Aus dem Institut für Molekulare Onkologie
Direktor: Prof. Dr. Thorsten Stiewe
des Fachbereichs Medizin der Philipps-Universität Marburg

Advanced preclinical CRISPR mouse models to explore context-dependent effects of *TP53* mutations in cancer

Inaugural-Dissertation
zur Erlangung des Doktorgrades der Naturwissenschaften
dem Fachbereich Medizin der Philipps-Universität Marburg
vorgelegt von

Nastasja Merle
aus Schwalmstadt

Marburg, 2023

Angenommen vom Fachbereich Medizin der Philipps-Universität Marburg am:
07.02.2023

Gedruckt mit Genehmigung des Fachbereichs Medizin.

Dekanin: Prof. Dr. Denise Hilfiker-Kleiner
Referent: Prof. Dr. Thorsten Stiewe
Korreferentin: Prof. Dr. Uta-Maria Bauer

To my dear parents & grandparents

Table of Contents

Summary

The tumor suppressor p53 is the most frequently mutated protein in cancer patients and exhibits a unique mutational spectrum that is dominated by missense mutations. In contrast to the most prevalent hotspot mutations, 70% of all missense mutations are non-hotspot mutations with yet poorly characterized functions in tumorigenesis. Non-hotspot mutants often retain some wildtype activity, which corresponds to a partial loss-of-function (pLOF). Mutations that affect the DNA binding cooperativity of p53 fall into this class of mutants.

This work demonstrates that the prototypical DNA binding cooperativity mutant E177R can either promote tumorigenesis or induce tumor regression dependent on the cellular and genetic context. Expression of E177R in normal tissues resulted in increased susceptibility to spontaneous and oncogene-driven tumor development, emphasizing the pathogenic role of pLOF mutants. In striking contrast, expression of E177R in p53-deficient tumor cells revealed that the residual transcriptional activity of the mutant is able to promote the regression of already manifested tumors. That the same p53 mutant can have opposite effects on tumor growth highlights how genetic context determines the consequences of a cancer mutation.

To investigate the impact of specific mutations in different genetic contexts, we have developed a new method for generating genetically defined mouse tumors for preclinical studies. We have applied the CRISPR technology to induce cancer mutations rapidly and precisely in somatic cells and present a flexible toolkit based on adenoviral vectors for *in vivo* delivery of CRISPR effectors. In addition, we have generated a conditional reporter mouse that expresses a *Gaussia princeps* luciferase (GLuc). When GLuc is secreted by tumor cells, it accumulates in the blood and serves as a tumor marker to monitor cancer development and therapy responses. By combining the use of CRISPR adenoviruses and GLuc reporter mice, we have established a preclinical mouse tumor model that allows the rapid and flexible induction of autochthonous tumors that are easily monitored using blood samples to study the impact of a cancer mutation on tumorigenesis and cancer therapy in a genetically defined context.

Zusammenfassung

Der Tumorsuppressor p53 ist das am häufigsten mutierte Protein in Krebspatienten und weist ein einzigartiges Mutationsspektrum auf, das von Missense-Mutationen dominiert wird. Im Gegensatz zu den am häufigsten vorkommenden Hotspot-Mutationen, sind 70% aller Missense-Mutationen Non-Hotspot-Mutationen, deren Funktion bei der Tumorentstehung noch nicht ausreichend bekannt ist. Non-hotspot-Mutationen behalten oft eine gewisse Wildtyp-Aktivität, was einem partiellen Funktionsverlust (pLOF) entspricht. Mutationen, die die DNA-Bindungskooperativität von p53 beeinträchtigen, fallen in diese Klasse von Mutanten.

Diese Arbeit zeigt, dass die prototypische DNA-Bindungskooperativitätsmutante E177R, je nach zellulärem oder genetischem Kontext, in der Lage ist, entweder Tumorentstehung oder Tumorregression zu fördern. Die Expression von E177R in normalen Geweben führte zu einer erhöhten Anfälligkeit für spontane und Onkogen-induzierte Tumorentwicklung, was die pathogenen Eigenschaften von pLOF-Mutanten verdeutlicht. In auffälligem Gegensatz dazu zeigte die Expression von E177R in p53-defizienten Tumorzellen, dass die transkriptionelle Restaktivität der Mutante die Regression von bereits manifestierten Tumoren ermöglicht. Dass ein und dieselbe p53-Mutante entgegengesetzte Auswirkungen auf das Tumorwachstum haben kann, verdeutlicht, wie der genetische Kontext die Folgen einer Tumormutation bestimmt.

Um den spezifischen Einfluss solcher Mutationen in unterschiedlichen genetischen Kontexten zu untersuchen, haben wir eine neue Methode zur Erzeugung genetisch definierter Maustumore für präklinische Studien entwickelt. Wir haben die CRISPR-Technologie eingesetzt, um Krebsmutationen schnell und präzise in somatischen Zellen zu induzieren, und stellen ein flexibles Toolkit vor, das auf adenoviralen Vektoren für den Transfer von CRISPR-Effektoren basiert. Darüber hinaus haben wir eine konditionelle Reportermauslinie generiert, die die *Gaussia princeps* Luciferase (GLuc) exprimiert. Von Tumorzellen sezernierte GLuc reichert sich im Blut an und dient dort als Tumormarker zur Überwachung der Tumorentwicklung und des Therapieansprechens. Durch die Kombination von CRISPR-Adenoviren und GLuc-Reportermäusen haben wir ein präklinisches Maustumormodell etabliert, das die schnelle und flexible Induktion von autochthonen Tumoren ermöglicht, die sich leicht anhand von Blutproben überwachen lassen, um die Auswirkungen einer Krebsmutation auf Tumorentwicklung und Krebstherapie in einem genetisch definierten Kontext zu untersuchen.

1. Introduction

1.1 The master transcription factor p53

Cancer is a multifaceted disease defined by the transformation of somatic cells towards a malignant state resulting from the activation of oncogenes or the inactivation of tumor suppressor genes. Tumor suppressors play a critical role in regulating cell proliferation, help to prevent uncontrolled cell growth and promote DNA repair and cell cycle checkpoint activation to maintain genomic integrity (Lee and Muller, 2010). One of the key operators of tumor suppression is the sequence-specific transcription factor p53 – the gene product of the *TP53* gene (Sabapathy and Lane, 2018). Considered as the "guardian of the genome" (Lane, 1992), p53 regulates various cellular processes like cell proliferation, senescence, apoptosis, or DNA repair. Upon multiple intrinsic or extrinsic stress signals such as DNA damage, hypoxia, or oxidative stress, p53 becomes stabilized and activates a myriad of target genes to prevent the proliferative expansion of genetically damaged cells (Brady and Attardi, 2010; Fischer, 2017; Kastenhuber and Lowe, 2017; Sullivan et al., 2018). The p53 protein consists of 393 amino acids, divided into an N-terminal transactivation domain, a proline-rich domain, a central DNA-binding domain, and C-terminally located regulatory and tetramerization domains. The latter enables cooperative binding as a tetramer to the DNA of target gene promoters. This is further enhanced by the oppositely charged amino acids E180 and R181, located within the H1 helix of the DNA binding domain, which form intermolecular salt bridges and stabilize the DNA-bound tetramer (Dehner et al., 2005; Klein et al., 2001; Schlereth et al., 2010; Timofeev et al., 2021; Weinberg et al., 2004). Being a transcription factor, DNA binding is essential for p53 to activate all the transcriptional effector programs that contribute to its tumor suppressive power.

1.2 The rainbow of p53 mutations

The *TP53* gene is mutated in more than half of human cancers, indicating a fundamental role for p53 in tumor suppression (Brady and Attardi, 2010). Unlike other tumor suppressors such as *RB1*, *PTEN,* or *APC*, which are inactivated in cancer by deletions or truncating mutations, the majority of *TP53* mutations are missense mutations causing the expression of a full-length mutant protein with impaired wildtype tumor suppressor activity, dominant-negative properties, and neomorphic oncogenic functions (Donehower et al., 2019; Levine and Oren, 2009; Muller and Vousden, 2012;

Stiewe and Haran, 2018). 30% of all missense mutations hit a few mutational hotspot residues within the DNA-binding domain (Baugh et al., 2018). These *TP53* hotspot mutations are well characterized and their functional impact on tumorigenesis has been explored in multiple studies. Hotspot mutations like R273H or R248Q affect residues that directly contact the DNA and are classified as “DNA-contact mutations” (Joerger et al., 2006). Mutations that disrupt the native folding of the protein and indirectly affect the DNA binding potential of p53 are considered as "structural mutations”, such as the R175H or R249S hotspot mutations (Bullock and Fersht, 2001; Joerger et al., 2006).

Mutations that do not affect hotspot residues account for the majority of missense mutations and are still poorly characterized. Unlike hotspot mutations that completely lack the transactivation potential of wildtype p53, non-hotspot mutations tend to retain residual transcriptional activity and, therefore, often exhibit only a partial loss-of-function (pLOF) (Campomenosi et al., 2001.; Jordan et al., 2010; Kato et al., 2003; Menendez et al., 2009). Such a pLOF phenotype is, for example, characteristic for a novel class of p53 mutants, the DNA binding cooperativity mutations, which disrupt the intermolecular salt bridge formed by the DNA binding domain residues E180 and R181 (Schlereth et al., 2010a; Schlereth et al., 2010b). Mutations involving these residues have been identified as both somatic and germline variants and account for approximately 34,000 cancer patients per year (Timofeev et al., 2013). The p53 binding cooperativity mutant E180R, for example, is mechanistically particularly well understood and shows a pronounced defect in apoptosis but retains cell cycle-inhibitory activity (Dehner et al., 2005; Schlereth et al., 2010; Schlereth et al., 2013).

The focus on p53 hotspot mutations in cancer research and the lack of knowledge on the more abundant non-hotspot mutations still hampers the use of p53 mutation status in clinical decision-making. Further studies on non-hotspot mutations and pLOF phenotypes are therefore essential to shed light on their role in tumorigenesis and develop targeted therapies.

1.3 Mouse models as a powerful tool in cancer research

The genetic landscape of cancer is extremely diverse and varies greatly between cancer patients. The most aggressive form of lung cancer, small cell lung cancer (SCLC), is defined by a combined inactivation of the two tumor suppressor genes *TP53* and *RB1*, for instance (George et al., 2015). Understanding the relationship between

cancer gene mutations and their contribution to carcinogenesis is critical for targeted therapeutic approaches. Animal models provide a valuable tool for studying the effects of various co-mutations and need to accurately reflect the diverse genetics of human tumors to be useful for the preclinical evaluation of molecular therapies (Kwon and Berns, 2013).

The spectrum of animal models available for cancer research is broad and xenograft models based on the transplantation of human tumor tissues or cancer cell lines are the most widely used (Breitenbach et al., 2018). Although such models precisely mirror the genetics of human cancer, they fail to develop the characteristic tumor microenvironment (TME) that is associated with the tumor phenotype and contributes to tumor progression or drug resistance (Guerin et al., 2020; Olson et al., 2018). Genetically engineered mouse models (GEMM) accurately represent the process of *de novo* tumorigenesis, whereby tumors arise from genetically engineered cells *in situ* (Kersten et al., 2017). GEMMs precisely represent the initiating events of tumorigenesis as well as the process of tumor progression, thus better reflecting the natural time course of tumor development. Tumorigenic mutations are typically introduced into the germline of mice using multiple conditional approaches, which requires extensive crossbreeding of transgenic mice to obtain animals with the desired complex genotype. This lengthy process is not only expensive and laborious but also contributes significantly to animal burden and poses ethical issues, as many mice are sacrificed due to an unwanted genotype.

The development of the CRISPR technology has revolutionized cancer research and is considered a game changer for animal cancer models. The CRISPR/Cas9 system simplified the generation of mouse models and can be used as a powerful tool to induce genetic changes directly in somatic cells, avoiding complex breeding schemes for genetically defined mouse models (Sánchez-Rivera and Jacks, 2015; van der Weyden et al., 2021; Weber and Rad, 2019). It also enables the development of tumors that progress along a natural timeline and accurately mimics cancer development as it occurs in patients. Moreover, CRISPR not only allows the introduction of almost every single genetic alteration found in human tumors but also combinations of cooperating mutations. For example, *in vivo* application of the CRISPR/Cas9 system has enabled the generation of complex chromosomal rearrangements leading to fusion oncogenes such as the Eml4-Alk fusion protein, a clinically important driver in non-small cell lung cancer (Maddalo et al., 2014). Application of the CRISPR technology advances the

generation of preclinical animal models and enables high throughput studies on relevant cancer gene mutations to provide detailed mechanistic insight into their role in cancer development, progression, and metastasis.

1.4 Monitoring tumor growth using secreted luciferases

Genetically transformed cells generally undergo sequential stages of tumorigenesis, resulting in slower and more variable tumor growth in different animals and groups. In addition, the dynamics of tumor growth are also affected by engineered co-mutations or secondary mutations that have been spontaneously acquired during the course of tumor development. To monitor differences in tumorigenesis caused by different cancer gene mutations, suitable methods are required for longitudinally tracking tumor growth. Most of these techniques rely on imaging technologies like magnetic resonance imaging (MRI), computed tomography (CT), positron-emission tomography (PET), or bioluminescence imaging (BLI) and require anesthesia of the animals, rendering such methods expensive and time-consuming (Wang et al., 2015). This, in turn, not only limits the overall examination frequency but also adds to animal burden and makes screening of large cohorts complicated.

As an alternative, secreted luciferases have been introduced for monitoring biological processes such as tumor growth (Markova et al., 2019; Tannous, 2009; Wurdinger et al., 2008). For example, the secreted luciferase from the copepod *Gaussia princeps* (GLuc) is actively secreted by cells and accumulates in the blood, so that tumor growth can be quantitively monitored *ex vivo* using GLuc activity levels in small-volume blood samples (Charles et al., 2014; Gremke et al., 2020; Wanzel et al., 2016). In addition, GLuc secretion is an energy-consuming process and thereby excludes necrotic cells that also contribute to tumor volume (Tannous, 2009). The ability to study large cohorts with GLuc-based tumor monitoring makes it suitable for time-resolved assessment and detection of differences in tumor growth caused by different mutations. Secreted luciferases are therefore a powerful tool for monitoring tumor growth, but as tumor cells have to be labeled with the luciferase *ex vivo*, this method is restricted to the monitoring of transplanted tumors and is not yet applicable to the more physiological GEMM or somatic CRISPR models.

2. p53 partial loss-of-function mutations sensitize to chemotherapy

Boris Klimovich*, Nastasja Merle*, Michelle Neumann, Sabrina Elmshäuser, Andrea Nist, Marco Mernberger, Daniel Kazdal, Albrecht Stenzinger, Oleg Timofeev and Thorsten Stiewe

* both authors contributed equally to this manuscript

Oncogene 41, 1011 – 1023 (2021). PubMed ID: 34907344

2.1 Introduction

Mutations affecting the tumor suppressive transcription factor *TP53* are common in many cancer entities and often result in an inactivation of the p53 protein. A large proportion of these mutations are missense mutations that cluster in the DNA binding domain where 30% of these mutations hit specific residues like R175, R248, or R273 which are referred to as hotspot mutations. These hotspot mutations are classified into “structural” mutations which destabilize the DNA binding domain and lead to protein denaturation, and “contact” mutations which affect residues directly contacting the DNA and thereby abrogate DNA binding (Joerger et al., 2006). The effects of hotspot mutations on p53 transcriptional activity are well studied. (Freed-Pastor and Prives, 2012; Kim and Lozano, 2018; Muller and Vousden, 2014; Stiewe and Haran, 2018). However, the remaining non-hotspot mutations account for the majority of all p53 mutations but their impact on cancer remains elusive. In contrast to hotspot mutants, most non-hotspot mutants retain some of their transcriptional activity, which classifies them as partial loss-of-function mutations (pLOF) (Giacomelli et al., 2018; Kotler et al., 2018).

The consequences of a p53 pLOF mutation and their impact on tumor development and therapy largely remain elusive. To investigate the functional consequences of pLOF mutations on tumor development and therapy response, we used the non-hotspot mutants involving residues E180 and R181, located within the H1 helix of p53, as a model, since they exhibit a mechanistically well-understood pLOF phenotype. These two oppositely charged amino acids form an ionic bond between the H1 helices of two p53 monomers, providing the structural basis for cooperative binding to DNA

(Dehner et al., 2005; Klein et al., 2001; Timofeev et al., 2021). Mutations affecting the E180 and R181 mutations are either somatic or germline variants and account for roughly 34,000 cancer patients each year (Timofeev et al., 2021). The *in vitro* and *in vivo* functional impact of the E180R mutation has been studied better than that of any other cooperative binding mutation, owing to the availability of a mutant mouse model with the equivalent murine E177R mutation (Klimovich et al., 2019; Timofeev et al., 2013). E177R retains residual transcriptional activity and is able to transactivate target genes involving the regulation of cell proliferation and senescence. However, the ability of E177R to induce apoptosis is selectively impaired (Timofeev et al., 2013). Moreover, complementation with the R178E mutant completely restores the E177R phenotype, indicating that the defect in cooperative DNA binding is responsible for the phenotype (Dehner et al., 2005; Schlereth et al., 2010; Schlereth et al., 2013; Timofeev et al., 2019). Since the effects of the multitude of other p53 pLOF mutations have not been adequately explored, we used the E177R mouse model together with other patient-derived cooperativity mutants to investigate the impact of such non-hotspot mutants on cancer initiation, progression, and therapy.

2.2 Summary and Discussion

To evaluate if non-hotspot mutations in the *TP53* gene are enriched for pLOF variants, we analyzed 1209 *TP53* missense mutations from the UMD *TP53* mutation database for their transcriptional activity (Fig. 1A). Variants with less than 10% transcriptional activity of p53 were classified as LOF mutations, those with 10-50% residual activity as pLOF mutants. Comparing the transcriptional activity of individual mutants with their frequency in cancer patients, pLOF variants were enriched among the mutations with low or medium frequency in patients (Fig. 1A and B). Nevertheless, a large proportion (27.6%) of *TP53* mutated malignancies harbored an intermediate p53 transcriptional activity, indicating that such pLOF mutants are common in p53 mutated tumors, especially among tumors with non-hotspot mutants (Fig. 1C and D). To investigate the transcriptional consequences of pLOF mutations in more detail, we expressed a set of patient-derived cooperativity mutants in p53-deficient tumor cells. Transcriptome analysis revealed that all cooperativity mutants showed a reduced regulation of target genes compared to wildtype p53 and that individual mutants differed in their residual transcriptional activity (Fig. 2A). We found canonical p53-target gene sets to be enriched in cells expressing the cooperativity mutants compared to cells with the

R175H hotspot mutant, reflecting the functional differences between p53 non-hotspot mutations and hotspot mutations (Fig. 2B-D). Notably, the E180R mutant showed a level of residual transcriptional activity between all analyzed patient-derived mutants, validating the E180R mutant as a model for p53 non-hotspot mutants with a pLOF.

We next aimed to evaluate the tumorigenic effects of the murine E180R equivalent E177R in models of *Kras*^{G12D}-driven pancreatic ductal adenocarcinoma (PDAC) and lung cancer (Fig. 3-4). Expression of E177R was sufficient to trigger tumor development and progression in the two independent models, albeit with slower dynamics compared to a complete loss of p53. Although hematopoietic cancer types are more susceptible to changes in p53 activity, expression of E177R in a model of acute myeloid leukemia (AML) led to the same observation as in solid tumors (Fig. 5). Of note, mutant protein accumulated in all samples and tumors retained residual p53 activity as analyzed by transcriptomic profiling (Fig. 3D, 4E and 5D-G). The residual transcriptional activity of E177R therefore transiently delayed tumor progression in multiple cancer models but was not sufficient to prevent tumor development and progression to lethal stages.

The therapeutic consequences and especially the effect of chemotherapy in the context of pLOF mutations remained elusive. Therefore, we next sought to evaluate potential tumor suppressive functions of E177R in response to chemotherapy and treated mice expressing either p53 null, E177R or wildtype (WT) in the AML model with a combination of cytarabine and doxorubicin. While p53-deficient AML continuously progressed, p53 WT and E177R animals showed good therapeutic responses, translating into an extended survival of the respective cohorts (Fig. 6A and B). Upon chemotherapy, p53 became rapidly stabilized in WT and E177R groups and immunohistochemical and transcriptomic analysis of leukemia samples showed upregulation of p53-related signaling pathways and indicated an apoptotic response of not only WT but also the p53 E177R mutant (Fig. 7). Activation of apoptosis was unexpected since multiple pLOF mutants, including E177R, were previously described to have a defect in apoptosis.

The amount and dynamics of wildtype p53 protein accumulation significantly affects the extent of apoptosis induction (Chen et al., 1996; Kracikova et al., 2013; Purvis et al., 2012). As we observed massive E177R protein accumulation in PDAC, lung adenocarcinoma, and AML cells, we speculated that elevated expression of pLOF mutants might rescue their apoptosis deficiency. We found the R181L, E180R, R181H,

and R181C mutants to be dysfunctional in their apoptotic program when expressed at the same levels as WT p53. However, when increasing the amount of mutant p53, the defect in apoptosis could be rescued, albeit to different extents for the individual mutants (Fig. 8D and E). Furthermore, DNA binding and transactivation of canonical target genes (including pro-apoptotic *PUMA/BBC3*) were restored to WT-like levels by overexpressing pLOF mutants (Fig. 8F and G).

In sum, the engineered E180R/E177R mutation proved to be a suitable model for p53 non-hotspot mutations with pLOF. Using multiple mouse tumor models, a pLOF mutation was shown to impact the tumor suppressive function of p53, resulting in profound cancer susceptibility. Similar to hotspot mutants, pLOF mutants accumulated at the protein level in tumor cells. However, different from hotspot mutants, which exert pro-tumorigenic properties upon accumulation, elevated expression of pLOF mutants exhibited tumor suppressive effects, especially in the context of chemotherapy, where their apoptotic defects were rescued. Our study, therefore, demonstrates that the class of p53 non-hotspot mutations with pLOF is functionally distinct from hotspot mutations and should be given special attention in terms of therapeutic and clinical implications.

2.3 Contribution Statement

In this study, I comprehensively characterized the pLOF phenotype of patient-derived p53 cooperativity mutants by transcriptomic profiling (Fig. 2) and demonstrated that their apoptosis defect is rescued at elevated expression levels using real-time apoptosis assays, Western Blots, and RT-qPCR analysis (Fig. 8, Supp. Fig. S3). I prepared the data for publication and participated in writing and proofreading the manuscript.

3. Partial p53 reactivation is sufficient to induce cancer regression

Boris Klimovich, Laura Meyer, Nastasja Merle, Michelle Neumann, Alexander M. König, Nikolaos Ananikidis, Corinna U. Keber, Sabrina Elmshäuser, Oleg Timofeev and Thorsten Stiewe

J Exp Clin Cancer Res 41, 80 (2022). PubMed ID: 35232479

3.1 Introduction

Over 50% of human cancer types show inactivation and impaired function of the tumor suppressor p53, most commonly caused by somatically acquired mutations that affect the *TP53* gene (Donehower et al., 2019). *TP53* mutations can vary widely in their functional impact (Donehower et al., 2019; Leroy et al., 2014). Notably, full p53 activity is critical for the most effective tumor suppression program, as even a partial loss of p53 increases cancer susceptibility (Frebourg et al., 1992; Liu et al., 2003; Timofeev et al., 2013; Wang et al., 2011). Most importantly, several studies have demonstrated that p53-deficient tumor cells become dependent on the continuous absence of p53, so that restoration of p53 triggers tumor regression (Lozano, 2019). This indicates that tumor cells become addicted to the loss of p53 activity, underscoring the therapeutic potential of p53 reactivation in cancer treatment (Feldser et al., 2010; Junttila et al., 2010; Ventura et al., 2007; Xue et al., 2007). Several compounds for p53 reactivation are currently being investigated for their therapeutic potential in clinical studies (Bykov et al., 2018; Sabapathy and Lane, 2018). Unfortunately, many of these compounds are yet inefficient and fail to fully restore wildtype activity to the mutant protein, raising the critical question of how much p53 activity is required to induce cancer regression.

To address this question and model an incomplete, partial p53 reactivation, we used a conditional mouse model with inducible expression of the p53 cooperativity mutant E177R, a partial loss-of-function (pLOF) mutant with reduced DNA binding and target gene activation.

3.2 Summary and Discussion

In this study, the conditional *Trp53*$^{LSL\text{-}E177R/+}$;*Rosa26*^{CreERT2} mouse strain was used to generate p53-deficient acute myeloid leukemia (AML) in which expression of the E177R pLOF mutant could be restored at will by treatment with tamoxifen (Fig. 1). Expression of E177R after tamoxifen treatment increased the expression of multiple p53 target genes (Fig. 1C-F) and triggered apoptosis (Fig. 2C and D). Thus, incomplete p53 reactivation, modeled by genetically switching AML cells from no p53 to a partially active p53, was sufficient to induce tumor-suppressive programs *in vitro*.

Next, we transplanted AML cells into mice and monitored leukemia growth via bioluminescence imaging (BLI) (Fig. 3A). Following successful leukemia engraftment, mice were treated with tamoxifen to induce expression of E177R and model partial p53 reactivation. Expression of E177R led to strongly decreased BLI signals and extended survival, indicating a strong response of tumor cells to partial p53 reactivation (Fig. 3A and B). CRISPR-mediated knockout of E177R prevented leukemia regression, confirming that the therapeutic response was indeed mediated by the expression of E177R (Fig. 3C and D).

To investigate the mechanisms by which E177R induces leukemia regression, we used immunohistochemistry (IHC) to analyze leukemia samples of mock-treated and tamoxifen-treated animals at different time points after therapy. Compared to mock-treated animals, p53 protein rapidly accumulated in tamoxifen-treated samples (Fig. 4A). This was followed by a decrease in cell proliferation, increased apoptosis and senescence, and immune cell infiltration, underscoring that partial p53 reactivation synergistically activates multiple tumor suppressive effector mechanisms not only *in vitro* but also *in vivo* (Fig. 4A-D).

Encouraged by the effects observed in the AML model, we investigated the consequences of partial p53 reactivation in a second model, where Burkitt-like B-cell lymphoma was induced by the *EμMyc* oncogene in the *Trp53*$^{LSL\text{-}E177R/+}$;*Rosa26*^{CreERT2} background. Mice transplanted with such lymphoma cells showed prolonged survival when treated with tamoxifen, indicating that E177R induction also causes tumor regression in B-cell lymphoma (Fig. 5A and B). Similar to the AML model, expression of E177R reduced the number of proliferating cells and increased apoptosis in primary lymphomas as well as at metastatic sites in the liver (Fig. 5C-F).

To explore the therapeutic potential of partial p53 activation in an autochthonous tumor model, we used the same experimental approach to generate thymic T-cell lymphoma.

Trp53$^{LSL\text{-}E177R/+}$;*Rosa26*^{CreERT2} animals were monitored by repeated magnetic resonance imaging (MRI) and developed p53-deficient thymic lymphoma spontaneously within 4 months. Induction of E177R with tamoxifen prolonged survival and led to a reduction in thymus size compared to non-reactivatable *Trp53*$^{LSL\text{-}E177R}$ control mice, where tumor size progressively increased even under tamoxifen treatment (Fig. 6). To conclude, expression of mutant p53 with pLOF was able to drive a tumor suppressive transcriptional program limiting the growth of several types of hematopoietic cancer, indicating that partial reactivation of p53 is sufficient to induce tumor regression.

Our study provides evidence that the pro-tumorigenic, pLOF mutant E177R can trigger cancer regression when activated in p53-deficient leukemia and lymphoma, emphasizing the sensitivity of cancer cells to even slight increases in p53 activity. The E177R mutant affects the cooperative binding of p53 to the DNA and results in a reduced degree of DNA binding but is still able to transactivate p53 target genes and regulate multiple other effector programs to a certain extent. By using a genetically defined expression level of the mutant, we demonstrate that partial reactivation of p53 leads to effective anti-proliferative programs *in vitro* and tumor regression *in vivo*, although potential non-cell-autonomous effects might help to suppress tumor growth *in vivo*. However, it remains to be investigated whether the effects observed in hematologic cancer, with a rather low apoptotic threshold, also apply to other solid cancers. Nevertheless, this study emphasizes the importance of research on mutant p53-reactivating drugs to improve the treatment of cancers with mutated p53.

3.3 Contribution Statement

In this project, I contributed to the studies on partial p53 reactivation in the AML model by generating and producing retroviral particles, transplanting AML cells into mice, treating mice with tamoxifen, and imaging leukemia progression by bioluminescence (Fig. 1-4). Furthermore, I prepared and analyzed data for the publication and participated in writing and proofreading the manuscript.

4. Monitoring autochthonous lung tumors induced by somatic CRISPR gene editing in mice using a secreted luciferase

Nastasja Merle, Sabrina Elmshäuser, Florian Strassheimer, Michael Wanzel, Alexander M. König, Julianne Funk, Michelle Neumann, Katharina Kochhan, Frederik Helmprobst, Axel Pagenstecher, Andrea Nist, Marco Mernberger, André Schneider, Thomas Braun, Tilman Borggrefe, Rajkumar Savai, Oleg Timofeev and Thorsten Stiewe

Mol Cancer 21, 191 (2022). PubMed ID: 36192757

4.1 Introduction

Cancer is a multigenetic disease and arises from mutations in somatic cells affecting tumor suppressor genes or proto-oncogenes. Each individual cancer subtype is defined by the combination of genetic mutations that result in differences in tumorigenesis, aggressiveness, and therapeutic vulnerabilities. Given the enormous genetic complexity of human cancer and the heterogeneous processes underlying human tumorigenesis, mouse tumors that model the key characteristics of human cancer in a defined (inbred) genetic background are valuable research tools. For preclinical studies on targeted therapies, these models need to accurately reflect the genetic alterations that have been observed in patients.

The spectrum of mouse models available for cancer research is diverse, with xenograft models based on the transplantation of human cancer cell lines or cancer tissues being the most common and widely used (Breitenbach et al., 2018; Guerin et al., 2020). Mouse xenograft models allow a quick evaluation of growth dynamics and response to drugs. However, to avoid rejection, human cancer cells or tissues need to be transplanted into immunocompromised hosts. As a consequence, the resulting tumors do not develop the characteristic tumor (immune) microenvironment (TME) that modulates tumor progression and therapy responses. The absence of a physiological TME hampers preclinical drug testing, thus limiting the value of xenograft models. Genetically engineered mouse models (GEMM) overcome this limitation since cancer arises in an autochthonous setting in an immunocompetent host, allowing for a more realistic representation of the human disease. Although GEMMs are well-established,

the generation of mice with multiple transgenic alleles is laborious, time-consuming, and expensive. Due to the extensive breeding schemes required to obtain animals with the desired complex genotype, the generation of GEMMs continues to contribute significantly to animal burden, as many mice with an unwanted genotype must be sacrificed. Recent advances in the CRISPR/Cas9 technology have made the use of non-transplanted, autochthonous mouse models easier than ever (Maddalo et al., 2014; Oser et al., 2019). CRISPR nucleases enable the generation of defined tumor mutations directly in somatic cells using, for example, modified adenoviruses as gene transfer vectors, thus avoiding the unnecessarily complicated germline manipulation of mice. In this approach, tumor development arises in a more natural way, directly from somatically transformed cells.

Tumor growth can vary greatly between animals as genetically modified cells undergo subsequent stages of tumorigenesis, making these models experimentally less predictable. Therefore, methods for longitudinal monitoring of tumor growth are indispensable for the precise tracking of cancer growth (Wang et al., 2015). The most commonly used monitoring by small animal imaging technologies is expensive, requires trained staff and anesthesia of the animals for immobilization. Together, this makes longitudinal and frequent monitoring a hurdle. Previous studies have shown that an alternative method of monitoring tumor development using secreted luciferases overcomes the obstacles associated with other sophisticated monitoring methods (Markova et al., 2019; Tannous, 2009; Wurdinger et al., 2008). The luciferase from the marine copepod *Gaussia princeps* (GLuc) is secreted by GLuc-labeled tumor cells and enters the blood stream so that luciferase activity in small-volume blood samples can be used to quantitatively monitor tumor growth. Moreover, GLuc is secreted in an energy-consuming process only by viable tumor cells, so that GLuc monitoring helps to distinguish tumor cells from other cell types in the tumor stroma, that contribute to tumor size but cannot be easily differentiated by small animal imaging. However, GLuc monitoring of tumors requires prior *ex vivo* labeling of the tumor cells, restricting the use of this animal-friendly monitoring method to the less physiological, transplanted mouse tumor models.

4.2 Summary and Discussion

To facilitate monitoring of autochthonous tumor growth with the help of the secreted luciferase from *Gaussia princeps*, we generated a reporter mouse strain

Gt(ROSA)26Sor$^{tm2(CAG-GLuc)Thst}$ (*Rosa26*$^{LSL-GLuc}$ or LSL-GLuc) with Cre-inducible expression of GLuc (Fig. 1A). As a proof-of-principle and to determine the expression of GLuc in different organs, we activated GLuc expression in the whole body by crossing to Prm-Cre mice. Compared to unrecombined animals, GLuc was detectable at comparable levels in all analyzed organs and secreted into the blood at a constant rate (Fig. 1B-E). Further, expression of GLuc was found to be not leaky since unrecombined LSL-GLuc mice had GLuc levels comparable to non-GLuc-transgenic animals, highlighting the suitability of the LSL-GLuc reporter mouse for longitudinally tracking tumor growth.

Next, we evaluated *in vivo* labeling of tumor cells in two classic, genetically engineered mouse models: an *EμMyc*-driven lymphoma model and a *Kras*^{G12D}-induced model for non-small cell lung cancer. In both models, GLuc secretion increased with disease progression (Fig. 2). Moreover, in the *EμMyc* model, GLuc blood levels accurately captured chemotherapy responses and therapy relapse with high temporal resolution, indicating suitability for treatment monitoring in preclinical drug studies (Fig. 2A-C).

The use of the CRISPR technology facilitated the design of somatically engineered mouse models and dramatically improved the generation of preclinical animal cancer models (Sánchez-Rivera et al., 2015; van der Weyden et al., 2021; Weber and Rad, 2019). However, the process of *in vivo* mutagenesis is still hampered by the inefficient delivery of CRISPR components into the target tissue. Recombinant adenoviruses represent a valuable tool for the efficient delivery of large cargo such as Cas9 enzymes and are well established as gene transfer vectors due to their large packaging capacity and their natural tropism for the respiratory epithelium (Weber and Rad, 2019). For that reason, we provide a cloning strategy to assemble multi-cistronic adenoviral vectors (AV) encoding for the CRISPR nuclease Cas9, multiple sgRNAs, and a Cre recombinase to facilitate the use in conditional transgenic mouse strains such as the conditional LSL-GLuc mice (Fig. 3). We applied this cloning strategy and generated AV constructs expressing Cre and Cas9 with sgRNAs targeting *Trp53* and *Rb1* to investigate whether knockout of these tumor suppressors induces autochthonous small cell lung tumors (Fig. 4A). Following validation of efficient gene targeting *in vitro*, we intratracheally infected LSL-GLuc reporter mice (Fig. 4B and C). Immunohistochemical staining of Cas9 and GLuc in lungs shortly after infection indicated successful cargo delivery to the lung epithelium. Detection of insertion and deletion mutations (InDels) at the *Trp53* and *Rb1* target loci by next generation

sequencing (NGS) of lung DNA confirmed the target-specific activity of the CRISPR nucleases (Fig. 4D-F). Compared to mice infected with a non-targeting control virus, mice infected with a Cas9-AV targeting *Trp53* and *Rb1* (PR.CC9) developed tumors within one year, resulting in a median survival of 363 days (Fig. 4H). Tumor development was dynamically monitored by classic magnetic resonance imaging (MRI) (Fig. 4G). The resulting tumors were identified as small cell lung cancer (SCLC) by immunohistochemical staining for multiple neuroendocrine markers and stained positive for GLuc (Fig. 5A). GLuc blood levels exceeded background levels starting 5 months after infection and progressively increased over time (Fig. 5D). To define the molecular origin of these tumors, we identified *Trp53* and *Rb1* mutations as driver lesions with approximately 80% modified reads in the NGS analysis (Fig. 5E).

Encouraged by the results and the flexibility of the toolkit for CRISPR-AV cloning, we aimed to explore the suitability of the CRISPR-GLuc model to investigate the impact of co-mutations on the dynamics of SCLC tumorigenesis. The retinoblastoma gene family member *Rbl2/p130* is recurrently mutated in SCLC patients (George et al., 2015) and loss of *Rbl2/p130* was previously shown to accelerate SCLC development in mice (Schaffer et al., 2010). We, therefore, aimed to generate and monitor development of SCLCs with triple mutations in *Trp53*, *Rb1*, and *Rbl2* using a CRISPR-AV co-expressing three sgRNAs. However, integration of a third sgRNA in our CRISPR-AV model led to inefficient virus packaging, mainly due to the limited packaging capacity of a 1st generation adenoviral vector. To overcome this limitation, we used a conditional double transgenic LSL-GLuc/LSL-Cas9 mouse strain which allowed us to omit Cas9 from the virus and generate constructs targeting either *Trp53* and *Rb1* (PR.Cre) or both in combination with *Rbl2/p130* (PRL.Cre) (Fig. 6A). Tumorigenesis in PR.Cre-infected mice was similar as with PR.CC9 mice, however, additional loss of *Rbl2/p130* led to accelerated tumor development and reduced survival to 210 days (Fig. 6F). Blood-GLuc levels accurately mirrored the differences in survival between the PR.Cre and PRL.Cre groups (Fig. 6G). GLuc blood levels increased above the background approximately three months before the animals reached the humane endpoint, proving GLuc to be suitable as an early detection marker in the SCLC mouse model (Fig. 6H-K). Of note, MRI confirmed the results observed with GLuc monitoring by visualizing total tumor burden in both groups (Fig. 7A). Similar as in PR.CC9 and PR.Cre-induced tumors, PRL.Cre tumors expressed neuroendocrine markers and universally carried mutations induced by the sgRNAs targeting *Trp53*, *Rb1*, and *Rbl2* (Fig.7B-D).

In conclusion, we established a toolkit to rapidly assemble CRISPR-AVs for *in vivo* mutagenesis of multiple cancer driver genes together with a novel reporter mouse strain which helps to easily capture the temporal dynamics of tumorigenesis using blood-based monitoring. Since personalized cancer therapy remains a clinical challenge and preclinical models are urgently needed to test therapeutic strategies in different genetically defined cancer subtypes, somatically engineered mouse models that can be generated fast and flexibly by, for example, CRISPR technology are indispensable. The CRISPR-GLuc mouse model is therefore a long-needed tool that will facilitate preclinical studies for precision medicine in autochthonous mouse models.

4.3 Contribution Statement

For this study, I planned and designed the cloning strategy for CRISPR-AV constructs (Fig. 3), generated the AVs used for the generation of SCLC in mice (Fig. 4A and 6A), validated their function *in vitro* (Fig. 4B and C and Fig. 6B and C), and planned and conducted all animal experiments involving these constructs (Fig. 4-7). In more detail, I performed the intratracheal infection of mice, collected blood samples, measured GLuc levels (Fig. 5D, 6G-K), assisted with mouse MRI (Fig. 4G, 7A), and monitored mice clinically (Fig. 4H, 6F, S1). I processed mouse tissues (lungs and tumors), characterized mouse tissues genetically by Sanger sequencing and amplicon NGS (Fig. 4E and F, 5E, 6E, 7D, S2-4; sequencing by Genomics Core Facility), established cell lines from SCLC tumors (Fig. S2), and analyzed immunohistochemical stainings of tissues (Fig. 4D, 5A-C, 6D, 7B and C; staining by Mouse Histopathology Core Facility). I prepared and analyzed the data, designed figures, and drafted the manuscript followed by correction and proofreading.

5. Summary and Perspectives

5.1 The impact of individual p53 mutations is highly context-dependent

Over the past decades, research on mutant p53 has made tremendous progress. Emerging evidence suggests that there is no single mutant p53 but rather a whole spectrum of distinct p53 variants in which the mutant proteins differ in their impact on tumorigenesis and offer distinct therapeutic vulnerabilities (Manfredi, 2019; Sabapathy and Lane, 2018). Unlike the well-characterized *TP53* hotspot mutations, which completely disrupt the transcriptional activity of p53, the functional impact of *TP53* non-hotspot mutations has remained largely elusive. Non-hotspot mutations are of particular clinical interest since they comprise 70% of all p53 mutations and often retain residual transcriptional activity, presenting a pLOF phenotype (Campomenosi et al., 2001; Jordan et al., 2010; Kato et al., 2003; Menendez et al., 2009).

In the first two publications, we investigated the class of p53 DNA binding cooperativity mutations as a model for non-hotspot mutations with a pLOF phenotype. Mutations that reduce the cooperative DNA binding of p53 do not affect DNA contact residues or disturb the proper folding of the entire DNA binding domain, like hotspot mutations do, but they interfere with the interaction of adjacent p53 DNA binding domains within the p53-DNA complex (Timofeev et al., 2013). Several mutations that destabilize these interactions and weaken the p53-DNA complex have been identified in cancer patients, which implies an important role of p53 DNA binding cooperativity for cancer development. In both studies, we used the E180R cooperativity mutation as a model. The biochemical and structural properties of the E180R mutation were well characterized and the availability of a mutant mouse strain with the homologous murine mutation E177R (Timofeev et al., 2013) facilitated the exploration of *in vivo* consequences on tumor development and cancer therapy responses.

In the first study, we observed that expression of E177R in multiple different tissues, including pancreas, lung, and bone marrow, sensitized to oncogene-driven tumorigenesis and was able to drive tumor development, further highlighting the pathogenicity of p53 pLOF mutants (Klimovich et al., 2021). In the second study, we observed that expression of E177R in fully established (p53-deficient) tumor cells triggers tumor regression (Klimovich et al., 2022). The intriguing fact that the E177R DNA cooperativity mutant, a single p53 mutant with a genetically defined DNA binding and transactivation level, behaves pro-tumorigenic in one model and tumor

suppressive in another, emphasizes the highly context-dependent activity of p53 mutants.

5.2 The power of CRISPR to investigate a genetically defined tumor context

In light of the findings from the first two studies, it is becoming increasingly important to study the impact of p53 mutations in a context-dependent manner, for example, in the presence of defined co-mutations. For this, methods are needed for the efficient and high-throughput generation of tumors with experimentally defined sets of mutations.

The generation of mouse models for cancer research improved significantly over the past years. It is essential that such models accurately recapitulate the genetic context of human cancers to provide an optimal tool for preclinical studies. The discovery of the CRISPR/Cas9 technology revolutionized genome editing, enabling rapid and precise editing of somatic cells (Katti et al., 2022; Sánchez-Rivera and Jacks, 2015; Weber and Rad, 2019). Recent advances of CRISPR have opened new avenues for manipulating mouse genomes and are currently transforming the process of mouse model generation, making a previously lengthy process easier than ever.

We applied the CRISPR technology in combination with adenoviral vectors as gene delivery vehicles to induce genetically defined lung tumors in mice. By introducing inactivating mutations in the *Trp53* and *Rb1* genes, which are a universal feature of human small cell lung cancer (George et al., 2015), mice developed autochthonous lung tumors of the small cell subtype. The CRISPR sgRNAs included in the viral constructs are defined by the genes of interest and can be customized to study the functional impact of different genetic contexts. However, successful delivery of large proteins such as Cas9 remains a challenge (Weber and Rad, 2019) and introduction of a third sgRNA, targeting the recurrently mutated *Rbl2* gene, failed to efficiently generate infectious AVs. Using our Cas9-based adenoviral system, it was not possible to explore the functional consequences of such additional mutations due to the limited cargo packaging capacity of adenoviruses. Utilization of size-optimized Cas enzymes such as CasMINI or split approaches could potentially improve and overcome challenges associated with large cargos (Ehrke-Schulz et al., 2017; Van der Weyden et al., 2021; Xu et al., 2021). Further, removal of Cas9 from the delivered constructs may enhance the complex design of adenoviral vectors. This strategy is supported by an available Cre-inducible Cas9 knock-in mouse strain, enabling stable Cas9

expression in the targeted tissue (Platt et al., 2014). Taking advantage of the availability of this mouse strain, we omitted Cas9 from our viral constructs, generating more space for additional sgRNAs. Introduction of a third mutation targeting *Rbl2* and thereby changing the genetic context of the cells, enhanced tumor development in our model, highlighting the importance to evaluate the context-specific effects of different genetic settings. CRISPR-AVs, therefore, present a valuable tool to functionally characterize the genetic alterations of human tumors rapidly and accurately.

However, cancer does not only involve inactivating mutations that can be easily generated by CRISPR/Cas9, but rather a combination of inactivating mutations in tumor suppressor genes and activating mutations in proto-oncogenes. Conversion of proto-oncogenes into oncogenes is usually a result of base substitutions (missense mutations). As elaborated above, *TP53* mutations are also most frequently missense mutations, which are notoriously difficult to engineer with classic CRISPR/Cas9 nucleases by exploiting homology-directed repair with a donor template. Fortunately, CRISPR technology has evolved in recent years and now offers a variety of tools, such as base editors (BE), to precisely introduce specific tumor-initiating cancer gene mutations. Engineering of a catalytically impaired Cas9 variant tethered to an adenine or cytosine deaminase led to the development of BEs that can induce missense mutations by A•T-to-G•C or C•G-to-T•A editing, respectively (Huang et al., 2021). Given the high prevalence of C>T transitions among all *TP53* missense mutations (Bouaoun et al., 2016), cytosine base editors (CBE) are of particular interest in the generation of specific *TP53* missense mutations. The invention of prime editors, whereby a catalytically inactive Cas9 is fused to a reverse transcriptase, further extended the spectrum of targeted mutations and offers the full potential to insert any kind of mutation by pegRNAs, which provide the desired sequence template (Anzalone et al., 2019). In first examples, *in vivo* base or prime editing was used to engineer specific pro-tumorigenic mutations in the *Pik3ca* or *Ctnnb1* genes, resulting in tumor formation (Annunziato et al., 2020; Liu et al., 2020).

Our adenoviral vector system can be easily adapted for the expression of CRISPR base- or prime editors to overcome the limitations associated with classical Cas9 approaches and aid in the introduction of specific missense mutations. Thus, investigating the oncogenic role of certain mutant proteins, such as p53 mutants, in a defined genetic context will be useful to further explore their impact on cancer.

5.3 High throughput monitoring of tumorigenesis using secreted luciferases

Specific genetic alterations caused by different mutations result in variable kinetics of tumor growth, which requires reliable methods to monitor growth dynamics. Especially the autochthonous growth of tumors in inner organs requires sophisticated imaging techniques like MRI, µCT, PET, or BLI that rely on anesthesia of the animal (Wang et al., 2015). This not only increases animal burden but limits the throughput of large cohorts and examination frequency, impairing preclinical drug testing, for instance. As an alternative, the luciferase from the copepod *Gaussia princeps* (GLuc) presents a valuable tool and monitoring option that has been previously shown to work in transplantable tumor models (Charles et al., 2014; Gremke et al., 2020; Vogiatzi et al., 2016; Wanzel et al., 2016).

To facilitate the use of GLuc monitoring in autochthonous tumors, we generated a Cre-inducible GLuc knock-in reporter mouse to monitor tumor growth. GLuc was suitable to monitor the growth of different types of lung cancer and was also suitable to capture differences in tumor growth in various genetic contexts, seen by an accelerated increase in GLuc blood levels in the *Trp53*/*Rb1*/*Rbl2* knockout SCLC model. Tumor growth dynamics are therefore highly dependent on genetic conditions, making GLuc exceptionally useful for high throughput monitoring of tumors that have specific underlying co-mutations.

Preclinical models are widely used for therapy studies, and tumors must be detectable at an early time point to adequately evaluate response to therapy. We successfully monitored therapy response in a lymphoma model and observed a strong decrease in GLuc activity upon therapy. This demonstrates the potential of GLuc as an early detection marker for accurate monitoring therapy responses.

Collectively, the combination of CRISPR-AVs for tumor induction and non-invasive tumor monitoring using GLuc facilitates the rapid generation and use of genetically defined mouse models for the preclinical evaluation of molecular therapies in different genetic contexts.

6. Publication Bibliography

Annunziato, Stefano; Lutz, Catrin; Henneman, Linda; Bhin, Jinhyuk; Wong, Kim; Siteur, Bjørn et al. (2020): In situ CRISPR-Cas9 base editing for the development of genetically engineered mouse models of breast cancer. In: *The EMBO Journal*, *39*(5).

Anzalone, Andrew; Randolph, Peyton B; Davis, Jessie R; Sousa, Alexander A; Koblan, Luke W; Levy, Jonathan M et al (2019): Search-and-replace genome editing without double-strand breaks or donor DNA. In: *Nature*, *576*(7785), 149–157.

Baugh, Evan H; Ke, Hua; Levine, Arnold J; Bonneau, Richard A; Chan, Chang S (2018): Why are there hotspot mutations in the TP53 gene in human cancers? In: *Cell Death and Differentiation*, *25*, 154–160.

Bouaoun, Liacine; Sonkin, Dmitriy; Ardin, Maude; Hollstein, Monica; Byrnes, Graham; Zavadil, Jiri; Olivier, Magali (2016): TP53 Variations in Human Cancers: New Lessons from the IARC TP53 Database and Genomics Data. In: *Human Mutation*, *37*(9), 865–876.

Brady, Colleen A; Attardi, Laura D (2010): p53 at a glance. In: *Journal of Cell Science*, *123*, 2527–2532.

Breitenbach, Michael; Holcmann, Martin; Cemazar, Maja; Lampreht Tratar, Ursa; Horvat, Simon (2018): Transgenic Mouse Models in Cancer Research. In: *Frontier in Oncology*, *8*, 268.

Bullock, Alex N; Fersht, Alan R (2001): Rescuing the function of mutant p53. In: *Nature Reviews Cancer*, *1*(1), 68–76.

Bykov, Vladimir JN; Eriksson, Sofi E; Bianchi, Julie; Wiman, Klas G (2018): Targeting mutant p53 for efficient cancer therapy. In: *Nature Reviews Cancer*, *18*(2), 89–102.

Campomenosi, Paola; Monti, Paola; Aprile, Anna; Abbondandolo, Angelo; Frebourg, Thierry; Gold, Barry et al. (2001): p53 mutants can often transactivate promoters containing a p21 but not Bax or PIG3 responsive elements. In: *Oncogene*, *20*, 3573–3579.

Charles, Joël P; Fuchs, Jeannette; Hefter, Mirjam; Vischedyk, Jonas B; Kleint, Maximilian; Vogiatzi, Fotini et al. (2014): Monitoring the dynamics of clonal tumour evolution in vivo using secreted luciferases. In: *Nature Communications*, *5*.

Chen, Xinbin; Ko, Linda J; Jayaraman, Lata; Prives, Carol (1996); p53 levels, functional domains, and DNA damage determine the extent of the apoptotic response of tumor cells. In: *Genes and Development*, *10*(19), 2438–2451.

Dehner, Alexander; Klein, Christian; Hansen, Silke; Müller, Lin; Buchner, Johannes; Schwaiger, Manfred; Kessler, Horst (2005); Cooperative binding of p53 to DNA: regulation by protein-protein interactions through a double salt bridge. In: *Angewandte Chemie*, *44*(33), 5247–5251.

Donehower, Lawrence A; Soussi, Thierry; Korkut, Anil; Liu, Yuexin; Schultz, A; Cardenas, M et al. (2019): Integrated Analysis of TP53 Gene and Pathway Alterations in The Cancer Genome Atlas. In: *Cell Reports*, *28*(5), 1370–1384.

Ehrke-Schulz, Eric; Schiwon, Maren; Leitner, Theo; Dávid, Stephan; Bergmann, Thorsten; Liu, Jing et al. (2017): CRISPR/Cas9 delivery with one single adenoviral vector devoid of all viral genes. In: *Scientific Reports*, *7*(17113), 1–11.

Feldser, David M; Kostova, Kamena K; Winslow, Monte M; Taylor, Sarah E; Cashman, Chris; Whittaker, Charles A et al. (2010): Stage-specific sensitivity to p53 restoration during lung cancer progression. In: *Nature*, *468*, 572–576.

Fischer, Martin (2017): Census and evaluation of p53 target genes. In: *Oncogene*, *36*, 3943–3956.

Frebourg, Thierry; Kassel, Jayne; Lam, Kelvin T; Gryka, Magdalena A; Barbier, Noele; Ikdahl Andersen, Tone; Friend, Stephen H (1992): Germ-line mutations of the p53 tumor suppressor gene in patients with high risk for cancer inactivate the p53 protein. In: *Genetics*, *89*, 6413–6417.

Freed-Pastor, William A; Prives, Carol (2012): Mutant p53: one name, many proteins. In: *Genes and Development*, *26*(12), 1268–1286.

George, Julie; Lim, Jing Shan; Jang, Se Jin; Cun, Yupeng; Ozretia, Luka; Kong, Gu et al. (2015): Comprehensive genomic profiles of small cell lung cancer. In: *Nature*, *524*(7563), 47–53.

Giacomelli, Andrew O; Yang, Xiaoping; Lintner, Robert E; McFarland, James M; Duby, Marc; Kim, Jaegil et al. (2018): Mutational processes shape the landscape of TP53 mutations in human cancer. In: *Nature Genetics 2018 50:10*, *50*(10), 1381–1387.

Gremke, Niklas; Polo, Pierfrancesco; Dort, Aaron; Schneikert, Jean; Elmshäuser, Sabrina; Brehm, Corinna et al. (2020): mTOR-mediated cancer drug resistance suppresses autophagy and generates a druggable metabolic vulnerability. In: *Nature Communications*, *11*(4686).

Guerin, Marion; Finisguerra, Veronica; van den Eynde, Benoit J; Bercovici, Nadege; Trautmann, Alain (2020): Preclinical murine tumor models: A structural and functional perspective. In: *ELife*, *9*, 1–24.

Huang, Tony P; Newby, Gregory A; Liu, David R (2021): Precision genome editing using cytosine and adenine base editors in mammalian cells. In: *Nature Protocols*, *16*, 1089–1128.

Joerger, Andreas C; Ang, Ching; Fersht, Alan R (2006): Structural basis for understanding oncogenic p53 mutations and designing rescue drugs. In: *Proceedings of the National Academy of Sciences*, *103*(41), 15056–15061.

Jordan, Jennifer J; Inga, Alberto; Conway, Kathleen; Edmiston, Sharon; Carey, Lisa A; Wu, Lin; Resnick, Michael A (2010): Cancer Genes and Genomics Altered-Function p53 Missense Mutations Identified in Breast Cancers Can Have Subtle Effects on Transactivation. In: *Molecular Cancer Research*, *8*(5), 701–716.

Junttila, Melissa R; Karnezis, Anthony N; Garcia, Daniel; Madriles, Francesc; Kortlever, Roderik M; Rostker, Fanya et al. (2010): Selective activation of p53-mediated tumour suppression in high-grade tumours. In: *Nature*, *468*, 567–572.

Kastenhuber, Edward R; Lowe, Scott W (2017): Putting p53 in Context. In: *Cell*, *170*(6), 1062–1078.

Kato, Shunsuke; Han, Shuang Yin; Liu, Wen; Otsuka, Kazunori; Shibata, Hiroyuki; Kanamaru, Ryunosuke; Ishioka, Chikashi (2003): Understanding the function-structure and function-mutation relationships of p53 tumor suppressor protein by high-resolution missense mutation analysis. In: *Proceedings of the National Academy of Sciences of the United States of America*, *100*(14), 8424–8429.

Katti, Alyna; Diaz, Bianca J; Caragine, Christina M; Sanjana, Neville E; Dow, Lukas E (2022): CRISPR in cancer biology and therapy. In: *Nature Reviews*, *22*, 259–279.

Kersten, Kelly; Visser, Karin E; Miltenburg, Martine H; Jonkers, Jos (2017): Genetically engineered mouse models in oncology research and cancer medicine. In: *EMBO Molecular Medicine*, *9*(2), 137–153.

Kim, Michael P; Lozano, Guillermina (2018): Mutant p53 partners in crime. In: *Cell Death and Differentiation*, *25*, 161–168.

Klein, Christian; Planker, Eckart; Diercks, Tammo; Kessler, Horst; Künkele, Klaus Peter; Lang, Kurt et al. (2001): NMR Spectroscopy Reveals the Solution

Dimerization Interface of p53 Core Domains Bound to Their Consensus DNA. In: *Journal of Biological Chemistry*, *276*(52), 49020–49027.

Klimovich, Boris; Merle, Nastasja; Neumann, Michelle; Elmshäuser, Sabrina; Nist, Andrea; Mernberger, Marco et al. (2022): p53 partial loss-of-function mutations sensitize to chemotherapy. In: *Oncogene*, *41*(7), 1011–1023.

Klimovich, Boris; Meyer, Laura; Merle, Nastasja; Neumann, Michelle; König, Alexander M; Ananikidis, Nikolaos et al. (2022): Partial p53 reactivation is sufficient to induce cancer regression. In: *Journal of Experimental and Clinical Cancer Research*, *41*(1).

Klimovich, Boris; Stiewe, Thorsten; Timofeev, Oleg (2019): Inactivation of Mdm2 restores apoptosis proficiency of cooperativity mutant p53 in vivo. In: *Cell Cycle*, *19*(1), 109–123.

Kotler, Eran; Shani, Odem; Goldfeld, Guy; Lotan-Pompan, Maya; Tarcic, Ohad; Gershoni, Anat et al. (2018): A Systematic p53 Mutation Library Links Differential Functional Impact to Cancer Mutation Pattern and Evolutionary Conservation. In: *Molecular Cell*, *71*(1), 178–190.

Kracikova, M; Akiri, G; George, A; Sachidanandam, R; Aaronson, SA (2013): A threshold mechanism mediates p53 cell fate decision between growth arrest and apoptosis. In: *Cell Death and Differentiation*, *20*(4), 576–588.

Kwon, Min chul; Berns, Anton (2013): Mouse models for lung cancer. In: *Molecular Oncology*, Vol. 7, pp. 165–177.

Lane, David (1992): p53, guardian of the genome. In: *Cancer*, *5*, 661–663.

Lee, Eva YHP; Muller, William J (2010): Oncogenes and Tumor Suppressor Genes. In: *Cold Spring Harbor Perspectives in Biology*, *2*.

Leroy, Bernard; Anderson, Martha; Soussi, Thierry (2014): TP53 Mutations in Human Cancer: Database Reassessment and Prospects for the Next Decade. In: *Human Mutation*, *35*, 672–688.

Levine, Arnold J; Oren, Moshe (2009): The first 30 years of p53: growing ever more complex. In: *Nature Reviews*, *9*, 749–758.

Liu, Geng; Parant, John M; Lang, Gene; Chau, Patty; Chavez-Reyes, Arturo; El-Naggar, Adel K et al. (2003): Chromosome stability, in the absence of apoptosis, is critical for suppression of tumorigenesis in Trp53 mutant mice. In: *Nature Genetics*, *36*(1).

Liu, Yao; Li, Xiangyang; He, Siting; Huang, Shuhong; Li, Chao; Chen, Yulin et al. (2020): Efficient generation of mouse models with the prime editing system. In: *Cell Discovery*, *6*(27).

Lozano, Guillermina (2019): Restoring p53 in cancer: the promises and the challenges. In: *Journal of Molecular Cell Biology*, (7), 615–619.

Maddalo, Danilo; Manchado, Eusebio; Concepcion, Carla P; Bonetti, Ciro; Vidigal, Joana A; Han, Yoon Chi et al. (2014): In vivo engineering of oncogenic chromosomal rearrangements with the CRISPR/Cas9 system. In: *Nature*, *516*(7531), 423–428.

Manfredi, James J (2019): p53 defies convention again: a p53 mutant that has lost tumor suppression but still can kill. In: *The EMBO Journal*, *38*(20).

Markova, Svetlana; Larionova, Marina D; Vysotski, Eugene S (2019): Invited Review Shining Light on the Secreted Luciferases of Marine Copepods: Current Knowledge and Applications. In: *Photochemistry and Photobiology*, *95*, 705–721.

Merle, Nastasja; Elmshäuser, Sabrina; Strassheimer, Florian; Wanzel, Michael; König, Alexander M; Funk, Julianne et al. (2022): Monitoring autochthonous lung tumors induced by somatic CRISPR gene editing in mice using a secreted luciferase. In: *Molecular Cancer*, 21, 91

Menendez, Daniel; Inga, Alberto; Resnick, Michael A (2009): The expanding universe of p53 targets. In: *Nature Reviews*, *9*, 724–737.

Muller, Patricia AJ; Vousden, Karen H (2012): p53 mutations in cancer. In: *Nature Cell Biology*, *15*(1).

Muller, Patricia AJ; Vousden, Karen H (2014): Mutant p53 in cancer: new functions and therapeutic opportunities. In: *Cancer Cell*, *25*(3), 304–317.

Olson, Brian; Li, Yadi; Lin, Yu; Liu, Edison T; Patnaik, Akash; Li, Y; Lin, Y (2018): Mouse Models for Cancer Immunotherapy Research. In: *Cancer Discovery*, 1358–1365.

Oser, Matthew G; Sabet, Amin H; Gao, Wenhua; Chakraborty, Abhishek A; Schinzel, Anna C; Jennings, Rebecca B et al. (2019): The KDM5A/RBP2 histone demethylase represses NOTCH signaling to sustain neuroendocrine differentiation and promote small cell lung cancer tumorigenesis. In: *Genes and Development*, *33*, 1718–1738.

Platt, Randall J; Chen, Sidi; Zhou, Yan; Yim, Michael J; Swiech, Lukasz; Kempton, Hannah R et al. (2014): CRISPR-Cas9 knockin mice for genome editing and cancer modeling. In: *Cell*, *159*(2), 440–455.

Purvis, Jeremy E; Karhohs, Kyle W; Mock, Caroline; Batchelor, Eric; Loewer, Alexander; Lahav, Galit (2012): p53 dynamics control cell fate. In: *Science*, *336*(6087), 1440–1444.

Sabapathy, Kanaga; Lane, David P (2018): Therapeutic targeting of p53: All mutants are equal, but some mutants are more equal than others. In: *Nature Reviews Clinical Oncology*, *15*(1), 13–30.

Sánchez-Rivera, Francisco J; Jacks, Tyler (2015): Applications of the CRISPR-Cas9 system in cancer biology. In: *Nature Reviews Cancer*, *15*(7), 387–395.

Schaffer, Bethany E; Park, Kwon-Sik; Yiu, Gloria; Conklin, Jamie F; Lin, Chenwei; Burkhart, Deborah et al. (2010): Loss of p130 Accelerates Tumor Development in a Mouse Model for Human Small-Cell Lung Carcinoma. In: *Cancer Research*, *70*(10), 3877–3883.

Schlereth, Katharina; Beinoraviciute-Kellner, Rasa; Zeitlinger, Marie K; Bretz, Anne C; Sauer, Markus; Charles, Joël P et al. (2010): DNA Binding Cooperativity of p53 Modulates the Decision between Cell-Cycle Arrest and Apoptosis. In: *Molecular Cell*, *38*(3), 356–368.

Schlereth, Katharina; Charles, Joël P; Bretz, Anne C; Stiewe, Thorsten (2010): Life or death p53-induced apoptosis requires DNA binding cooperativity. In: *Cell Cycle*, *929*, 4068–4076.

Schlereth, Katharina; Heyl, Charlotte; Krampitz, Anna Maria; Mernberger, Marco; Finkernagel, Florian; Scharfe, Maren et al. (2013): Characterization of the p53 cistrome-DNA binding cooperativity dissects p53's tumor suppressor functions. In: *PLoS Genetics*, *9*(8).

Stiewe, Thorsten; Haran, Tali E (2018): How mutations shape p53 interactions with the genome to promote tumorigenesis and drug resistance. *Drug Resistance Updates*, *38*, 27–43.

Sullivan, Kelly D; Galbraith, Matthew D; Andrysik, Zdenek; Espinosa, Joaquin M (2018): Mechanisms of transcriptional regulation by p53. In: *Cell Death and Differentiation*, *25*, 133–143.

Tannous, Bakhos A (2009): Gaussia luciferase reporter assay for monitoring biological processes in culture and in vivo. In: *Nature Protocols*, *4*(4), 582–591.

Timofeev, Oleg; Klimovich, Boris; Schneikert, Jean; Wanzel, Michael; Pavlakis, Evangelos; Noll, Julia et al. (2019): Residual apoptotic activity of a tumorigenic p53 mutant improves cancer therapy responses. In: *The EMBO Journal*, *38*(20).

Timofeev, Oleg; Schlereth, Katharina; Wanzel, Michael; Braun, Attila; Nieswandt, Bernhard; Pagenstecher, Axel et al. (2013): p53 DNA binding cooperativity is essential for apoptosis and tumor suppression in vivo. In: *Cell Reports*, *3*(5), 1512–1525.

Timofeev, Oleg; Stiewe, Thorsten; Yamaguchi, Masayoshi (2021): Rely on Each Other: DNA Binding Cooperativity Shapes p53 Functions in Tumor Suppression and Cancer Therapy. In: *Cancers*, *13*(2422).

van der Weyden, Louise; Jonkers, Jos; Adams, David J (2021): The use of CRISPR/Cas9-based gene editing strategies to explore cancer gene function in mice. In: *Current Opinion in Genetics and Development*, *66*, 57–62.

Ventura, Andrea; Kirsch, David G; McLaughlin, Margaret E; Tuveson, David A; Grimm, Jan; Lintault, Laura et al. (2007): Restoration of p53 function leads to tumour regression in vivo. In: *Nature*, *445*(7128), 661–665.

Vogiatzi, Fotini; Brandt, Dominique T; Schneikert, Jean; Fuchs, Jeannette; Grikscheit, Katharina; Wanzel, Michael et al. (2016): Mutant p53 promotes tumor progression and metastasis by the endoplasmic reticulum UDPase ENTPD5. In: *Proceedings of the National Academy of Sciences*, 8433–8441.

Wang, Yongxing; Suh, Young-Ah; Fuller, Maren Y; Jackson, James G; Xiong, Shunbin; Terzian, Tamara et al. (2011): Restoring expression of wild-type p53 suppresses tumor growth but does not cause tumor regression in mice with a p53 missense mutation. In: *The Journal of Clinical Investigation*, *121*, 893.

Wang, Yuchuan; Tseng, Jen-Chieh; Sun, Yanping; Beck, Andrew H; Kung, Andrew L (2015): Noninvasive Imaging of Tumor Burden and Molecular Pathways in Mouse Models of Cancer. In: *Cold Spring Harbor Laboratory Press*, 135–144.

Wanzel, Michael; Vischedyk, Jonas B; Gittler, Miriam P; Gremke, Niklas; Seiz, Julia R; Hefter, Mirjam et al. (2016): CRISPR-Cas9-based target validation for p53-reactivating model compounds. In: *Nature Chemical Biology*, *12*.

Weber, Julia; Rad, Roland (2019): Engineering CRISPR mouse models of cancer. In: *Current Opinion in Genetics and Development*, *54*, 88–96.

Weinberg, Richard L; Veprintsev, Dmitry B; Fersht, Alan R (2004): Cooperative binding of tetrameric p53 to DNA. In: *Journal of Molecular Biology*, *341*(5), 1145–1159.

Wurdinger, Thomas; Badr, Christian; Pike, Lisa; de Kleine, Ruben; Weissleder, Ralph; Breakefield, Xandra O; Tannous, Bakhos A (2008): A secreted luciferase for ex vivo monitoring of in vivo processes. In: *Nature Methods*, *5*(2), 171–173.

Xu, Xiaoshu; Chemparathy, Augustine; Zeng, Leiping; Kempton, Hannah R; Shang, Stephen; Nakamura, Muneaki; Qi, Lei S (2021): Engineered miniature CRISPR-Cas system for mammalian genome regulation and editing. In: *Molecular Cell*, *81*(20), 4333–4345.

Xue, Wen; Zender, Lars; Miething, Cornelius; Dickins, Ross A; Hernando, Eva; Krizhanovsky, Valery et al. (2007): Senescence and tumour clearance is triggered by p53 restoration in murine liver carcinomas. In: *Nature*, *445*, 656–660.

7. Appendix

List of abbreviations

AML	Acute myeloid leukemia
APC	Adenomatous polyposis coli protein
AV	Adenovirus
BE	Base Editing
BLI	Bioluminescence Imaging
CBE	Cytosine Base Editing
CRISPR	Clustered Regularly Interspaced Short Palindromic Repeats
CT	Computed Tomography
DNA	Desoxyribonucleic acid
GEMM	Genetically engineered mouse model
GLuc	Gaussia Luciferase
GOF	Gain-of-function
IHC	Immunohistochemistry
InDel	Insertion/Deletion
KO	Knockout
LOF	Loss-of-function
LSL-GLuc	lox-Stop-lox-GLuc
MRI	Magnetic Resonance Imaging
NGS	Next Generation Sequencing
pegRNA	prime-editing RNA
pLOF	partial loss-of-function
PDAC	Pancreatic ductal adenocarcinoma
PET	Positron Emission Tomography
Pten	Phosphatase and Tensin Homolog
RB1	Retinoblastoma protein 1
RNA	Ribonucleic acid
SCLC	Small cell lung cancer
sgRNA	short guide RNA
TME	Tumor microenvironment
WT	Wildtype

Curriculum Vitae

[removed for final print]

List of academic teachers

My academic teachers at the Philipps University in Marburg were:

Batschauer, Baumeister, Bolte, Borchers, Bölker, Brandl, Brändle, Bremer, Buttgereit, Dahlke, Essen, Exner, Feuser, Galland, Grolig, Hassel, Heider, Homberg, Imhof, Kostron, Lingelbach, Linklater, Lohöfer, Maier, Moog, Mösch, Önel, Pokorny, Przyborski, Pütz-Rathke, Rath, Renkawitz-Pohl, Schallenberg-Rüdinger, Schneider, Stiewe, Thanbichler, Ullrich, Zauner.

Acknowledgments

First and foremost, I would like to express my gratitude to Prof. Dr. Thorsten Stiewe for giving me the opportunity to work on this exciting project. Thank you for your guidance, advice, and trust throughout the years!

Sabi(-Wan), this would not have been possible without you! I am infinitely grateful to you for not only teaching me how to work with experimental animals and everything related to them, but also for your introduction to the Star Wars universe. Thank you for becoming a friend, for never getting tired of my endless questions, and for sharing countless cat photos with me.

I would like to thank all members from the Stiewe lab for the pleasant working atmosphere and the technical and scientific advice at any time:

Miri and Siggi for your organizational help and for always having an open ear no matter what. Siggi, thank you for your commitment to all the IHC and for always being there for me! Oleg, thank you for sharing your expertise on mouse experiments. Special thanks to Andrea, Geli, Alex, Marco, and Katharina for helping with the NGS preparations and analysis! Andrea, thank you for sharing your knowledge about SCLC cell culture. Björn for your tireless support with cloning. Thanks to Imke for being the best student ever and extending this project to base editing. I'm excited for what's to come! Many thanks to Michelle, Katharina, Julia, Jan, Michael, Niklas, Amir, Evangelos, and all former and current MD, Master, and Bachelor students for the warm and pleasant working atmosphere in the lab.

I would also like to thank other members of the University for their support:

Janine, Jarmila and Dr. Alexander König for MRI imaging and analysis of our mice. My special thanks go to all employees of the Animal Facility, especially Julia, Tanja, Katja and Sandra for their excellent care of experimental animals. I want to thank the Core Facility Mouse Pathology, Dr. Frederik Helmprobst and Prof. Dr. Axel Pagenstecher for their collaboration and dedicated work on IHC stainings and analysis.

I am very grateful to all former members of the Stiewe group for their help and support during my first years: Boris, Pier, Maria, Joël, Berni, Angela, Ronja and Laura.

Michelle, Katharina, Julia, and Jan: Thank you not only for the countless scientific discussions but also for the emotional support, frozen yogurts, endless coffee breaks and - most importantly - your friendship! Michelle, thank you for becoming a safe space for me to share good and bad times with you.

Finally, I owe my deepest gratitude to my parents and especially to my dear Max, who have always been supporting me in every aspect of life. Thank you!

Ehrenwörtliche Erklärung

[removed for final print]

Publications

ARTICLE OPEN

Check for updates

p53 partial loss-of-function mutations sensitize to chemotherapy

Boris Klimovich[1,4], Nastasja Merle[1,4], Michelle Neumann[1], Sabrina Elmshäuser[1], Andrea Nist[2], Marco Mernberger[1], Daniel Kazdal[3], Albrecht Stenzinger[3], Oleg Timofeev[1✉] and Thorsten Stiewe[1,2✉]

The tumor suppressive transcription factor p53 is frequently inactivated in cancer cells by missense mutations that cluster in the DNA binding domain. 30% hit mutational hotspot residues, resulting in a complete loss of transcriptional activity and mutant p53-driven chemotherapy resistance. Of the remaining 70% of non-hotspot mutants, many are partial loss-of-function (partial-LOF) mutants with residual transcriptional activity. The therapeutic consequences of a partial-LOF have remained largely elusive. Using a p53 mutation engineered to reduce DNA binding, we demonstrate that partial-LOF is sufficient to enhance oncogene-driven tumorigenesis in mouse models of lung and pancreatic ductal adenocarcinoma and acute myeloid leukemia. Interestingly, mouse and human tumors with partial-LOF mutations showed mutant p53 protein accumulation similar as known for hotspot mutants. Different from the chemotherapy resistance caused by p53-loss, the partial-LOF mutant sensitized to an apoptotic chemotherapy response and led to a survival benefit. Mechanistically, the pro-apoptotic transcriptional activity of mouse and human partial-LOF mutants was rescued at high mutant protein levels, suggesting that accumulation of partial-LOF mutants enables the observed apoptotic chemotherapy response. p53 non-hotspot mutants with partial-LOF, therefore, represent tumorigenic p53 mutations that need to be distinguished from other mutations because of their beneficial impact on survival in a therapy context.

Oncogene; https://doi.org/10.1038/s41388-021-02141-5

INTRODUCTION

The tumor suppressor gene *TP53* is mutated in roughly half of all cancer patients [1]. In contrast to other tumor suppressor genes, *TP53* mutations are most often missense mutations giving rise to mutant proteins which accumulate in tumor cells to high levels. The *TP53* gene product p53 responds to various types of cellular stress, DNA damage being the most prominent, and functions as a transcription factor that binds DNA in a sequence-specific manner to regulate a host of transcriptional programs, any or all of which can contribute to suppressing tumorigenesis [2]. Reflecting the functional importance of p53 DNA binding for tumor suppression, missense mutations cluster in the exons encoding the DNA binding domain (DBD). Overall, more than 2000 different missense variants have been reported in cancer cells and yield a complex mutation spectrum [1, 3].

Some codons like R175, R248 and R273 are more frequently mutated than others and the top 10 'hotspot' mutations together account for ~30% of all missense mutations. The hotspot mutations are structurally well-characterized and subdivided into 'contact' mutations, which remove essential DNA-contact residues, and 'structural' mutations affecting residues that are critical for the overall architecture of the DNA binding protein surface [4]. Studies in cell culture and knock-in mouse models have yielded a thorough mechanistic understanding of the functional impact of hotspot mutations, which have largely lost the tumor suppressive activity of the wild-type proteins (LOF, loss-of-function) and, by oligomerization, exert additional dominant-negative activity towards wild-type p53 expressed from a remaining non-mutated allele [5]. Moreover, several hotspot mutants have acquired neomorphic properties (also termed gain-of-function, GOF) that, in an oncogene-like fashion, actively promote tumor progression to a more aggressive and therapy-resistant state [6–8]. These properties of mutant p53 proteins help to explain the preference for missense over null mutations and the poor prognosis associated with p53 mutations in several cancer types [9].

Importantly, our current knowledge on mutant p53 is mostly based on studies of hotspot mutants. The functional consequences of non-hotspot mutants, that comprise the majority (~70%) of all patients with *TP53* missense mutations, are still poorly understood. A landmark study that systematically profiled the transcriptional activity of 2314 p53 variants in a yeast-based reporter assay revealed substantial differences in transactivation [10]. Loss of transactivation correlated with mutant frequency supporting a selection bias for loss-of-transactivation mutants during cancer development. In other words, while hotspot mutants completely lack transcriptional activity, the less frequent non-hotspot mutants tend to retain

[1]Institute of Molecular Oncology, Universities of Giessen and Marburg Lung Center (UGMLC), Member of the German Center for Lung Research (DZL), Philipps-University, Marburg, Germany. [2]Genomics Core Facility, Philipps-University, Marburg, Germany. [3]Institute of Pathology, Heidelberg University Hospital, Translational Lung Research Center Heidelberg (TLRC-H), Member of the German Center for Lung Research (DZL), Heidelberg, Germany. [4]These authors contributed equally: Boris Klimovich, Nastasja Merle.

Received: 9 June 2021 Revised: 19 November 2021 Accepted: 26 November 2021
Published online: 14 December 2021

residual activity which was independently confirmed for a set of selected mutants in yeast and mammalian cells [11, 12]. In line, more recent systematic screens based on mutant p53 cDNA expression in human tumor cell lines have observed highly heterogenous antiproliferative activity among thousands of p53 variants [13, 14]. The loss of antiproliferative activity was more pronounced for hotspot than non-hotspot mutants, confirming that non-hotspot variants are often only partial loss-of-function (partial-LOF) variants. Of note, mice carrying a hypomorphic p53 allele or the murine partial-LOF variant R172P (corresponding to human R175P) succumb prematurely to cancer proving that partial-LOF mutations are pathogenic despite their residual tumor suppressive activity [15, 16]. However, the extent of cancer susceptibility is strongly context-dependent. For example, the murine R172P mutant is apoptosis-deficient and fails to prevent tumorigenesis in a mouse model of *Myc*-driven B-cell lymphomagenesis [17], where p53 is known to limit tumorigenesis primarily by means of apoptosis [18]. In contrast, R172P efficiently suppresses $Kras^{G12D}$-triggered development of pancreatic ductal adenocarcinoma (PDAC) through its residual senescence-inducing activity [19]. Together these findings suggest that partial-LOF and LOF mutants promote the development of different tumor types so that partial-LOF mutations should be more frequent in, for example, Burkitt lymphoma with chromosomal *Myc*-translocations than in *Kras*-driven PDAC. However, this hypothesis is challenged by a similar overall frequency of p53 partial-LOF mutations in different cancer types [20].

Mutations at R175 (mouse R172) affect zinc coordination in the DBD, but our structural understanding of the partial-LOF associated with R175P versus a complete LOF in R175H remains still incomplete [21]. Mechanistically better understood are non-hotspot mutations affecting the DBD surface residues E180 and R181 (mouse E177 and R178). These residues form an intermolecular salt-bridge which stabilizes the DNA-bound tetramer and enables p53 DBDs to bind response elements in a cooperative manner [20, 22–26]. Several mutations of these residues have been described as somatic or germline variants in ~0.5% of tumors with frequencies of individual variants up to 0.114% in the case of R181C [1, 3, 20]. Based on the world-wide cancer incidence, all E180/R181 mutations together account for an estimated number of 34,000 cancer patients per year [20]. The distribution of these cooperativity mutations across different tumor types is similar as for hotspot mutations and other frequent p53 mutations supporting a comparable causal role as drivers of tumorigenesis [20]. The charge-inverting E180R mutation is not a single-nucleotide variant and has therefore not been found in cancer patients so far, but it is mechanistically characterized better than any other cooperativity mutant regarding protein structure, cooperative DNA binding, and target gene activation [23, 27, 28]. In addition, the murine equivalent E177R is available as a knock-in mouse for in vivo studies [29, 30]. E177R mice show a preferential defect in apoptosis induction resulting in increased susceptibility to sporadic and Myc-driven lymphomagenesis [30, 31]. Moreover, the E177R mutant phenotype is explained entirely by a lack of DNA binding cooperativity as it is fully rescued in vitro and in vivo by complementation with the human R181E (mouse R178E) mutant [23, 27, 28, 32].

Here we have used the E177R mutant knock-in mouse along with a panel of cancer patient-derived cooperativity mutants to explore the role of a partial LOF in tumorigenesis and cancer therapy. We demonstrate that a p53 partial-LOF cooperates with oncogenes to drive tumorigenesis in multiple tissues. Most interestingly, we found that the residual transcriptional activity of partial-LOF mutants is retained in tumors and can be therapeutically boosted to provide a beneficial therapy outcome, superior to LOF mutations.

RESULTS

Non-hotspot mutations are enriched for partial loss-of-function variants

We extracted from the UMD *TP53* mutation database (https://p53.fr/tp53-database) a total of 1209 *TP53* missense mutations, that were identified in patient tumor samples at least once and map to the DNA binding domain (aa100-300), along with their transcriptional activity as measured in a yeast-based reporter assay using response elements (REs) of 8 prototypical p53 target genes [10]. We defined a loss of transcriptional activity (loss-of-function, LOF) as less than 10% residual activity and partial loss-of-function (partial-LOF) with low (10–20%) or high (20-50%) residual activity. When plotting the transcriptional activity of mutants sorted by their frequency in the set of tumor samples, we noted the characteristic enrichment of LOF variants in the mutants with a high frequency of >0.05% (Fig. 1A and B). Importantly, we also observed an unexpectedly high number of partial-LOF variants with low or high residual transcriptional activity in the various mutant frequency groups (Fig. 1A and B). In particular, mutants with medium abundance in cancer patients often display partial-LOF. While the median transcriptional activity of hotspots mutants was strongly reduced to 2.59% of the wild-type, the other frequency classes show substantially higher median residual activity ranging between 8.23% for very frequent mutants and 78.2% for unique variants (Fig. 1B). This was observed for the calculated median transcriptional activity (Fig. 1B), but also for the transcriptional activity at all individual tested REs (Supplementary Fig. S1A). The same trend is observed when analyzing the relative fitness score (RFS) of variants which reflects their loss of antiproliferative activity and was measured upon enforced expression in p53-null H1299 cells [13]. Again, many of the mutants with medium abundance in the cancer population often show an intermediate RFS ($-2<RFS<0$) indicative of residual antiproliferative activity (Supplementary Fig. S1B). Supporting the idea that partial-LOF mutants are driver mutations rather than neutral bystanders or sequencing artefacts, mutations in all the different frequency groups are marked as damaging in the UMD p53 mutation database based on several pathogenicity prediction algorithms such as SIFT, MutAssessor and PROVEAN (Fig. 1A, right panel).

When assessing transcriptional activity on the basis of individual patient tumors – not p53 variants – the distribution is similar, revealing a large proportion of *TP53* mutant malignancies (both solid and hematological) with an intermediate p53 mutant transcriptional activity (Fig. 1C and D; Supplementary Fig. S1C and D). A total of 31.6% of variants and 27.6% of tumors with *TP53* missense mutations fall within the partial-LOF activity range (Fig. 1D). When excluding the top 10 hotspot mutants, the percentage of non-hotspot tumors harboring a partial-LOF mutant increases to 36.8% (Fig. 1D). In summary, p53 mutants with residual transcriptional activity, i.e., partial-LOF, are common in p53-mutated tumors and particularly prevalent among non-hotspot mutants.

p53 cooperativity mutations as a model for partial-LOF mutations

To better explore the in vivo consequences of *TP53* partial-LOF mutations, we focused on the mechanistically well-studied subclass of cooperativity mutations (labelled orange in Fig. 1A). They commonly reduce DNA binding and show a median transcriptional activity of 47.5% (13.7-67.4%) in the yeast-based reporter assay (Figs. 1B and D), classifying them as non-hotspot mutants with partial-LOF. Given that yeast are lacking p53-relevant transcriptional components and properties present in humans, we aimed to further characterize the transcriptional activity of cooperativity mutants in a more physiological system. For this, we expressed the cancer patient-derived mutants E180K, R181L, R181H, R181C, R181P, and the engineered mutant E180R in

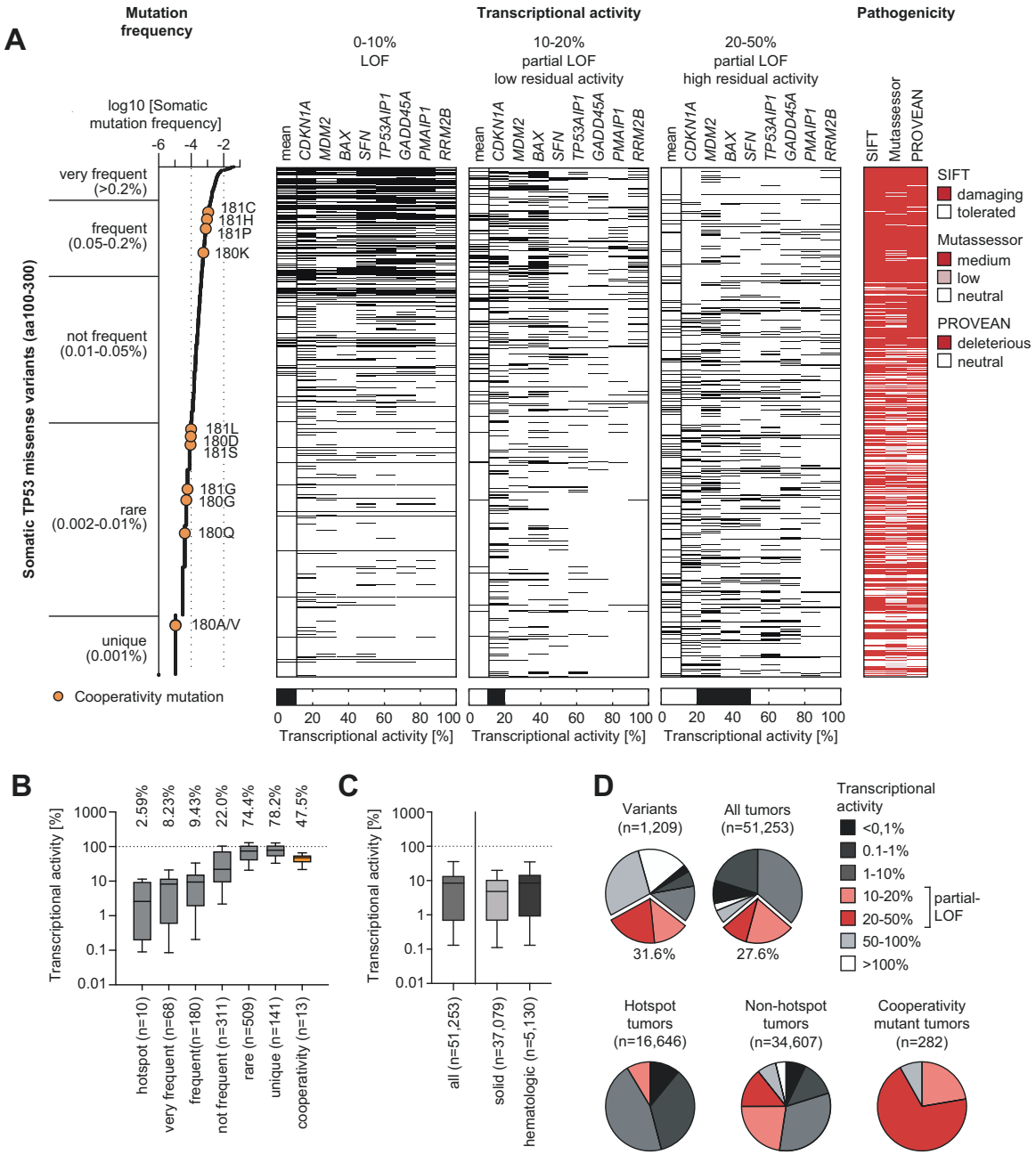

Fig. 1 Prevalence of p53 partial-LOF mutations in human cancer patients. A Frequency, transcriptional activity, and in silico predicted pathogenicity of 1,209 somatic *TP53* missense mutations affecting the p53 DNA binding domain (amino acids 100–300). Three black-white heatmaps depict the mean and response element-specific transcriptional activity of missense variants. The left heatmap illustrates the distribution of loss-of-function (LOF) events (0-10% transcriptional activity), the middle heatmap partial LOF events with low (10–20%) residual activity and the right heatmap partial LOF events with high (20-50%) residual activity. The pathogenicity plot shows variants predicted to be damaging by SIFT, Mutassessor or PROVEAN in red. All data were extracted from the UMD *TP53* mutation database (http://p53.fr/tp53-database). Transcriptional activity data were determined in a yeast-based reporter assay [10]. Cooperativity mutations at residues E180 and R181 are highlighted in orange. **B** Non-hotspot *TP53* missense mutants retain substantial transcriptional activity. Shown is the range of transcriptional activity for somatic *TP53* mutations grouped according to mutation frequency in cancer patients. Cooperativity mutations are highlighted separately in orange. **C**, **D** Range and distribution of transcriptional activity in p53 mutant cancer patients. In all box plots, boxes indicate median and interquartile range, whiskers the 10–90 percentile. Pie charts depict the percentage of variants (or tumors) falling into different categories of transcriptional activity as indicated. 31.6% of p53 variants and 27.6% of tumors with p53 missense mutations fall into the partial-LOF category defined by a residual transcriptional activity of 10–50%.

comparison to WT, the R175H hotspot mutant, and GFP as a negative control in p53-deficient Saos-2 osteosarcoma cells. Transcriptome analysis by RNA-seq revealed more genes to be activated by WT than repressed (Fig. 2A), in line with p53 being primarily a transactivator [33]. Compared to WT, all cooperativity mutants showed a strongly reduced regulation of target genes, but individual mutants differed substantially forming a continuum of residual activity (Fig. 2A). R181L, E180R, and R181H showed the highest residual activity, whereas R181P – consistent with proline functioning as a helix breaker – displayed a complete LOF indistinguishable from R175H and GFP (Fig. 2A-E). Consistent with distinct degrees of LOF, functional annotation analysis revealed a

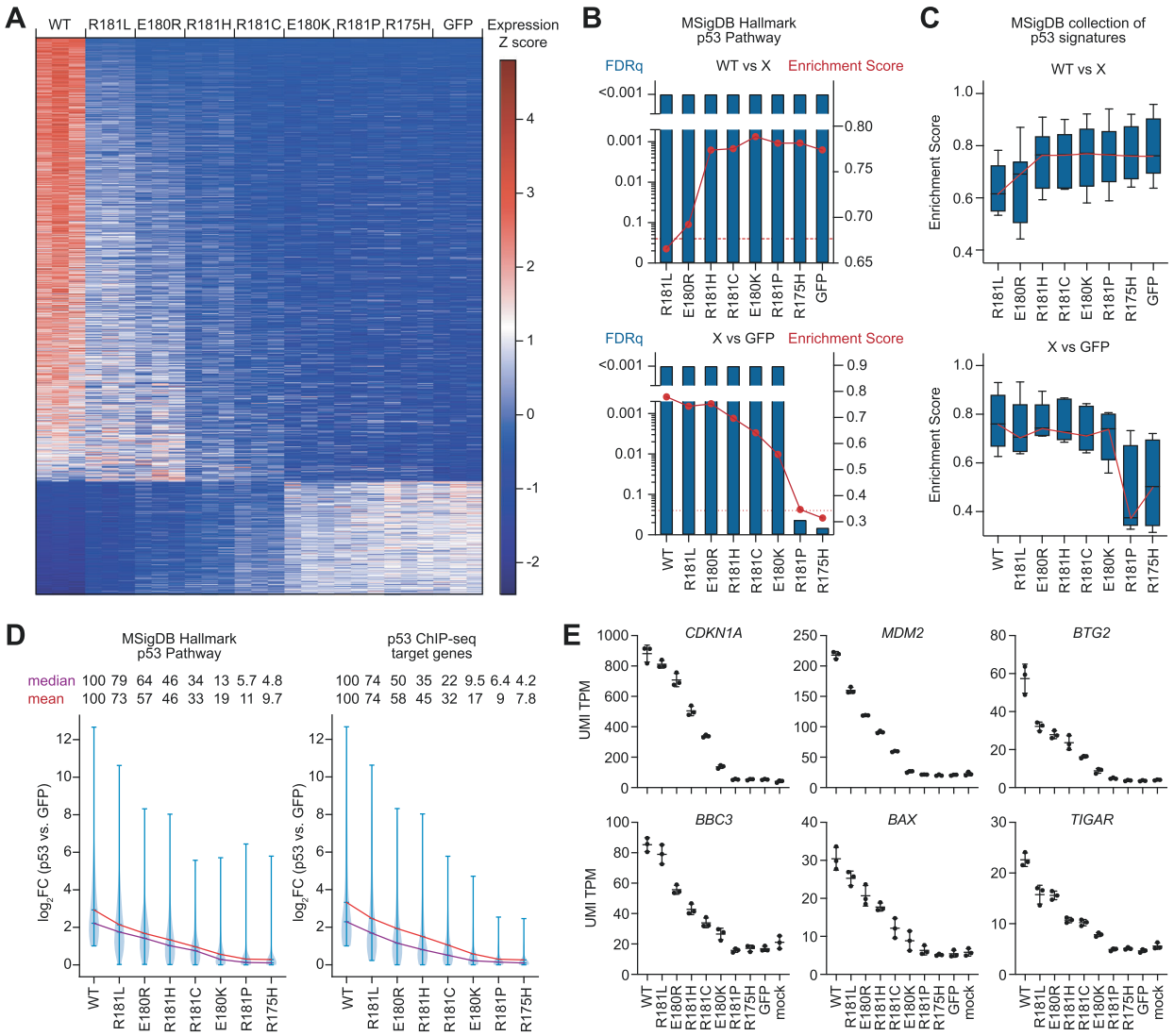

Fig. 2 Partial loss of transcriptional activity in p53 cooperativity mutations. A Heat-map shows z-transformed RNA expression values (FPKM) for 1592 differentially expressed genes (mean $\log_2$FC ≥ 1, corrected p-value ≤ 0.05) detected by RNAseq in p53-null Saos-2 cells transduced with wild-type p53, indicated p53 missense mutants or GFP as negative control. $n = 3$ for each genotype. **B** RNAseq data from **A** were used for gene set enrichment analysis (GSEA). Depicted are the false discovery rate (FDRq, blue bars) and enrichment score (red curve) for the MSigDB Hallmark p53 Pathway gene set in pairwise comparisons between cells expressing wild-type p53 and different mutants (X) (upper panel) or all variants (X) vs. GFP-transfected (p53-null) cells (lower panel). **C** Depicted is the distribution of enrichment scores of multiple p53-related signatures of the MSigDB collection (Table S1) in pairwise comparisons like in **B**. **D** Expression of p53-target genes in WT- or mutant p53-transfected cells relative to GFP-transfected (p53-null) cells. Violin plots show the distribution of $\log_2$FC values for genes belonging to the MSigDB Hallmark p53 Pathway gene set (left panel) and a gene set obtained from p53 ChIP-seq (right panel, Table S1). Red and purple lines indicate mean and median $\log_2$FC, respectively. **E** Expression of prototypical p53 target genes obtained from **A**. UMI TPM, unique molecular identifier tags per million. Shown is the mean±SD of $n = 3$ biological replicates.

varying enrichment of p53-related expression signatures such as the Hallmark p53 pathway gene set from the Molecular Signatures Database (MSigDB) in WT transcriptomes when compared to each one of the mutants (Fig. 2B and C, Supplementary Table 1). Importantly, p53-related gene sets were also significantly enriched in R181L, E180R, R181H, R181C, and E180K mutant transcriptomes compared to the GFP control, highlighting their residual transcriptional activity, i.e. their partial-LOF phenotype (Fig. 2B and C). In detail, partial-LOF cooperativity mutants displayed 5–79% residual transactivation of genes belonging to the Hallmark p53 pathway set or genes that were found to be directly bound and regulated by WT in Saos-2 cells (Fig. 2D). These findings were confirmed for the prototypical p53 target genes *CDKN1A* (p21), *MDM2*, *BTG2*, *BBC3* (Puma), *BAX,* and *TIGAR* (Fig. 2E).

Of note, the ability of cooperativity mutants to repress genes mirrored their transactivation potential (Fig. 2A). Gene set enrichment analysis indicated these repressed genes to be significantly enriched for E2F and Myc target genes sets related to cell proliferation (Supplementary Fig. 2, Supplementary Table 1). Similar as seen above for transactivated gene sets, these repressed gene sets were enriched in the WT transcriptome compared to most of the mutants and enriched in R181L, E180R, R181H, R181C, and E180K compared to the GFP control attesting to their partial-LOF with respect to gene repression. Although p53 can function as a direct transrepressor [34], the majority of cell proliferation genes are known to be repressed indirectly through p53-mediated transactivation of the p21-DREAM pathway [33]. The impaired target gene repression by partial-LOF mutants is

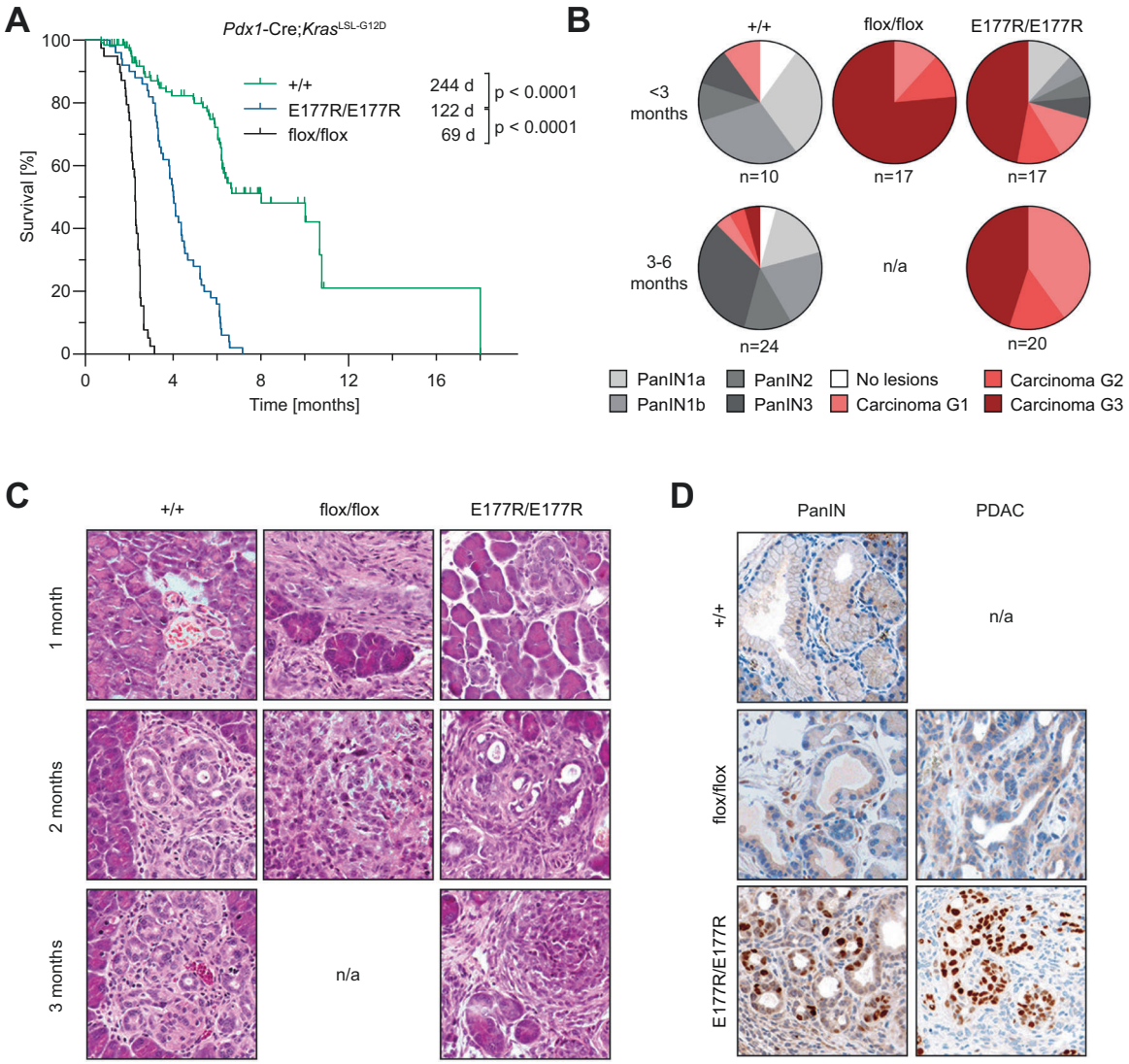

Fig. 3 Trp53E177R mutant in Ras-driven PDAC. A Kaplan-Meier curves show overall survival of mice with indicated p53 genotypes and pancreas-specific expression of oncogenic mutant *Kras*^{G12D}. *Trp53*$^{+/+}$ $n = 45$, *Trp53*$^{E177R/E177R}$ $n = 50$, *Trp53*$^{flox/flox}$ $n = 39$, log-rank Mantel-Cox test. **B** Pie charts show percentage of mice with (pre)neoplastic pancreas lesions (highest grade that was detected in each sample). Samples were collected at different time-points from animals as in **A**. PanIN, pancreatic intraepithelial neoplasia. n/a, no sample available for analysis as all *Trp53*$^{flox/flox}$ mice were dead by 3 months of age. **C** Representative micrographs of pancreas samples from **B**, hematoxylin and eosin (H&E) staining. **D** Immunochemical staining of p53 in representative PanIN (left) and PDAC samples (right).

therefore most likely a consequence of their reduced transactivation potential.

In all these analyses, the E180R mutant integrated into the continuum of transcriptional activities displaying a level of residual activity in between the cancer-derived mutants R181L and R181H, which validates the E180R (mouse E177R) cooperativity mutant as a suitable model for non-hotspot mutants with partial-LOF.

p53 partial loss-of-function cooperates with Ras oncogenes in tumorigenesis

Previous work has demonstrated an increased susceptibility of mice with the R172P and E177R partial-LOF mutations to both sporadic and Myc-driven lymphoma [17, 30]. In light of reports that R172P-triggered senescence prevents *Kras*^{G12D}-induced pancreatic ductal adenocarcinoma (PDAC) [19], we also analyzed the E177R cooperativity mutant in this model. We noted that E177R extended the median survival from 69 days in p53$^{flox/flox}$ mice to 122 days indicative of tumor-suppressive activity. However, p53$^{+/+}$ animals survived twice as long (Fig. 3A). All E177R mice succumbed to PDAC within half a year and almost half showed high-grade PDAC by less than 3 months of age when the majority of p53$^{+/+}$ only showed high-grade PanIN lesions which only rarely progressed to PDAC later on (Fig. 3B and C). Similar to R172H-mutant PDAC [19], both PanIN and PDAC lesions in E177R mice showed strong nuclear p53 staining, indicating that PDAC formation is not necessarily driven by the loss of p53 and is, in fact, compatible with sustained high-level expression of E177R (Fig. 3D). We conclude that E177R – different from R172P – delays, but fails to completely suppress PDAC development.

To study tumor suppression by E177R in a different Kras-driven tumor type, we extended our studies with E177R mice and crossed them to *Kras*^{LA1} mice which develop lung tumors due to spontaneous activation of a latent oncogenic *Kras*^{G12D} allele [35]. In the presence of wild-type p53 these mice develop multiple adenomas that only rarely progress to carcinomas, whereas hetero- or homoallelic inactivation of the *Trp53* gene leads to the early development of adenocarcinomas with 100% penetrance [35]. When comparing cohorts of *Kras*^{LA1} mice with

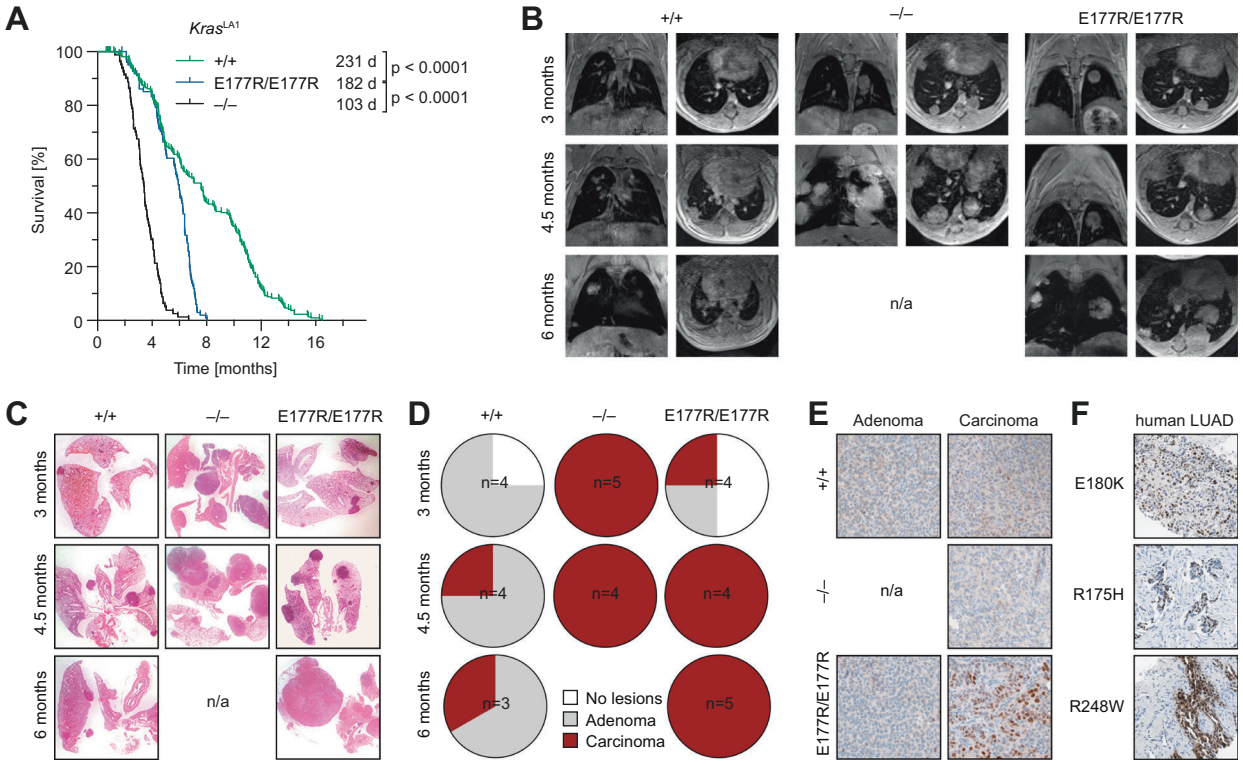

Fig. 4 Trp53E177R mutant in Ras-driven lung cancer. A Kaplan-Meier curves show the overall survival of *Kras*^{LA1} mice with indicated p53 genotypes. *Trp53*$^{+/+}$ $n = 228$, *Trp53*$^{E177R/E177R}$ $n = 105$, *Trp53*$^{-/-}$ $n = 80$, log-rank Mantel-Cox test. **B** A group of mice from **A** was monitored for lung tumorigenesis by MRI tomography. Representative MRI images collected at indicated time-points are shown. n/a, no mice available for analysis, as all *Trp53*$^{-/-}$ mice were dead by 6 months of age. **C**–**E** Lung samples were collected at different time-points from *Kras*^{LA1} mice with indicated p53 genotypes. **C** Representative micrographs, H&E staining. **D** Pie charts show percentage of mice with tumors (highest grade). **E** Immunochemical staining of p53 in representative lung adenoma (left panel) and carcinoma samples (right). **F** IHC detection of mutant p53 protein in human lung adenocarcinomas (LUAD) with indicated hotspot (R175H, R248W) and non-hotspot (E180K) *TP53* mutations.

different p53 genotype, we observed a significantly reduced lifespan in E177R compared to p53$^{+/+}$ mice (Fig. 4A). Similar as observed in the PDAC model, survival of E177R mice was significantly longer in comparison to p53-null animals, indicating that residual tumor suppression by E177R slowed down *Kras*-driven tumorigenesis (Fig. 4A).

Of note, many p53-null mice with lung tumors were also burdened with thymic lymphoma, the most common tumor arising spontaneously upon loss of p53 [36]. To exclude a confounding effect on survival, we monitored lung tumor growth longitudinally with magnetic resonance imaging and analyzed lung tissues histologically at different time points (Fig. 4B–D). We observed early appearance and fast progression of adenocarcinomas in p53-deficient *Kras*^{LA1} animals, none of which reached the last time point because of the high tumor burden. In contrast, in p53 wild-type mice lung tumors were barely detectable at 3 months of age and had advanced only slowly at later time points mostly retaining a benign adenoma morphology. MRI showed presence of tumors in 2 of 4 E177R mice at 3 months, and in all animals at 4.5 months, but tumor progression was slower than in p53 knockouts. Histologically, E177R mice showed an intermediate morphology with examples of both adenoma and carcinoma at 3 months that progressed to mostly adenocarcinomas at later time points. We conclude that the residual activity of E177R provided a temporary defense against oncogenic *Kras* early during tumorigenesis, but its tumor-suppressive potential was insufficient to block progression to more malignant tumor stages.

Similar as in PDAC samples, immunohistochemical analysis showed accumulation of the E177R protein in advanced adenocarcinomas, but not in adenomas (Fig. 4E). Of note, a human lung adenocarcinoma with the E180K mutation showed strongly positive p53 immunostaining indistinguishable from hotspot mutants, confirming aberrant stabilization of a partial-LOF mutant also for human cancer tissues (Fig. 4F).

p53 partial loss-of-function cooperates with Ras in leukemogenesis

Having demonstrated efficient cooperation of the E177R partial-LOF mutation with oncogenic Ras in two solid tumor models, we next explored this cooperation in a model of acute myeloid leukemia (AML), which is driven by the combination of *Nras*^{G12D} and *AML1/ETO9a* oncogenes and in which p53 is known to be tumor suppressive [37]. As hematopoietic bone marrow cells are in general more vulnerable to p53 activity than other cells [38–41], we speculated that E177R might be more tumor suppressive in leukemia than in solid tumors. We isolated hematopoietic fetal liver stem cells from p53$^{+/+}$, p53$^{-/-}$ and homozygous E177R embryos and transduced cells with two bicistronic retroviral constructs – one expressing *Nras*^{G12D} and firefly luciferase, the second *AML1/ETO9a* and EGFP, which allowed disease monitoring (Fig. 5A). Five independent batches of transduced hematopoietic cells of each genotype were transplanted into 5-8 lethally irradiated recipients. Consistent with published data [37], loss of p53 dramatically accelerated AML development (median survival 49 vs. 103 days, $P < 0.0001$). Mice transplanted with oncogene-transduced E177R fetal liver cells demonstrated an intermediate survival of 74 days which differed significantly from both p53$^{+/+}$ and p53$^{-/-}$ AML ($P = 0.0008$ and $P = 0.0004$, respectively) (Fig. 5B). As p53 is induced by oncogenes via Cdkn2a/p19ARF [42], we analyzed p19ARF in established AML samples. Immunohistochemistry revealed low levels of Cdkn2a/p19ARF and p53 in wild-type AML, indicating strong selection pressure against an intact

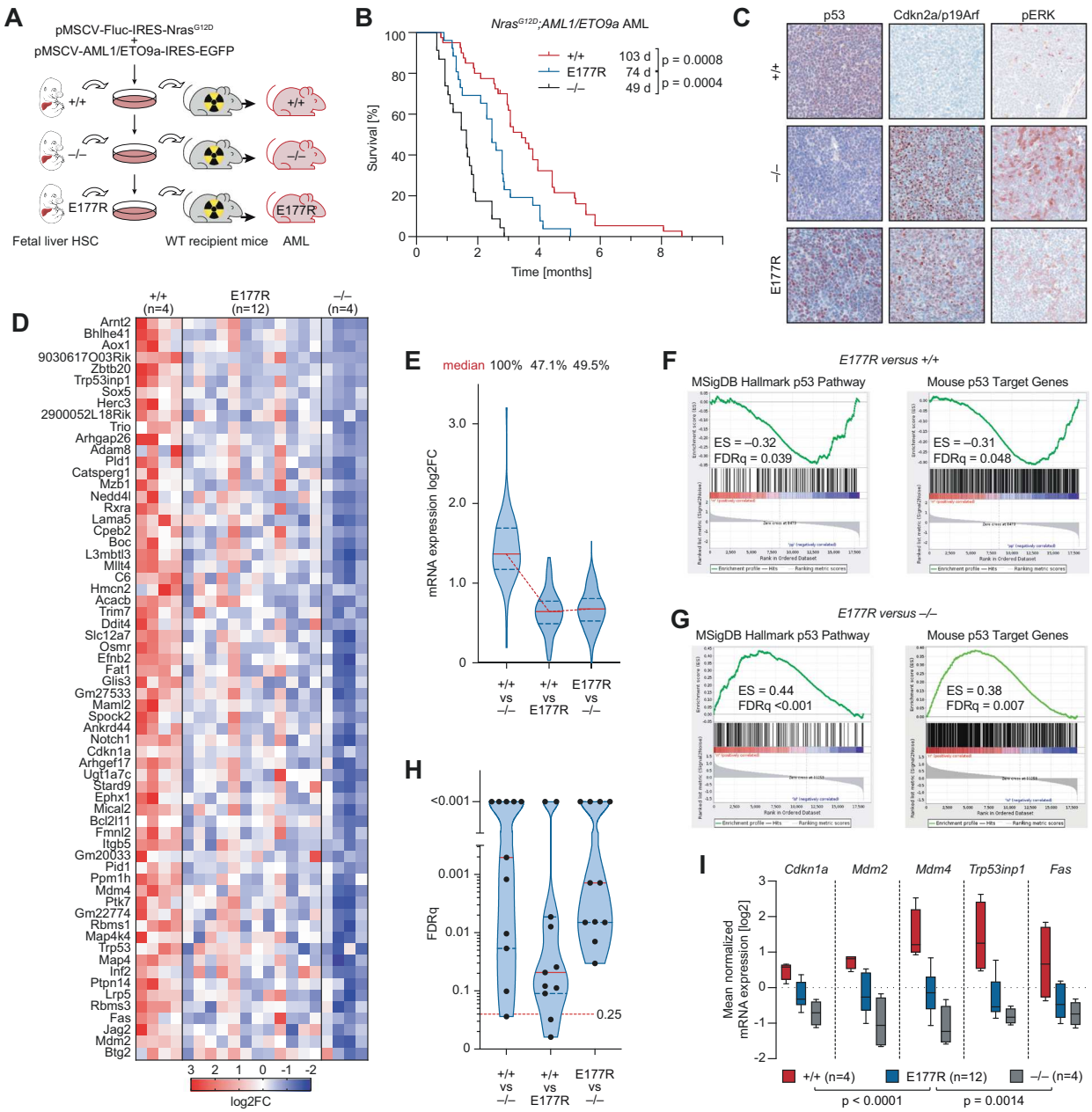

Fig. 5 Trp53E177R mutant in leukemia mouse model. A Fetal liver cells were isolated from *Trp53*$^{+/+}$, *Trp53*$^{E177R/E177R}$, and *Trp53*$^{-/-}$embryos at E14-16 and infected with retroviruses carrying *AML1/ETO9a* and *Nras*^{G12D} oncogenes co-expressed with GFP and firefly luciferase, correspondingly. After four rounds of infection, 1 million cells were transplanted into lethally irradiated (7 Gy) 129×1/SvJ albino primary recipients. **B** Kaplan–Meier survival plots for animals from **A**. *Trp53*$^{+/+}$ $n = 38$, *Trp53*$^{E177R/E177R}$ $n = 26$ and *Trp53*$^{-/-}$ $n = 23$, log-rank Mantel-Cox test. **C** Representative micrographs show immunochemical staining of p53 (left panel), Cdkn2a/p19ARF (middle panel), and phospho-ERK (right panel) in spleen samples of mice with advanced leukemia. **D**, RNAseq was performed with purified AML cells isolated from terminally ill primary recipients. Shown are 62 p53 target genes defined by the presence of a p53 ChIPseq peak in wild-type MEFs and differential expression (mean $\log_2$FC ≥ 1) between *Trp53*$^{+/+}$ and *Trp53*$^{-/-}$ AML cells. **E** Violin plots (with median and interquartile range) depict expression changes between the indicated samples for all genes from **D**. **F**–**G** RNAseq data were used for gene set enrichment analysis (GSEA). Shown are enrichment plots (with enrichment scores and FDRq-values) for the denoted gene sets in pairwise comparisons of the indicated p53 genotypes. **H** Violin plots for FDRq-values from GSEA enrichment analyses show significant enrichment (FDRq < 0.25) of multiple p53-target gene sets (Table S1) in the indicated pairwise comparisons. **I** Expression of prototypical p53 target genes obtained from **A**. Box plots (Tukey) show the mean normalized mRNA expression.

p19ARF-p53 axis. In contrast, the E177R AML samples were positive for p19ARF like p53$^{-/-}$ AML and accumulated high levels of mutant p53 protein (Fig. 5C). Thus, even though E177R exhibits sufficient residual activity to significantly delay leukemogenesis, the developing leukemia cells eventually tolerate E177R expression and do not experience selective pressure to uncouple it from activating oncogenic signals transmitted through p19ARF.

Global transcriptome profiling of primary leukemia samples by RNA-seq revealed an intermediate level of transcriptional p53 activity in E177R mutant AML (Fig. 5D). When examining a set of direct p53 target genes that contain validated p53 binding sites [32] and that are differentially expressed between p53$^{+/+}$ and p53$^{-/-}$ AML, their median expression is reduced in E177R AML by 47.1% (Fig. 5D and E). Indicative of a loss of function, canonical

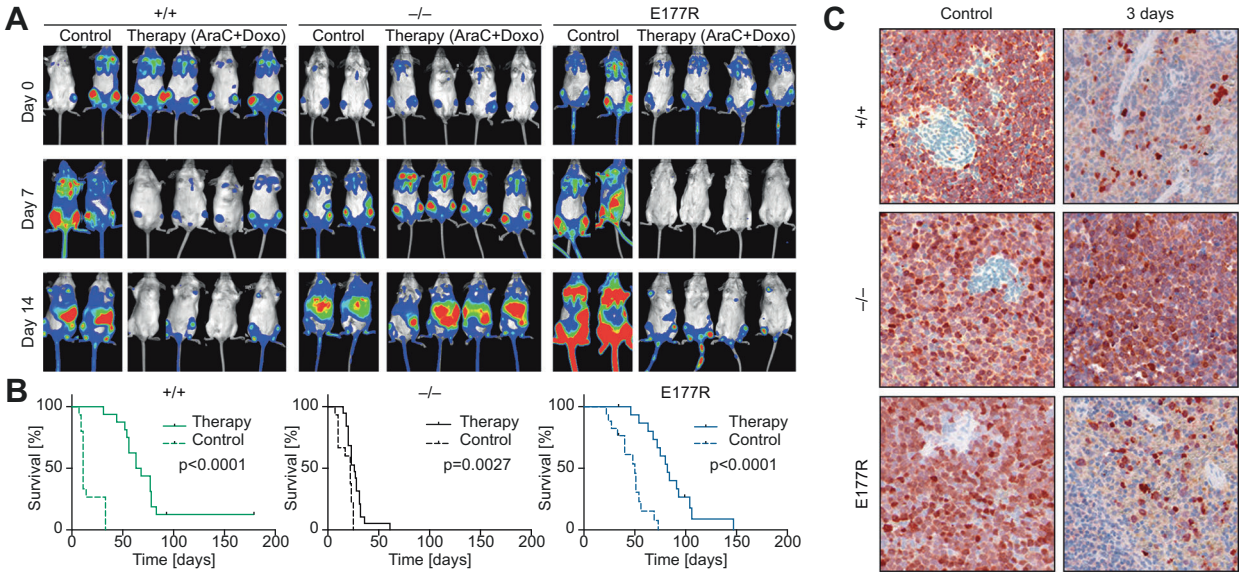

Fig. 6 Trp53E177R mutant supports chemotherapy response and improves survival in AML. A Exemplary bioluminescence imaging (BLI) pictures of representative albino mice transplanted with leukemia cells of the indicated p53 genotype at indicated time points after start of chemotherapy. **B** Kaplan–Meier survival plots for control and therapy groups. *Trp53*$^{+/+}$ control: $n = 15$, therapy: $n = 16$; *Trp53*$^{-/-}$ control: $n = 15$, therapy: $n = 19$; *Trp53*$^{E177R/E177R}$ control: $n = 17$, therapy: $n = 20$; $n = 3$ independent leukemias per genotype. **C** Immunohistochemical staining of GFP used as a surrogate marker of leukemia cells in spleens collected from control (left panel) and treated animals (right panel).

p53 signatures were significantly enriched in p53$^{+/+}$ compared with E177R AML (Fig. 5F–H). Nevertheless, confirming residual transcriptional activity of E177R, the same signatures were significantly enriched in E177R vs. p53$^{-/-}$ AML (Fig. 5G, H). Last but not least, several prototypical p53 target genes were expressed in E177R AML at a level in-between p53$^{+/+}$ and p53$^{-/-}$ AML (Fig. 5I).

We conclude that the E177R partial-LOF mutation delays, but does not prevent development of Ras-driven cancer in several mouse models. Furthermore, transcriptomic profiling of tumor samples confirms retention of residual p53 activity in such tumors along with accumulation of the mutant protein.

p53 partial-LOF supports chemotherapy response and improves survival

Despite the abundance of p53 partial-LOF mutations in cancer patients, little is known about their therapeutic implications. While p53-loss and, in particular, p53 hotspot mutants are generally considered a marker of poor therapy response and drug resistance [7, 9, 43], it is unclear if this also applies to non-hotspot mutants with residual transcriptional activity. To investigate residual tumor-suppressive functions of E177R in the context of chemotherapy, we generated cohorts of mice transplanted with p53$^{+/+}$, p53$^{-/-}$, and E177R AML and subjected them to a standard chemotherapy for leukemia. As expected, the therapy had only a marginal effect on p53-null leukemias that continued to progress under treatment as indicated by BLI, whereas p53$^{+/+}$ leukemias demonstrated a very good response (Fig. 6A). Surprisingly, in all treated mice from the E177R cohort we observed a strong reduction in luciferase signal after therapy (Fig. 6A). Predictably, the wild-type p53 group showed the best therapy outcome with a median survival benefit of 54 days ($P < 0.0001$), compared to a very modest 7-day survival advantage in the p53-null cohort ($P = 0.0405$). Importantly, treated mice with E177R leukemia demonstrated a substantial survival benefit of 32 days ($P < 0.0001$, Fig. 6B). Consistently, infiltration by GFP-positive AML cells was decreased within 3 days in both p53$^{+/+}$ and E177R spleens, confirming that E177R was not only acting in a cytostatic manner by cell cycle inhibition, but was also effectively eliminating leukemia cells (Fig. 6C).

To explore the underlying mechanism, we collected spleen samples from control and treated mice at 2 and 6 h after start of therapy. All untreated control samples independently of genotype showed high levels of proliferation and low background levels of apoptosis (Fig. 7A–C). Upon chemotherapy p53 became rapidly stabilized in p53$^{+/+}$ leukemias with an expression peak at 2 h (Fig. 7B). E177R expression was already high before treatment but increased further at 6 hours. Two hours after start of therapy, a strong decrease in BrdU-positive cells was detected in both p53$^{+/+}$ and E177R leukemias, attesting to the known ability of E177R in mounting a cell cycle arrest [30], whereas p53-null leukemia retained high levels of proliferation (Fig. 7A). Moreover, we observed a massive peak in apoptosis after two hours in p53$^{+/+}$ AML, while apoptosis levels remained low in p53-null leukemia (Fig. 7C and D). Remarkably, treated E177R AML cells also showed significant activation of apoptosis which was only slightly delayed compared to p53$^{+/+}$ cells (Fig. 7C and D).

To gain deeper molecular insight, we analyzed untreated and treated AML samples by RNA-seq. Various p53-related transcriptional signatures, including the MSigDB Hallmark p53 Pathway, were upregulated in treated mice with high statistical significance in both p53$^{+/+}$ and E177R, but not in p53-null leukemias (Fig. 7E and F). Similar as observed by immunohistochemistry of spleen samples, 2 h after treatment upregulation of the signatures was already highly significant in p53$^{+/+}$ leukemias, but still variable in E177R leukemias. At 6 h, the various signatures were also uniformly enriched in E177R samples. The delayed but significant upregulation of p53 target gene expression was also confirmed by quantitative RT-PCR for the canonical target genes *Cdkn1a/p21* and *Bbc3/Puma* using a larger set of mouse samples (Fig. 7G).

Elevated protein levels rescue the transcriptional apoptosis defect of partial-LOF mutants

The apoptotic chemotherapy response and transcriptional induction of pro-apoptotic p53 target genes seen in treated E177R leukemia cells were rather unexpected, given that various partial-LOF mutants, including E177R, were previously described to have a selective apoptosis defect [16, 28, 30, 44–46]. However, the extent of apoptosis induced by wild-type p53 is strongly determined by the amount and dynamics of p53 protein accumulation [47–50]. We,

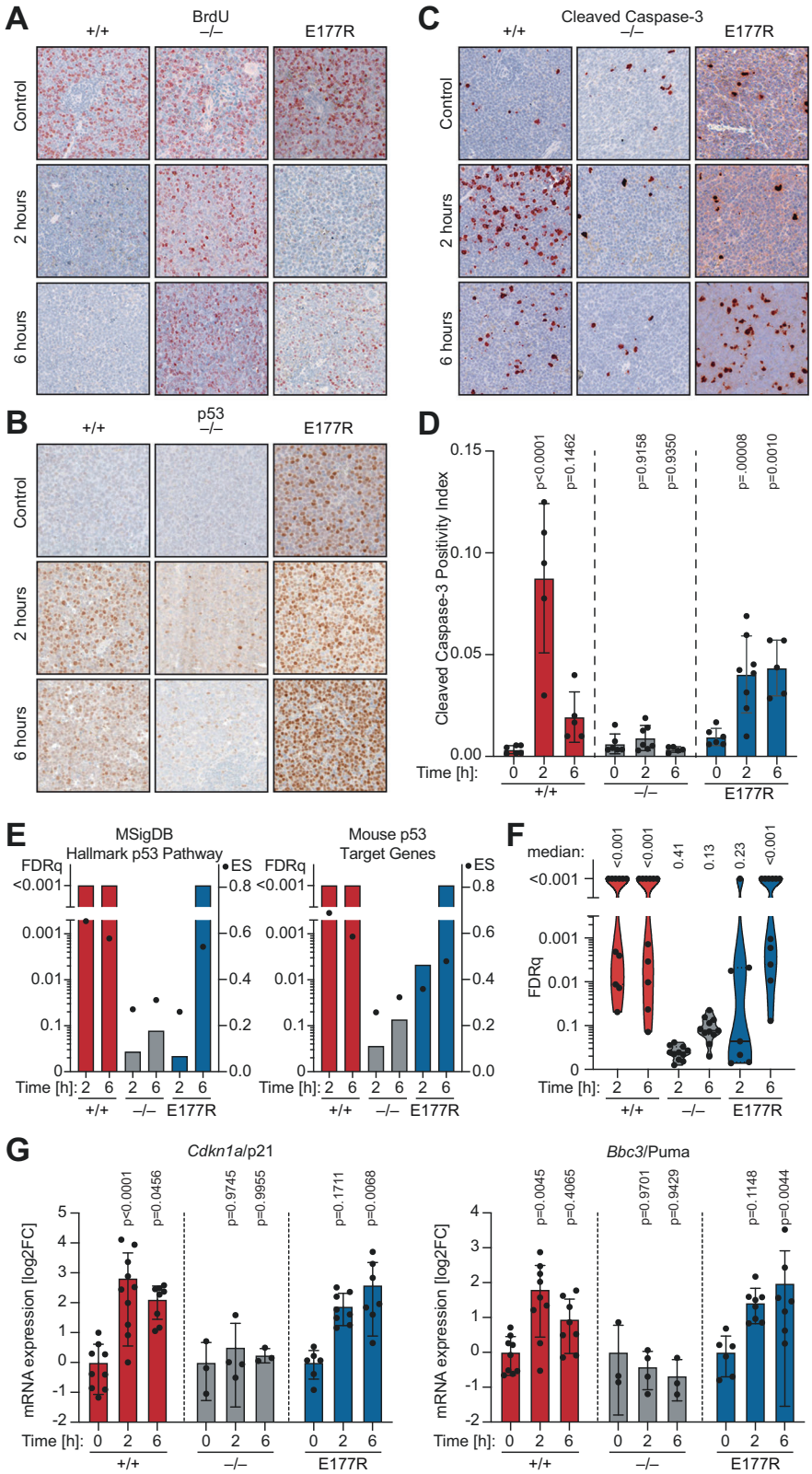

therefore, speculated that the apoptosis deficiency of partial-LOF mutants is rescued when mutant proteins are expressed at elevated levels or with sustained dynamics. To investigate whether human partial-LOF mutants can be rescued to trigger apoptosis by increasing their expression level, we transfected p53-null cells with increasing amounts of wild-type and mutant p53-expressing GFP-adenoviruses. As a human cancer model, we chose the p53-deficient Saos-2 osteosarcoma cell line, in which the apoptosis-deficiency of cooperativity and other partial-LOF mutants has originally been described [44, 45]. To ensure that adenoviral p53 expression is close

Fig. 7 Apoptotic chemotherapy response in Trp53E177R AML. A–C, Representative IHC images of spleen samples stained for **A** BrdU as proliferation marker, **B** p53 protein, and **C** cleaved caspase 3 (CC3) as apoptosis marker. **D** Quantification of CC3 in 10 fields of view per mouse sample. Shown are mean ± SD; datapoints represent individual mice; 2way ANOVA with Dunnett's multiple comparisons test. **E**, **F** Leukemia samples were collected from control and treated mice at 2 and 6 hours after therapy and analyzed by RNAseq and GSEA. **E** Graphs depict GSEA results for the indicated gene sets in pairwise comparisons between control and treated leukemias. Bars, false discovery rate (FDRq); dots, enrichment score. **F** Violin plots illustrate distribution of FDRq values from GSEA with multiple p53-related gene sets (Table S1). Each data point represents one gene set. **G** mRNA expression (RT–qPCR) of p53 target genes *Cdkn1a* and *Bbc3* normalized to *Actb* (β-actin). Shown is the mean ± SD log2-fold change in treated leukemia samples relative to untreated; 2way ANOVA with Dunnett's multiple comparisons test; datapoints represent individual mice.

to physiological, we carefully titrated the adenoviruses to reach protein expression levels that are similar to activated endogenous wild-type p53. For this reference, we treated p53 wild-type HCT116 colorectal cancer cells with the highly-specific Mdm2-inhibitor Nutlin-3a (Supplementary Fig. S3A and B). To control for adenovirus-induced toxicity, the total adenovirus dose was kept constant by adding GFP-expressing control adenovirus and validating GFP-protein levels to be equal in all samples accordingly. We measured the cell-cycle inhibitory properties by EdU immunofluorescence staining for S-phase cells and, in parallel, used a real-time Annexin V-based split-nanoluciferase complementation assay to quantify apoptosis in a time-resolved manner. When expressed at equal levels, similar to activated endogenous p53 in HCT116 cells, all patient-derived cooperativity mutants (R181C, R181H, and R181L) as well as E180R (corresponding to murine E177R) were indistinguishable from wild-type p53 (WT) in causing cell-cycle arrest (Fig. 8A) but showed the expected decrease in apoptosis characteristic for partial-LOF mutants (Fig. 8B). By comparing with a titration of WT protein (Fig. 8C), peak apoptosis levels were decreased by at least 60% for R181L and by >80% for the other mutants. Importantly, for R181L and R181H apoptosis was fully rescued to WT-levels when mutant protein expression was raised 4- to 8-fold (Fig. 8D and E). For E180R and R181C, apoptosis was partially rescued at 8-fold higher expression, reaching 60% and 30% peak levels, respectively. Moreover, while all partial-LOF mutants were able to transactivate *CDKN1A/p21* above mock level, they were strongly compromised at inducing *BBC3/Puma* mRNA when expressed at the same level as WT (Fig. 8F). Notably, *BBC3/Puma* expression was fully or partially rescued to the WT-level at 8-fold higher expression (Fig. 8F).

Moreover, the rescue was confirmed at the level of promoter binding by chromatin immunoprecipitation (Fig. 8G). When expressed at WT-like levels (1× mut), all partial-LOF mutants yielded a binding signal significantly different from the IgG control at the *CDKN1A/p21* promoter, but not at the *BBC3/Puma* promoter. When expressed at 8× higher levels, p53 binding increased and reached at both promoters a level that was significantly different from the background and comparable to binding of wild-type expressed at 1×.

These experiments reveal that multiple patient-derived partial-LOF mutants can bind and transactivate a pro-apoptotic target gene promoter when expressed at increased levels, indicating that the previously reported transcriptional apoptosis-deficiency is not absolute and can be overcome by an increase in mutant protein level.

DISCUSSION

A pan-cancer *TP53* mutome analysis revealed a high prevalence of p53 partial LOF mutations that include p53 DNA binding cooperativity mutations affecting residues E180 and R181 (Fig. 1). RNA-seq profiling of the E180R (murine E177R) mutant demonstrated that its transcriptional activity is representative of the class of cooperativity mutants and validated this mouse strain as a suitable in vivo model for p53 partial-LOF mutations (Fig. 2). In tissues as different as pancreas, lung, and bone marrow the E177R mutant sensitized to *Ras* oncogene-driven tumorigenesis, highlighting the pathogenicity of a partial-LOF mutation. Interestingly, a similar degree of cancer susceptibility has also been observed in $p53^{neo}$ mice which exhibit partial-LOF owing to reduced expression levels of wild-type p53 resulting from the intronic insertion of a neomycin cassette [15]. Levels of p53 expression in $p53^{neo/-}$ and $p53^{neo/neo}$ MEFs were 7.4% and 16.1% of the level of p53 expression in $p53^{+/+}$ MEFs, resulting in a reduced median lifespan of 251 and 395 days, respectively [15]. As such, $p53^{neo}$ mice are remarkably similar to $p53^{E177R}$ mice, the resulting tumors are nevertheless notably different. Tumors in $p53^{neo}$ mice were reported as negative for p53 by immunostaining, whereas tumors in $p53^{E177R}$ mice were strongly immunopositive for p53 in all models we studied (Figs. 3–5). In this respect, E177R tumors were more similar to tumors with p53 hotspot mutations than tumors with reduced levels of wild-type p53.

Nevertheless, E177R tumors were very different from p53-null and hotspot-mutant tumors in their response to chemotherapy. While wild-type p53 can promote or diminish chemotherapy responses in a manner depending on cellular context and pathway activation [51], many hotspot-mutations exert GOF activities that render tumors more drug-resistant than the loss of p53 [7]. In contrast, E177R-mutant leukemias were more sensitive to standard chemotherapy than p53-null leukemias. The chemotherapy response was apoptotic and associated with induction of pro-apoptotic p53 target genes (Fig. 7C-G). This finding was rather surprising, given that E177R is unable to bind non-canonical REs in many pro-apoptotic target genes and E177R mice are characterized by a defect in p53-mediated apoptosis [30]. However, this apoptosis defect is not absolute and it was recently shown that in *Mdm2*-knockout embryos E177R triggers widespread apoptosis and leads to embryonic lethality [29]. Possible causes are the massive E177R stabilization caused by *Mdm2*-deficiency combined with the low apoptosis threshold of highly-proliferating embryonal tissues. We speculated that similar conditions are present in E177R leukemia cells. First, hematopoietic cells are exceptionally vulnerable to p53-mediated apoptosis as demonstrated by the strong hematopoietic phenotypes of mice with elevated p53 activity and the bone marrow toxicity of Mdm2 inhibitors [38, 39, 52, 53]. Second, E177R is constitutively stabilized in murine leukemia cells similar as cooperativity mutants in cancer patients. It can be assumed that sustained high-level expression of E177R restores binding to pro-apoptotic promoters by mass action, so that additional exogenous stress in the form of chemotherapy drives E177R leukemia cells into apoptosis. In support of this hypothesis, we experimentally validated that the apoptotic activity of E177R/E180R (and various patient-derived partial-LOF mutants) is rescued at elevated expression levels. Notably, non-transcriptional mitochondrial and cytoplasmic activities also contribute to p53-mediated apoptosis and support p53's transcriptional apoptotic activity [54–56]. Furthermore, non-transcriptional apoptotic functions can be retained by tumorigenic p53 mutants and drive a beneficial chemotherapy response [32]. It is therefore conceivable that additional non-transcriptional functions of E177R further contribute to the survival-promoting therapy response seen in our AML mouse study.

In summary, our study further emphasizes the functional diversity among p53 mutations and reveals that partial-LOF mutations have a distinct translational impact on the course of

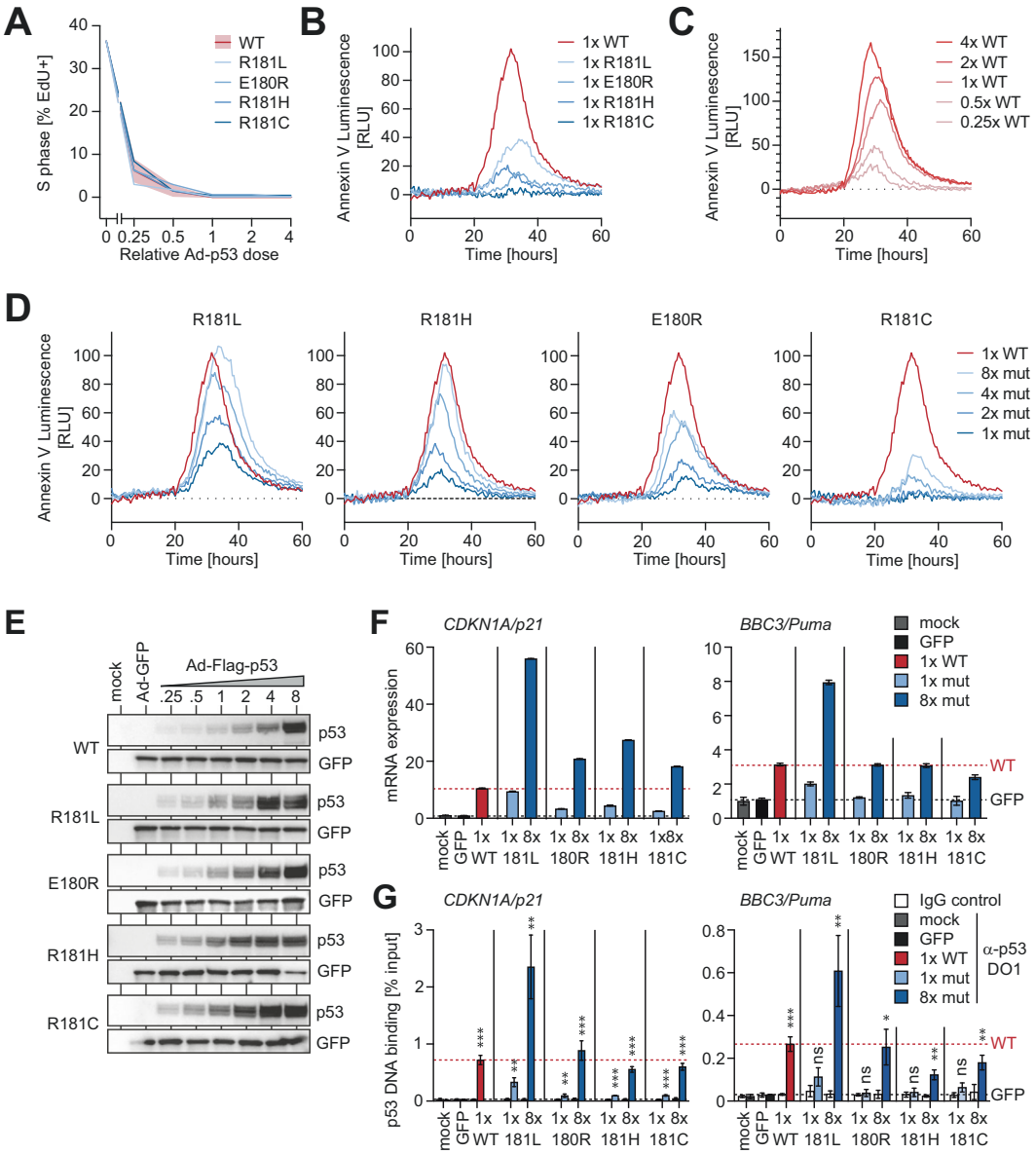

Fig. 8 Elevated protein levels rescue the transcriptional apoptosis defect of partial-LOF mutants. Saos-2 cells were transduced with different relative amounts of p53/GFP-coexpressing vectors. Total amount of vector was adjusted to equal levels with GFP-only vector. **A** Immunofluorescence quantification of S-phase as mean percentage of EdU+ cells ($n = 3$). **B**–**D** Real-time quantification of apoptosis shown as mean Annexin V luminescence relative to GFP-only control ($n = 3$). **E** WB for p53-mutant protein levels. Equal vector load is confirmed by GFP. **F** mRNA expression of p53 target genes *CDKN1A/p21* and *BBC3/Puma* (relative to GFP-only control vector). Expression values were normalized to *GAPDH* and are shown as mean ± SD ($n = 3$ replicates). **G**, Chromatin immunoprecipitation analysis of indicated p53 variants at the *CDKN1A/p21* and *BBC3/Puma* promoter 18 hours after transduction. Chromatin samples were immunoprecipitated with α-p53 antibody or IgG as background control. Shown is DNA binding as % input chromatin (mean ± SD, $n = 3$ replicates). *P*-values (***$P < 0.001$; **$P < 0.01$; *$P < 0.05$; ns not significant; two-sided t-test) indicate statistical significance of the DNA binding signal relative to the respective IgG background control.

tumorigenesis and cancer therapy and should be distinguished from classical hotspot mutations when using p53 mutations for predicting prognosis or deciding between treatment options.

MATERIALS AND METHODS

Animal experiments

All mouse experiments were performed according to the German Animal Welfare Law (TierSchG) and approved by the Regierungspräsidium Gießen based on recommendations of their animal welfare committee. The size of animal cohorts was determined a priori based on a biometric plan aimed at achieving statistically significant results at an effect size (Cohen's d) of 1, error of $\alpha = 0.05$, and power of $1\text{-}\beta = 0.80$. The approved animal study protocols specified pre-established humane endpoint criteria. Animals that reached the endpoint before the end of the experiment were excluded from the analysis (or censored in survival studies). In treatment studies, animals were randomized to treatment cohorts by investigators and monitored by caretakers blinded to cohort allocation. Mice were housed in open cages, on a 12 h light/dark cycle, fed a standard housing/breeding diet (Altromin), and received water ad libitum.

Conditional 129 S2-*Trp53*^{tm1Thst}/Thst (*Trp53*$^{LSL\text{-}E177R}$) knock-in mice have been described [30]. Homozygous *Trp53*$^{LSL\text{-}E177R/LSL\text{-}E177R}$ mice with the intact LSL cassette (deficient for p53 expression) were used as p53-null

controls. For the PDAC model, triple-transgenic animals were generated through the breeding of double-heterozygous B6.129S/Sv-Kras^{tm4Tyj}/JThst (*Kras*$^{+/LSL\text{-}G12D}$), B6.FVB-Tg(Pdx1-cre)6Tuv/JThst (*Pdx-Cre*) with homozygous 129S2-*Trp53*$^{tm1.1Thst}$/Thst (*Trp53*$^{E177R/E177R}$) or B6.129P2-*Trp53*^{tm1Brn}/JThst (*Trp53*$^{flox/flox}$) animals. For the LUAD model, B6.129S2-*Kras*^{tm2Tyj}/NciThst (*Kras*^{LA1}) knock-in mice were intercrossed with *Trp53*$^{E177R/E177R}$ or *Trp53*$^{LSL\text{-}E177R/LSL\text{-}E177R}$ animals. MRI-assisted lung examination was done with a 7 T Clinscan 70/30 USR (Brucker) as described before [53]. Generation of the leukemia mouse model, monitoring of disease development by BLI, and therapy were performed as described earlier [32, 37]. Experiments with leukemia control cohorts (*Trp53*$^{+/+}$ and *Trp53*$^{-/-}$) depicted in Fig. 6 have been described previously [32] and were performed in parallel to the *Trp53*$^{E177R/E177R}$ cohort. 129X1Sv/J and 129.B6F1 albino mice were used as recipients in the leukemia model.

Real-time apoptosis assay

Saos-2 cells were infected in white 96-well clear-bottom plates with p53-expressing Ad-vectors and cultures in a CO_2-independent medium (Thermo Fisher). RealTime-Glo™ Annexin V Apoptosis Assay (Promega) reagents were added 1 h post-infection according to the manufacturer's protocol. Luminescence was recorded over 72 h after infection using a Cytation 3 Plate Reader (Biotek).

Statistical analysis

GraphPad Prism 8 software was used for statistical analysis. Graphs show mean values obtained with n technical or biological replicates, and error bars in all figures represent standard deviation (SD), unless indicated otherwise. To assess comparisons between multiple groups, ANOVA followed by Dunnett's multiple comparisons test was performed. To assess comparisons between two groups, the Student's t-test was used. Data were validated to have similar variances and meet the assumption of (log) normal distribution by Kolmogorov-Smirnov test. p-values <0.05 were considered significant. Gene Set Enrichment Analyses were evaluated based on enrichment scores (ES) and FDRq-values, considering FDRq<0.25 as significant.

REFERENCES

1. Donehower LA, Soussi T, Korkut A, Liu Y, Schultz A, Cardenas M, et al. Integrated analysis of TP53 gene and pathway alterations in the Cancer Genome Atlas. Cell Rep. 2019;28:1370–84.
2. Mello SS, Attardi LD. Deciphering p53 signaling in tumor suppression. Curr Opin Cell Biol. 2018;51:65–72.
3. Leroy B, Anderson M, Soussi T. TP53 mutations in human cancer: database reassessment and prospects for the next decade. Hum Mutat. 2014;35:672–88.
4. Joerger AC, Fersht AR. Structural biology of the tumor suppressor p53. Annu Rev Biochem. 2008;77:557–82.
5. Stiewe T, Haran TE. How mutations shape p53 interactions with the genome to promote tumorigenesis and drug resistance. Drug Resist Updat. 2018;38:27–43.
6. Kim MP, Lozano G. Mutant p53 partners in crime. Cell Death Differ. 2018;25:161–8.
7. Muller PA, Vousden KH. Mutant p53 in cancer: new functions and therapeutic opportunities. Cancer Cell. 2014;25:304–17.
8. Freed-Pastor WA, Prives C. Mutant p53: one name, many proteins. Genes Dev. 2012;26:1268–86.
9. Robles AI, Jen J, Harris CC Clinical Outcomes of TP53 Mutations in Cancers. Cold Spring Harb Perspect Med. 2016; 6:a026294.
10. Kato S, Han SY, Liu W, Otsuka K, Shibata H, Kanamaru R, et al. Understanding the function-structure and function-mutation relationships of p53 tumor suppressor protein by high-resolution missense mutation analysis. Proc Natl Acad Sci USA. 2003;100:8424–9.
11. Resnick MA, Inga A. Functional mutants of the sequence-specific transcription factor p53 and implications for master genes of diversity. Proc Natl Acad Sci USA. 2003;100:9934–9.
12. Menendez D, Inga A, Resnick MA. The biological impact of the human master regulator p53 can be altered by mutations that change the spectrum and expression of its target genes. Mol Cell Biol. 2006;26:2297–308.
13. Kotler E, Shani O, Goldfeld G, Lotan-Pompan M, Tarcic O, Gershoni A, et al. A Systematic p53 mutation library links differential functional impact to cancer mutation pattern and evolutionary conservation. Mol Cell. 2018;71:178–90.
14. Giacomelli AO, Yang X, Lintner RE, McFarland JM, Duby M, Kim J, et al. Mutational processes shape the landscape of TP53 mutations in human cancer. Nat Genet. 2018;50:1381–7.
15. Wang Y, Suh YA, Fuller MY, Jackson JG, Xiong S, Terzian T, et al. Restoring expression of wild-type p53 suppresses tumor growth but does not cause tumor regression in mice with a p53 missense mutation. J Clin Invest. 2011;121:893–904.
16. Liu G, Parant JM, Lang G, Chau P, Chavez-Reyes A, El-Naggar AK, et al. Chromosome stability, in the absence of apoptosis, is critical for suppression of tumorigenesis in Trp53 mutant mice. Nat Genet. 2004;36:63–8.
17. Post SM, Quintas-Cardama A, Terzian T, Smith C, Eischen CM, Lozano G. p53-dependent senescence delays Emu-myc-induced B-cell lymphomagenesis. Oncogene. 2010;29:1260–9.
18. Schmitt CA, Fridman JS, Yang M, Baranov E, Hoffman RM, Lowe SW. Dissecting p53 tumor suppressor functions in vivo. Cancer Cell. 2002;1:289–98.
19. Morton JP, Timpson P, Karim SA, Ridgway RA, Athineos D, Doyle B, et al. Mutant p53 drives metastasis and overcomes growth arrest/senescence in pancreatic cancer. Proc Natl Acad Sci USA. 2010;107:246–51.
20. Timofeev O, Stiewe T Rely on Each Other: DNA Binding Cooperativity Shapes p53 Functions in Tumor Suppression and Cancer Therapy. Cancers (Basel) 2021; 13:2422.
21. Blanden AR, Yu X, Blayney AJ, Demas C, Ha JH, Liu Y et al. Zinc shapes the folding landscape of p53 and establishes a pathway for reactivating structurally diverse cancer mutants. Elife 2020; 9:e61487.
22. Klein C, Planker E, Diercks T, Kessler H, Kunkele KP, Lang K, et al. NMR spectroscopy reveals the solution dimerization interface of p53 core domains bound to their consensus DNA. J Biol Chem. 2001;276:49020–7.
23. Dehner A, Klein C, Hansen S, Muller L, Buchner J, Schwaiger M, et al. Cooperative binding of p53 to DNA: regulation by protein-protein interactions through a double salt bridge. Angew Chem Int Ed Engl. 2005;44:5247–51.
24. Weinberg RL, Veprintsev DB, Fersht AR. Cooperative binding of tetrameric p53 to DNA. J Mol Biol. 2004;341:1145–59.
25. Kitayner M, Rozenberg H, Rohs R, Suad O, Rabinovich D, Honig B, et al. Diversity in DNA recognition by p53 revealed by crystal structures with Hoogsteen base pairs. Nat Struct Mol Biol. 2010;17:423–9.
26. Kitayner M, Rozenberg H, Kessler N, Rabinovich D, Shaulov L, Haran TE, et al. Structural basis of DNA recognition by p53 tetramers. Mol Cell. 2006;22:741–53.
27. Schlereth K, Heyl C, Krampitz AM, Mernberger M, Finkernagel F, Scharfe M, et al. Characterization of the p53 cistrome-DNA binding cooperativity dissects p53's tumor suppressor functions. PLoS Genet. 2013;9:e1003726.
28. Schlereth K, Beinoraviciute-Kellner R, Zeitlinger MK, Bretz AC, Sauer M, Charles JP, et al. DNA binding cooperativity of p53 modulates the decision between cell-cycle arrest and apoptosis. Mol Cell. 2010;38:356–68.
29. Klimovich B, Stiewe T, Timofeev O. Inactivation of Mdm2 restores apoptosis proficiency of cooperativity mutant p53 in vivo. Cell Cycle. 2020;19:109–23.
30. Timofeev O, Schlereth K, Wanzel M, Braun A, Nieswandt B, Pagenstecher A, et al. p53 DNA binding cooperativity is essential for apoptosis and tumor suppression in vivo. Cell Rep. 2013;3:1512–25.
31. Mellert H, Espinosa JM. Tumor suppression by p53: Is apoptosis important or not? Cell Rep. 2013;3:1335–6.
32. Timofeev O, Klimovich B, Schneikert J, Wanzel M, Pavlakis E, Noll J, et al. Residual apoptotic activity of a tumorigenic p53 mutant improves cancer therapy responses. EMBO J. 2019;38:e102096.
33. Engeland K. Cell cycle arrest through indirect transcriptional repression by p53: I have a DREAM. Cell Death Differ. 2018;25:114–32.
34. Tiwari B, Jones AE, Caillet CJ, Das S, Royer SK, Abrams JM. p53 directly represses human LINE1 transposons. Genes Dev. 2020;34:1439–51.
35. Johnson L, Mercer K, Greenbaum D, Bronson RT, Crowley D, Tuveson DA, et al. Somatic activation of the K-ras oncogene causes early onset lung cancer in mice. Nature. 2001;410:1111–6.
36. Donehower LA, Harvey M, Slagle BL, McArthur MJ, Montgomery CA Jr, Butel JS, et al. Mice deficient for p53 are developmentally normal but susceptible to spontaneous tumours. Nature. 1992;356:215–21.
37. Zuber J, Radtke I, Pardee TS, Zhao Z, Rappaport AR, Luo W, et al. Mouse models of human AML accurately predict chemotherapy response. Genes Dev. 2009;23:877–89.
38. Abbas HA, Maccio DR, Coskun S, Jackson JG, Hazen AL, Sills TM, et al. Mdm2 is required for survival of hematopoietic stem cells/progenitors via dampening of ROS-induced p53 activity. Cell Stem Cell. 2010;7:606–17.
39. Ringshausen I, O'Shea CC, Finch AJ, Swigart LB, Evan GI. Mdm2 is critically and continuously required to suppress lethal p53 activity in vivo. Cancer Cell. 2006;10:501–14.
40. Mendrysa SM, O'Leary KA, McElwee MK, Michalowski J, Eisenman RN, Powell DA, et al. Tumor suppression and normal aging in mice with constitutively high p53 activity. Genes Dev. 2006;20:16–21.
41. Terzian T, Wang Y, Van Pelt CS, Box NF, Travis EL, Lozano G. Haploinsufficiency of Mdm2 and Mdm4 in tumorigenesis and development. Mol Cell Biol. 2007;27:5479–85.
42. Lin AW, Lowe SW. Oncogenic ras activates the ARF-p53 pathway to suppress epithelial cell transformation. Proc Natl Acad Sci USA. 2001;98:5025–30.

43. Sabapathy K, Lane DP. Therapeutic targeting of p53: all mutants are equal, but some mutants are more equal than others. Nat Rev Clin Oncol. 2018;15:13–30.
44. Rowan S, Ludwig RL, Haupt Y, Bates S, Lu X, Oren M, et al. Specific loss of apoptotic but not cell-cycle arrest function in a human tumor derived p53 mutant. EMBO J. 1996;15:827–38.
45. Ludwig RL, Bates S, Vousden KH. Differential activation of target cellular promoters by p53 mutants with impaired apoptotic function. Mol Cell Biol. 1996;16:4952–60.
46. Ryan KM, Vousden KH. Characterization of structural p53 mutants which show selective defects in apoptosis but not cell cycle arrest. Mol Cell Biol. 1998;18:3692–8.
47. Kracikova M, Akiri G, George A, Sachidanandam R, Aaronson SA. A threshold mechanism mediates p53 cell fate decision between growth arrest and apoptosis. Cell Death Differ. 2013;20:576–88.
48. Purvis JE, Karhohs KW, Mock C, Batchelor E, Loewer A, Lahav G. p53 dynamics control cell fate. Science. 2012;336:1440–4.
49. Chen X, Ko LJ, Jayaraman L, Prives C. p53 levels, functional domains, and DNA damage determine the extent of the apoptotic response of tumor cells. Genes Dev. 1996;10:2438–51.
50. Paek AL, Liu JC, Loewer A, Forrester WC, Lahav G. Cell-to-Cell Variation in p53 dynamics leads to fractional killing. Cell. 2016;165:631–42.
51. Jackson JG, Pant V, Li Q, Chang LL, Quintas-Cardama A, Garza D, et al. p53-mediated senescence impairs the apoptotic response to chemotherapy and clinical outcome in breast cancer. Cancer Cell. 2012;21:793–806.
52. Andreeff M, Kelly KR, Yee K, Assouline S, Strair R, Popplewell L, et al. Results of the phase I Trial of RG7112, a small-molecule MDM2 antagonist in leukemia. Clin Cancer Res. 2016;22:868–76.
53. Timofeev O, Koch L, Niederau C, Tscherne A, Schneikert J, Klimovich M, et al. Phosphorylation control of p53 DNA-binding cooperativity balances tumorigenesis and aging. Cancer Res. 2020;80:5231–44.
54. Mihara M, Erster S, Zaika A, Petrenko O, Chittenden T, Pancoska P, et al. p53 Has a direct apoptogenic role at the mitochondria. Mol Cell. 2003;11:577–90.
55. Chipuk JE, Bouchier-Hayes L, Kuwana T, Newmeyer DD, Green DR. PUMA couples the nuclear and cytoplasmic proapoptotic function of p53. Science. 2005;309:1732–5.
56. Chipuk JE, Kuwana T, Bouchier-Hayes L, Droin NM, Newmeyer DD, Schuler M, et al. Direct activation of Bax by p53 mediates mitochondrial membrane permeabilization and apoptosis. Science. 2004;303:1010–4.

ACKNOWLEDGEMENTS

Authors thank Sigrid Bischofsberger, Antje Grzeschiczek, Angela Mühling, Björn Geißert, Marlen Lahmann and employees of the animal facility of Marburg University for technical and experimental support. We acknowledge support by the Medical Core Facilities (Genomics: Alexandra Schneider and Angelika Filmer; Flow Cytometry: Gavin Giel; Small Animals Imaging: Marina Tatura; 7T-MRT: Janine Schweigert; Small Animals Molecular Imaging: Claudia Weiß; X-ray: Ulrike Schötz). This work was supported by grants from Deutsche Krebshilfe (111250, 70112623 to TS and 111444 to OT), Deutsche José Carreras Leukämie Stiftung e.V. (09 R/2018 to OT and TS), Deutsche Forschungsgemeinschaft (TRR81/3 109546710 Project A10 to TS, TI 1028/2-1 to OT, STI 182/13-1 to TS, GRK2573), German Center for Lung Research (DZL) to TS, BMBF (031L0063 to TS), von Behring-Röntgen Stiftung (65-0004 and 66-LV06 to TS).

AUTHOR CONTRIBUTIONS

Conceptualization: OT, TS; Molecular biology experiments: BK, NM, and MN; Animal experiments: BK, SE, and OT; Human pathology: DK, AS; Bioinformatics: MM; Genomics: AN; Writing – Original Draft: OT, TS; Writing – Review and Editing: all.

FUNDING

Open Access funding enabled and organized by Projekt DEAL.

COMPETING INTERESTS

The authors declare no competing interests.

ADDITIONAL INFORMATION

Supplementary information The online version contains supplementary material available at https://doi.org/10.1038/s41388-021-02141-5.

Correspondence and requests for materials should be addressed to Oleg Timofeev or Thorsten Stiewe.

Reprints and permission information is available at http://www.nature.com/reprints

Publisher's note Springer Nature remains neutral with regard to jurisdictional claims in published maps and institutional affiliations.

SUPPLEMENTARY INFORMATION

p53 Partial Loss-of-Function Mutations Sensitize to Chemotherapy

Boris Klimovich[1,*], Nastasja Merle[1,*], Michelle Neumann[1], Sabrina Elmshäuser[1], Andrea Nist[2], Marco Mernberger[1], Daniel Kazdal[3], Albrecht Stenzinger[3], Oleg Timofeev[1], and Thorsten Stiewe[1,2]

[1] Institute of Molecular Oncology, Universities of Giessen and Marburg Lung Center (UGMLC), Member of the German Center for Lung Research (DZL), Philipps-University, Marburg, Germany;

[2] Genomics Core Facility, Philipps-University, Marburg, Germany;

[3] Institute of Pathology, Heidelberg University Hospital, Translational Lung Research Center Heidelberg (TLRC-H), Member of the German Center for Lung Research (DZL), Heidelberg, Germany.

[*] These authors contributed equally.

Correspondence to Oleg Timofeev: timofeev@staff.uni-marburg.de; Thorsten Stiewe: stiewe@uni-marburg.de.

SUPPLEMENTARY MATERIALS AND METHODS

Cell culture and gene transfer

For experiments, all cells were maintained at ambient oxygen in a humidified cell culture incubator (37°C, 5% CO2) in high-glucose Dulbecco's Modified Eagle's Medium (DMEM) supplemented with 10% fetal bovine serum (FBS, Sigma-Aldrich), 100 U/ml penicillin and 100 µg/ml streptomycin (Life technologies). Recombinant adenoviral vectors co-expressing GFP and FLAG-tagged p53 mutants were produced in Ad293 cells (Agilent) using the pAdEasy system (Agilent) and used for infection of Saos-2 cells as described before [1]. Ad-vectors were titrated to precisely regulate the amount of ectopically expressed p53, while equalizing the total amount of Ad-vector encoding GFP only, using Western blotting and GFP flow cytometry.

EdU immunofluorescence analysis

Saos-2 cells were plated in black clear-bottom 96-well plates (Greiner), infected with Ad-vectors and harvested 30 hours post-infection. S phase cells were labeled with 10 µM EdU (Baseclick) added to the culture medium 1.5 hours before fixation. Cells were fixed at room temperature (RT) on plates (3.7% PFA in PBS, 15 min), washed twice (3% BSA in PBS) and permeabilized (0.5% Triton-X100, 20 minutes). EdU was detected using Click-It cocktail (4 mM CuSO4, 1 µM Eterneon Red Azide, 100 mM ascorbic acid in PBS) for 30 minutes at RT. After washing twice with 3 % BSA in PBS, nuclei were counterstained with 0.1 µg/ml DAPI in PBS. Fluorescence images were obtained using the high-content automated BD Pathway (BD Biosciences) microscope. Images were taken as a 3x3 montage with A647 (EdU) and DAPI filters for each well and analyzed with the Attovision software (BD Biosciences) to determine the percentage of EdU-positive cells.

Western blot and immunohistochemistry (IHC)

Cells were collected 18 hours after infection and lysed in NP-40 Lysis Buffer (50 mM Tris-HCl, 150 mM NaCl, 5 mM EDTA, 2% NP-40, pH 8.0) supplemented with protease inhibitor (complete ULTRA tablets EASYpack, Roche) and sonicated with a Bioruptor (Diagenode) for 5 min. Western blotting was performed as described [2] using the following antibodies against: human p53 (DO-1, Santa Cruz Biotechnology [SC], 1:5000), GFP (B-2, #sc-9996, SC, 1:500), β-actin (AC-15, #ab6276, Abcam, 1:10000). Detection was performed with

secondary anti-mouse or anti-rabbit IgG-HRP (GE Healthcare, 1:5,000) and SuperSignal ECL kit (Thermo Fisher). β-actin was detected using goat anti-mouse Alexa-488 conjugate (A-11029, Thermo Fisher). Formalin fixed and paraffin embedded (FFPE) mouse samples were processed for histology and IHC as described [2] using the following antibodies against: cleaved caspase-3 (#9661, Cell Signaling, 1:100), mouse p53 (NCL-p53-505, Leica Microsystems, 1:1000), human p53 (DO-1, SC, 1:1000), BrdU (BU1/75(ICR1), #OBT0030G, 1:100), GFP (ab6556, Abcam, 1:500), p19Arf (5-C3-1, #sc-32748, SC 1:50), phosho-Erk (E-4, #sc-7383, SC, 1:100), biotinylated goat anti-rabbit IgG (E0 432, DAKO, 1:500) and biotinylated rabbit anti-mouse IgG (31834, Invitrogen, 1:500). Human specimen of pulmonary adenocarcinoma (ADC) used in this study were resected at the Thoraxklinik at Heidelberg University Hospital and diagnosed according to the criteria of the current WHO Classification (2015) for lung cancer [3] in the Institute of Pathology at Heidelberg University Hospital. The use of FFPE samples was approved by the ethics committee of Heidelberg University (S-145/2017). Immunohistochemical staining for p53 in human tumor specimen was carried out automatically using a BenchMark ULTRA autostainer (Ventana Medical Systems Inc., Tucson, AZ, USA) according to the manufacturer's instructions, in order to apply a ready to use solution of the anti-p53 mouse monoclonal antibody, clone Bp53-11 (F. Hoffmann-La Roche AG, Basel, CH) to the sections. IHC images were acquired with the Leica Aperio Versa slide-scanner and Leica Aperio eSlide Manager software v. 1.0.3.37. Analysis of IHC images was done using Aperio ImageScope software v. 12.3.2.8013. Quantification was performed using the Positive Pixel Count Algorithm v.9 and calculated as the ratio $N_{positive}/N_{total}$ pixels in 10 fields of view (1000X1000 pixel each) per sample.

mRNA expression analysis by RT-qPCR

RNA was isolated from cells or tissue samples using the RNeasy Mini kit (Qiagen). cDNA was generated with the SuperScript VILO cDNA Synthesis Kit (Invitrogen) and used for quantitative PCR with SYBR Green (Thermo Fisher Scientific) and the following primer pairs: mouse β-*Actin* 5'- CATTGCTGACAGGATGCAGAAGG (sense), 5'-TGCTGGAAGGTGGACAGTGAGG (antisense); *Cdkn1a/p21* 5'-CAAGAGGCCCAGTACTTCCT (sense), 5'-ACACCAGAGTGCAAGACAGC (antisense); *Bbc3/Puma* 5'- GTACGAGCGGCGGAGACAAG (sense), 5'-GCACCTAGTTGGGCTCCATTTCTG (antisense), human *GAPDH* 5'-CTATAAATTGAGCCCGCAGCC (sense), 5'- ACCAAATCCGTTGACTCCGA (antisense); *BBC3/Puma* 5'- ACCTCAACGCACAGTACGAG (sense), 5'-

GAGATTGTACAGGACCCTCCA (antisense). Gene expression was analyzed on a LightCycler 480 (Roche) with the ΔΔCt method using β-*Actin* or *GAPDH* for normalization.

Chromatin immunoprecipitation

Saos-2 cells growing on 15 cm dishes were fixed at 80% confluency with freshly prepared 18.5% (w/v) paraformaldehyde (PFA) for 10 min at RT, aiming at a final concentration of 0.88% (v/v) PFA for fixation. Crosslinking of DNA and proteins was terminated by quenching unreacted PFA by addition of glycine to 125 mM end concentration and further incubation of the cells for 5 min at RT. Cells were rinsed twice with ice-cold PBS, scraped off the dishes in 1 ml PBS supplemented with protease inhibitor. After pelleting at 700 x g for 5 min at 4°C, cells were lyzed at a concentration of $2x10^7$ cells/ml in SDS lysis buffer containing protease inhibitor. 250 µl lysate per tube was sonicated to shear DNA to a fragment size of 200 - 1000 bp, using the Sonicator Bioruptor Twin UCD-400 (Diagenode) for 5 cycles of 30 s ON/ 30 s OFF. After sonication, cell debris was pelleted by centrifugation for 10 min at 10,000 x g at 20°C. Supernatant containing the sheared chromatin was aliquoted á 100 µl and either frozen at - 80°C for later use or directly processed. For each antibody in the subsequent immunoprecipitation, one 100 µl aliquot was used and diluted 1: 10 with dilution buffer. Pre-clearing was performed for 1 h at 4 °C using 50 µl blocked Protein G-coupled sepharose beads (1:1 slurry with 20% EtOH) per sample. Supernatant of pelleted beads (3000 x g, 1 min, 4°C) was transferred into a new tube and 1% was removed as input DNA and stored at 4°C. Samples were rotated over night at 4°C with 2.5 µg antibody: human p53 (DO-1, Abcam ab 1101) or isotype control (E5Y6Q, Cell Signaling #61656). For precipitation, protein-DNA complexes were bound to blocked beads (50 µl per sample) for 4 h at 4°C on the next day. Hereafter, beads were washed once with each Low Salt, High Salt and LiCl Immune Complex washing buffers and twice with TE buffer. Crosslinking was reverted by incubating the immunoprecipitated samples and inputs at 99°C for 10 min with 100 µl of 10% (w/v) Chelex 100 solution (in ddH2O). Proteins were digested by proteinase K for 30 min at 55°C and this enzyme was subsequently inactivated at 99°C for 10 min. DNA was eluted in two steps with ddH2O, first with 55 µl and then with 100 µl each time by centrifugation (1 min at 12,000 x g). Analysis of bound DNA fragments was performed using qPCR with 1 µl DNA per reaction with the primer pairs: *BBC3/Puma* 5'-GCGAGACTGTGGCCTTGTGT (sense), 5'- CGTTCCAGGGTCCACAAAG (antisense); *CDKN1A/p21* 5'- AGCAGGCTGTGGCTCTGATT (sense), 5'-CAAAATAGCCACCAGCCTCTTCT (antisense).

RNA seq data analysis

RNA was isolated using the RNeasy Mini kit (Qiagen) and RNA quality was assessed using the Experion RNA StdSens Analysis Kit (Bio-Rad). RNA-seq libraries were prepared from total RNA using the QuantSeq 3′ mRNA-Seq Library Prep Kit FWD for Illumina (Lexogen) in combination with the UMI Second Strand Synthesis Module for QuantSeq FWD (Illumina, Read 1) (Lexogen) according to the manufacturer's instructions. Quality of sequencing libraries was controlled on a Bioanalyzer 2100 using the Agilent High Sensitivity DNA Kit (Agilent). Pooled sequencing libraries were quantified with digital PCR (QuantStudio 3D, Thermo Fisher), sequenced on the NextSeq550 platform (Illumina) with 75 base single reads and archived at EBI ArrayExpress (E-MTAB-10216, E-MTAB-10245).

Unique molecular identifiers (UMI) were extracted from the sequenced reads and the first four nucleotides corresponding to the QuantSeq FWD-UMI 3' spacer were removed. Trimmed reads were mapped to the *Homo sapiens* (revision 96, GRCh38) or *Mus musculus* (revision 92, mm10) Ensembl reference genome, using STAR (version 2.6.1d). After alignment, UMIs were deduplicated using UMI-tools (version 1.0.0), UMI per gene were quantified and normalized to CPM (counts per million). Genes that did not yield a CPM count of at least one in a single sample were discarded. Differential expression was assessed using DEseq2 (version 1.22.2) and obtained p-values were corrected via Benjamini-Hochberg correction. Genes with log2FC ≥ 1 as well as corrected p-values smaller than 0.05 were considered differentially expressed. For heatmaps, expression values were z-transformed and genes were clustered using k-means clustering. Clustering and dimensionality reduction was performed using the sklearn package (version 0.22.1). Gene set enrichment analysis was performed using Molecular Signatures Database (MSigDB) gene sets (Table S1) and GSEA software (version 3.0) [4, 5].

Supplementary References

1 Schlereth K, Beinoraviciute-Kellner R, Zeitlinger MK, Bretz AC, Sauer M, Charles JP *et al*. DNA binding cooperativity of p53 modulates the decision between cell-cycle arrest and apoptosis. *Mol Cell* 2010; 38: 356-368.

2 Timofeev O, Schlereth K, Wanzel M, Braun A, Nieswandt B, Pagenstecher A *et al*. p53 DNA binding cooperativity is essential for apoptosis and tumor suppression in vivo. *Cell Rep* 2013; 3: 1512-1525.

3 Travis WD, Brambilla E, Nicholson AG, Yatabe Y, Austin JHM, Beasley MB *et al*. The 2015 World Health Organization Classification of Lung Tumors: Impact of Genetic, Clinical and Radiologic Advances Since the 2004 Classification. *J Thorac Oncol* 2015; 10: 1243-1260.

4 Liberzon A, Subramanian A, Pinchback R, Thorvaldsdottir H, Tamayo P, Mesirov JP. Molecular signatures database (MSigDB) 3.0. *Bioinformatics* 2011; 27: 1739-1740.

5 Liberzon A, Birger C, Thorvaldsdottir H, Ghandi M, Mesirov JP, Tamayo P. The Molecular Signatures Database (MSigDB) hallmark gene set collection. *Cell Syst* 2015; 1: 417-425.

6 Kato S, Han SY, Liu W, Otsuka K, Shibata H, Kanamaru R *et al*. Understanding the function-structure and function-mutation relationships of p53 tumor suppressor protein by high-resolution missense mutation analysis. *Proc Natl Acad Sci U S A* 2003; 100: 8424-8429.

7 Kotler E, Shani O, Goldfeld G, Lotan-Pompan M, Tarcic O, Gershoni A *et al*. A Systematic p53 Mutation Library Links Differential Functional Impact to Cancer Mutation Pattern and Evolutionary Conservation. *Mol Cell* 2018; 71: 178-190.e178.

SUPPLEMENTARY FIGURES

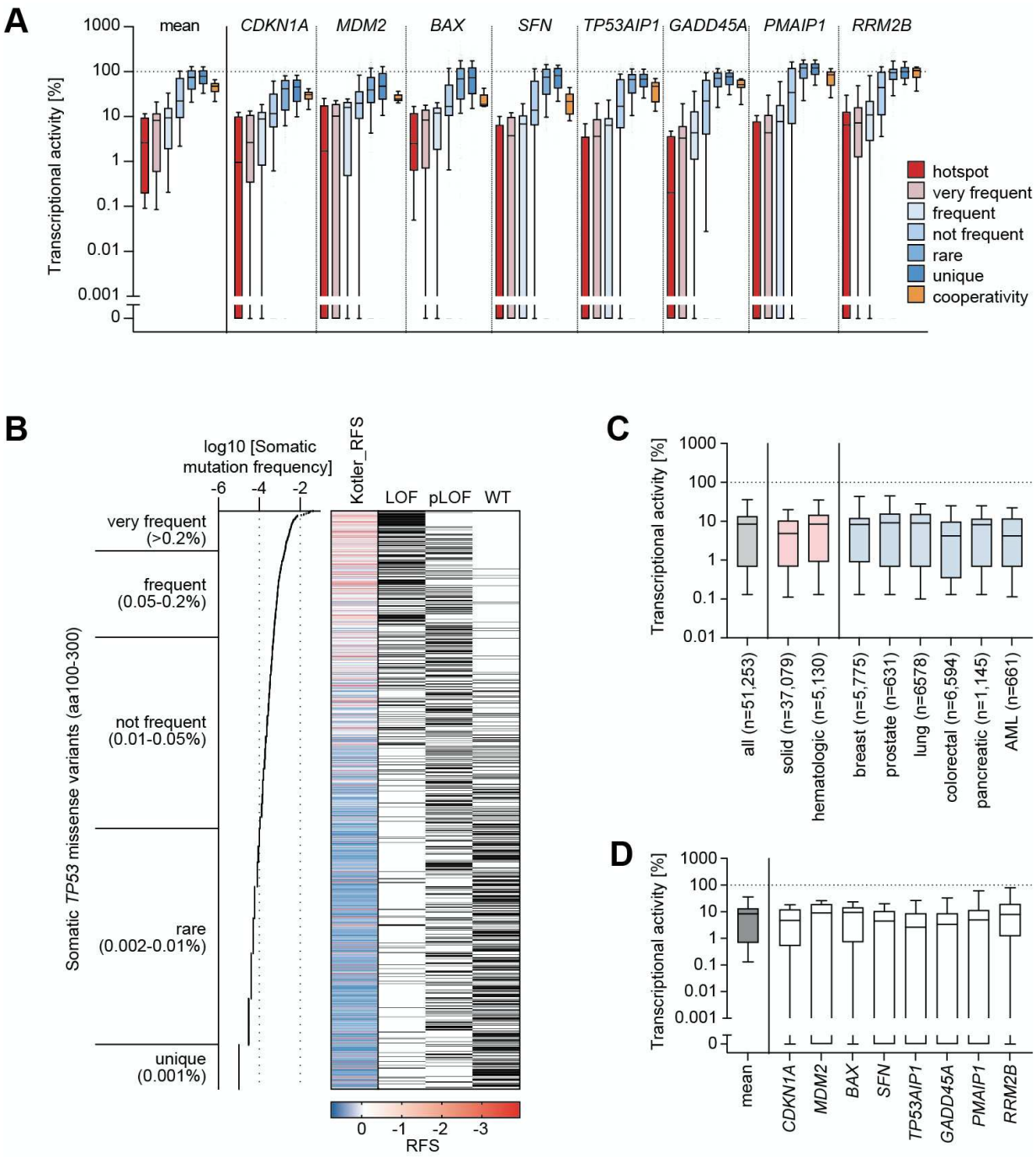

Supplementary Figure S1. Transcriptional activity of 1,209 missense mutations from the UMD p53 mutation database. A, Transcriptional activity of somatic *TP53* mutations grouped according to mutation frequency in cancer patients. **B**, Relative fitness score (RFS) of *TP53* mutations ordered from top to bottom by mutation frequency in cancer patients. LOF, loss of function: RFS>0; pLOF, partial loss of function: 0<RFS<-2; WT, wildtype-like: RFS<-1. **C-D**, Transcriptional p53 activity in cancer patients with *TP53* missense mutations according to **C** tumor type and **D** target gene. Transcriptional activity data from [6], relative fitness scores from [7].

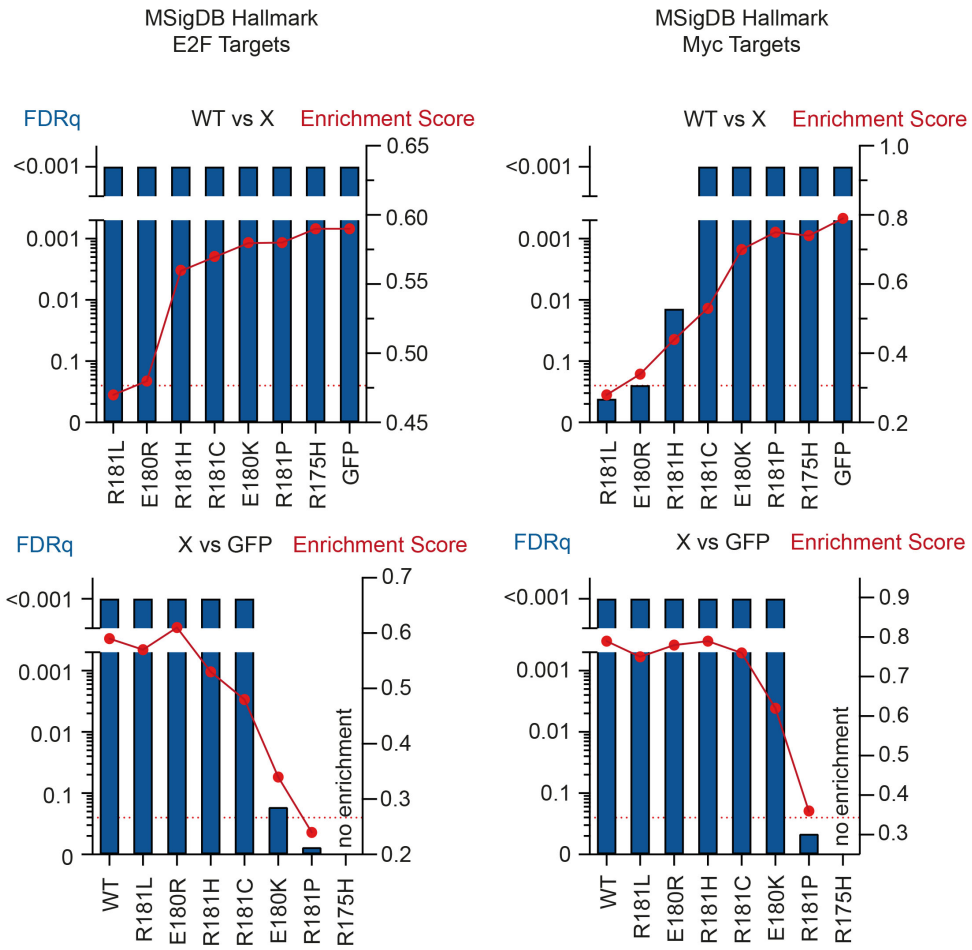

Supplementary Figure S2. Partial loss of transcriptional repression in p53 cooperativity mutants. RNAseq data from Fig. 2A were used for gene set enrichment analysis (GSEA). Depicted are the false discovery rate (FDRq, blue bars) and enrichment score (red curve) for the MSigDB Hallmark E2F and Myc Target gene sets in pairwise comparisons between cells expressing wild-type p53 and different mutants (upper panels) or all variants versus GFP-transfected (p53-null) cells (lower panels).

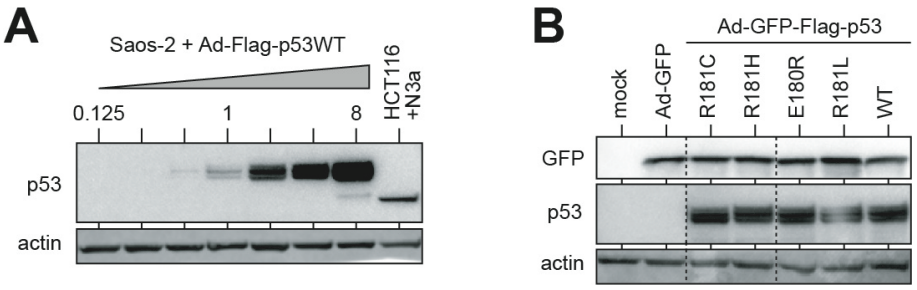

Supplementary Figure S3. Elevated protein levels rescue the transcriptional apoptosis defect of partial-LOF mutants. **A**, Western blot of FLAG-tagged wild-type p53 ectopically expressed in Saos-2 cells upon vector titration (0.125-8X). Protein lysate from p53 wild-type HCT116 cells treated with Nutlin 3a was included as a reference for endogenous p53 expression levels. **B**, WB confirming equal vector load (GFP) and p53 protein levels for all p53 variants ectopically expressed in Saos-2 cells (4X titer is shown).

Journal of Experimental & Clinical Cancer Research

RESEARCH

Open Access

Partial p53 reactivation is sufficient to induce cancer regression

Boris Klimovich[1], Laura Meyer[1], Nastasja Merle[1], Michelle Neumann[1], Alexander M. König[2], Nikolaos Ananikidis[1], Corinna U. Keber[3], Sabrina Elmshäuser[1], Oleg Timofeev[1,4*†] and Thorsten Stiewe[1,4,5*†]

Abstract

Background: Impaired p53 function is one of the central molecular features of a tumor cell and even a partial reduction in p53 activity can increase the cancer risk in mice and men. From a therapeutic perspective it is noteworthy that tumor cells often become addicted to the absence of p53 providing a rationale for developing p53 reactivating compounds to treat cancer patients. Unfortunately, many of the compounds that are currently undergoing preclinical and clinical testing fail to fully reactivate mutant p53 proteins, raising the crucial question: how much p53 activity is needed to elicit a therapeutic effect?

Methods: We have genetically modelled partial p53 reactivation using knock-in mice with inducible expression of the p53 variant E177R. This variant has a reduced ability to bind and transactivate target genes and consequently causes moderate cancer susceptibility. We have generated different syngeneically transplanted and autochthonous mouse models of p53-deficient acute myeloid leukemia and B or T cell lymphoma. After cancer manifestation we have activated E177R expression and analyzed the in vivo therapy response by bioluminescence or magnetic resonance imaging. The molecular response was further characterized in vitro by assays for gene expression, proliferation, senescence, differentiation, apoptosis and clonogenic growth.

Results: We report the conceptually intriguing observation that the p53 variant E177R, which promotes de novo leukemia and lymphoma formation, inhibits proliferation and viability, induces immune cell infiltration and triggers cancer regression in vivo when introduced into p53-deficient leukemia and lymphomas. p53-deficient cancer cells proved to be so addicted to the absence of p53 that even the low-level activity of E177R is detrimental to cancer growth.

Conclusions: The observation that a partial loss-of-function p53 variant promotes tumorigenesis in one setting and induces regression in another, underlines the highly context-specific effects of individual p53 mutants. It further highlights the exquisite sensitivity of cancer cells to even small changes in p53 activity and reveals that changes in activity level are more important than the absolute level. As such, the study encourages ongoing research efforts into mutant p53 reactivating drugs by providing genetic proof-of-principle evidence that incomplete p53 reactivation may suffice to elicit a therapeutic response.

Keywords: p53, Tumor suppressor gene, p53 reactivation, Molecular therapy, Leukemia, Lymphoma, Mouse models

Background

The tumor suppressor gene *TP53* encodes the p53 transcription factor, which regulates target genes in multiple pathways to counteract the expansion of malignant cells [1–3]. p53 thereby poses a major barrier to tumor development, explaining why tumorigenesis strongly selects

*Correspondence: timofeev@staff.uni-marburg.de; stiewe@uni-marburg.de
†Oleg Timofeev and Thorsten Stiewe contributed equally to this work.
[1] Institute of Molecular Oncology, Universities of Giessen and Marburg Lung Center (UGMLC), Philipps-University, Marburg, Germany
[5] Genomics Core Facility, Philipps-University, Marburg, Germany
Full list of author information is available at the end of the article

for cells with inactivated p53 [3]. Loss of p53 function (LOF) can result from p53 degradation or sequestration by viral oncoproteins or cellular inhibitors like Mdm2 or Mdmx [4, 5]. In approximately 50% of all tumors, LOF is caused by somatically acquired genetic alterations affecting the *TP53* gene directly [5]. This includes large deletions encompassing the entire gene as well as small non-sense, frameshift or missense mutations, which can differ massively in their functional impact [5, 6]. Different from other tumor suppressor genes, most *TP53* mutations are missense mutations, explained in part by dominant-negative and tumor-promoting neomorphic (gain-of-function, GOF) properties of at least some of the mutant proteins [7–10]. Of note, full p53 activity is essential for optimal tumor suppression as even a partial loss of p53 function increases the cancer risk in mice and causes hereditary cancer susceptibility in humans [11–17].

Importantly, restoration of p53 in p53-deficient tumor cells was found to be detrimental, usually resulting in cell death or loss of proliferative capacity due to senescence or differentiation [18]. For example, in p53ER^{TAM} mice with tamoxifen-switchable p53 activity, EμMyc-driven Burkitt-like lymphomas develop in the p53-off state, but undergo rapid regression when p53 is switched on [19]. This was observed even when p53 inactivation was not the tumor-initiating driver lesion and acquired only later during tumor progression [20]. Together with other studies in independent mouse cancer models, this firmly established that tumor cells can become addicted to the loss of p53 [21–24]. Moreover, these studies demonstrated the therapeutic potential of p53 reactivation and provided critical support for the development of p53-reactivating drugs as cancer therapeutics [25, 26].

Meanwhile a growing number of p53 reactivating compounds has been developed. While Mdm2 and Mdmx inhibitors are being evaluated for treatment of tumors with wild-type p53, diverse strategies have been proposed to target tumors with *TP53* mutations [25, 26]. As straightforward as reactivation may seem, as challenging it turns out in practice. The most common *TP53* mutations either destroy DNA contact residues or destabilize the thermodynamically labile p53 DNA binding domain and cause its denaturation at normal body temperature [27]. The most direct reactivation approaches aim to refold the pool of mutant p53 proteins, that have accumulated in the tumor cells, into a native conformation [28, 29]. However, as more than 2000 different mutant proteins have been identified in cancer patients, a universal reactivation strategy is unrealistic. As such, many reactivation compounds target only single or groups of mutants [30]. For example, PhiKan083 specifically targets a surface crevice created by the Y220C mutation [31]. Metallochaperones increase the intracellular availability of zinc to rescue folding of zinc-binding site mutants like R175H [32]. Arsenic trioxide (ATO) binds to a cryptic allosteric site formed by Arsenic-coordinating cysteines and stabilizes the native fold of a subset of p53 mutants [33]. The clinically most advanced compound APR-246 (PRIMA-1^{Met}, Eprenetapopt), is converted to the thiol-reactive metabolite methylene quinuclidinone (MQ) and proposed to alkylate and thereby reactivate structural mutants, but also, in a mechanistically poorly understood manner, some DNA contact mutants [34–36]. In combination with azacytidine, APR-246 showed promising therapeutic responses in phase II studies involving myelodysplastic syndrome (MDS) and acute myeloid leukemia (AML) patients [37, 38]. However, MQ also reacts with numerous other cellular cysteines, forming a thiol-bound drug reservoir, and through depletion of glutathione (GSH) and inhibition of the GSH and thioredoxin antioxidant systems exhibits cytotoxic activities [39, 40]. Other reactivating compounds also display considerable p53-independent toxicity that certainly adds to, if not determines, the therapeutic effects [30]. This raises the critical question: how much of the observed cytotoxicity is due to p53 reactivation [18]? Last but not least, the mutant p53 refolding activity of various reactivating compounds differs by at least two orders of magnitude not only between compounds but also between individual mutants [33]. Together these findings indicate that pharmacological mutant p53 reactivation is continuously improving, but is currently still far from optimal. This brings up an even more important question: to what extent does p53 have to be restored [18]? Is full reactivation required to achieve a therapeutic response or is partial reactivation already sufficient?

Here, we have modelled partial p53 reactivation using a conditional knock-in mouse with inducible expression of the partial LOF variant p53^{E177R} (short: E177R), which corresponds to human E180R. The E177R mutation disrupts an intermolecular salt-bridge with R178 (human R181) that is required for cooperative DNA binding [41–43]. The decrease in cooperativity reduces DNA binding and target gene activation [15, 44, 45]. As a result, E177R causes cancer susceptibility and cooperates with various oncogenes to promote cancer development, including lung and pancreatic adenocarcinoma and various types of leukemia and lymphoma [15, 43, 46, 47]. Here, we report that in p53-deficient leukemia and lymphoma models the effects of E177R expression are entirely opposite: E177R inhibits cell proliferation and viability and induces cancer regression. p53-deficient cancer cells prove to be so addicted to the absence of p53 that the residual activity

of E177R is detrimental for cancer growth. As such, the study provides genetic proof-of-concept that incomplete p53 reactivation can make a therapeutic impact.

Materials and methods

Animal experiments

All mouse experiments were performed according to the German Animal Welfare Law (TierSchG) and were approved by the local authorities. Mice were housed in open cages, on a 12 h light/dark cycle, fed a standard housing/breeding diet (Altromin) and received water ad libitum. The following mouse strains were used: B6.129S/Sv-Trp53tm1Thst (*Trp53*$^{LSL\text{-}E177R}$) [15], B6.129-Gt (ROSA)26Sortm1(cre/ERT2)Tyj/J (CreER^{T2}) [22], B6.Cg-Tg (IghMyc)22Bri/J (EμMyc) [48], and B6.129-Trp53 < tm1Brd>/TacThst (p53KO) [49]. In transplantation experiments, F1 hybrids of C57BL/6 J (B6) and 129S1/SvImJ (129) or B6(Cg)-Tyrc-2 J/J (B6 albino) and 129X1/SvJ (129 albino) were used as recipients. Generation of the leukemia and lymphoma, monitoring of disease development by bioluminescence imaging (BLI) and therapy were performed as described earlier [50].

For the AML model with Cre-inducible expression of p53^{E177R}, double-heterozygous *Trp53*$^{LSL\text{-}E177R/+}$; Rosa26$^{CreERT2/+}$ mice were intercrossed. Fetal liver cells from *Trp53*$^{LSL\text{-}E177R/LSL\text{-}E177R}$; Rosa26^{CreERT2} embryos (E14–16) were isolated, transduced with retroviruses expressing the *AML1/ETO9a* fusion oncogene (co-expressed with GFP) and *Nras*^{G12D} oncogene (co-expressed with firefly luciferase) and 10^6 cells were transplanted into 129 albino recipients as described [46, 50]. Recipients were lethally irradiated (7 Gy) 24 h before transplantation using the X-RAD 320iX system. Recipients were provided with neomycin-supplemented water (1.6 g ml^{-1}, pH 3) starting 2 days before transplantation until 3 weeks after. For in vivo p53 reactivation, recipient 129 albino/B6 albino F1 hybrid mice were sublethally irradiated and injected i.v. with 10^6 AML cells. Both male and female mice were used as recipients for female AML cells with and without reactivatable p53. Leukemia progression was monitored by BLI: mice were imaged under isoflurane anesthesia 5 min after i.p. injection of 100 μl of D-luciferin solution (15 mg ml^{-1}) using an IVIS 100 imaging system (Xenogen).

For the EμMyc lymphoma model, double-heterozygous *Trp53*$^{LSL\text{-}E177R/+}$; *Rosa26*$^{CreERT2/+}$ females were bred with EμMyc transgenic males. Lymphomas from EμMyc; *Trp53*$^{LSL\text{-}E177R/LSL\text{-}E177R+}$ offspring mice with or without CreER^{T2} were used for transplantation into 129/B6 F1 hybrid recipient mice as described [50]. After disease onset was confirmed by palpation of enlarged mandibular, axillary or subiliac lymph nodes, mice were treated 1 week with daily i.p. injections of 1 mg tamoxifen. Mice were euthanized when pre-defined humane endpoint criteria were reached. Control experiments for Cre-mediated toxicity were performed with EμMyc; *Rosa26*$^{CreERT2/+}$ lymphomas. Both male and female donor and recipient mice were used.

For the spontaneous T-lymphoma model, both male and female *Trp53*$^{LSL\text{-}E177R/LSL\text{-}E177R}$; *Rosa26*^{CreERT2} mice were examined with magnet-resonance tomography using 7 T Clinscan 70/30 USR (Bruker) as described [51]. T2 weighted sequences triggered on respiration in transverse and coronal orientation were used for anatomical imaging of the thymus. The total measurement time was approximately 28 min per mouse. Tumor size was measured using RadiAnt DICOM Viewer and tumor volume was calculated with the ellipsoid formula V = 4/3*π*abc. *Trp53*$^{LSL/LSL}$ mice without Cre were used as a control cohort. The first imaging was performed at the age of 120 days or earlier for mice that showed clinical symptoms of thymic lymphoma (weight loss, hunchback posture, shortness of breath).

For reactivation of E177R expression via Cre-mediated recombination in vivo, mice were injected i.p. for 7 consecutive days with 100 μl of 10 mg ml^{-1} tamoxifen (Sigma) in sterile corn oil. For mock treatment, mice were injected with 100 μl of corn oil only.

Cell culture

For generation of mouse AML cell lines, primary tumors (spleen, bone marrow) were mechanically disrupted by mashing through 70 μm EASYstrainer (Greiner). After erythrocyte lysis (5 min at RT in ACK buffer, Thermo Fisher), cells were collected by centrifugation, resuspended and cultured in B-cell medium (DMEM:IMDM 1:1, Life Technologies), 20% fetal bovine serum (FBS, Sigma-Aldrich), 100 U ml^{-1} penicillin/streptomycin (Life technologies), 5×10^{-5} M 2-mercaptoethanol) supplemented with 0.2 ng ml^{-1} murine IL3, 2 ng ml^{-1} IL6 and 20 ng ml^{-1} SCF (all from Immunotools). Cells were maintained on multi-well plates for suspension cells (Greiner) at ambient oxygen in a humidified cell culture incubator (37 °C with 5% CO_2). For colony formation assay, 50,000 cells were plated in MethoCult™ GF M3434 medium (STEMCELL Technologies, 1.5 ml per well on 6-well plate) and colonies were counted after 7 days.

CRISPR-Cas9

For generation of AML cells with CRISPR-mediated p53 knock-out, *Trp53*$^{LSL\text{-}E177R/LSL\text{-}E177R}$; *Rosa26*^{CreERT2} leukemia cells were transduced with pMSCV-Cas9-Blast retrovirus. For pMSCV-Cas9-Blast plasmid, the puromycin resistance (*pac*) gene in the pMSCV-Cas9-Puro plasmid (RRID: Addgene_65655) was replaced with the blasticidin-S resistance gene (*bsr*) PCR-amplified from

lentiCas9-Blast plasmid (RRID: Addgene_52962) using primer pair 5′-catgcAAGCTTccaccatggccaagcctttgtctcaag and 5′-gatcgATCGATttagccctcccacacataacc using HindIII and ClaI restriction sites, respectively. MSCV-Cas9-Blast retrovirus was packaged using Platinum-E cells as described [51] and used for spin-infection in B-cell medium supplemented with 6 µg ml^{-1} polybrene (Sigma). AML cells were spin-infected 4 times (600×g, 40 min) in 24-well tissue culture plates (Greiner) coated with 40 µg ml^{-1} RetroNectin (Takara). After 1 week of selection with 50 µg ml^{-1} Blasticidin S (Invivogen), 5000 cells were plated on 35 mm tissue culture dish (Greiner) in MethoCult™ GF M3434 medium and grown for 2 weeks. Single colonies were picked, expanded and screened for Cas9 expression by Western blotting. One validated single cell clone (AML-Cas9) was used for CRISPR editing. Oligos, encoding control (scrambled) sgRNA (sense 5′-caccgaaatgtgagatcagagtaat-3′, antisense 5′-aaacattactctgatctcacatttc-3′) or sgRNA targeting *Trp53* locus [50], were cloned into lentiviral SGL40C.EFS.RFP657 vector (gift from Dirk Heckl, RRID:Addgene_69147 [52]) via BsmBI site using Golden Gate cloning. Lentiviruses were produced in HEK293-T cells and used for infection of the AML-Cas9 cell clone [20]. Infection efficiency was analyzed by flow cytometry for RFP 48 h after infection and the pool of cells was directly used for transplantation. CRISPR-mediated *Trp53* knock-out was confirmed by Sanger sequencing and InDel analysis using the TIDE algorithm [53].

Flow cytometry

Immunophenotyping and analysis of differentiation of leukemia cells was performed as described [50] on an Accuri C6 Plus flow cytometer (BD Biosciences) with the following antibodies: mouse Gr1-PE (Milteny Biotec #130–102-426, RRID: AB_2659861), mouse CD11b-APC (Milteny Biotec #130–091-241, RRID: AB_244268), mouse Ly-6A/E (Sca-1)-PE/Cy5 (BioLegend #108109, RRID: AB_313346), mouse CD117 (c-kit)-PE (BioLegend #105807, RRID: AB_313217), Rat IgG2a, κ Isotype Ctrl-PE/Cy5 (BioLegend #400509), Rat IgG2b, κ Isotype Ctrl-PE (BioLegend #400607; RRID: AB_326551). BrdU labeling of S-phase cells and flow cytometry analysis were done using A488-conjugated anti-BrdU antibodies (BD Biosciences #347580, RRID: AB_400326) as described [50]. For apoptosis assay, Annexin V-APC (MabTag) or CaspGLOW™ Red Active Caspase-3 Staining Kit (Biovision) kits were used according to the manufacturer's protocols.

Immunohistochemistry and western blot

Immunoblotting (WB) was performed as described [15]. Cells were lysed in NP-40 lysis buffer (50 mM Tris-HCl, 150 mM NaCl, 5 mM EDTA, 2% NP-40, pH 8.0) supplemented with protease inhibitor (cOmplete ULTRA tablets EASYpack, Roche) and phosphatase inhibitor (PhosSTOP, Roche). For WB the following antibodies were used: anti-p53 (NCL-p53–505, Leica Microsystems, 1:2000, RRID: AB_563932), anti-p21 (F-5, #sc-6246, Santa-Cruz, 1:200, RRID: AB_628073), anti-Cas9 (E7M1H, #19526, Cell Signaling, 1:1000, RRID: AB_2798820), anti-β-actin (AC-15, #ab6276, Abcam, 1:10000, RRID: AB_2223210). Secondary anti-mouse or anti-rabbit IgG-HRP (GE Healthcare, 1:5000) and Super-Signal ECL kit (Thermo Fisher) were used for detection. Tissue samples for histology and immunohistochemistry (IHC) were formalin-fixed and processed as described before [15]. For IHC the following antibodies and kits were used: anti-cleaved caspase-3 (#9661, Cell Signaling, 1:100, RRID: AB_2341188), DeadEnd TM colorimetric TUNEL System (Promega), anti-p53 (NCL-p53–505, Leica Microsystems, 1:1000, RRID: AB_563932), anti-GFP (ab6556, Abcam, 1:500, RRID: AB_305564), anti-BrdU (BU1/75(ICR1), #OBT0030G, Bio-Rad, 1:100, RRID: AB_609567) and biotinylated rabbit anti-mouse IgG (31,834, Invitrogen, 1:500). Detection of senescence-associated β-galactosidase activity (SA-βGal) in frozen tissue sections and in cytospin samples was performed as described [15, 50]. Images were acquired using the Leica Aperio Versa slide scanner and Leica Aperio eSlide Manager software v. 1.0.3.37. Aperio ImageScope software v. 12.3.2.8013 was used for IHC image analysis, quantification was performed using Positive Pixel Count Algorithm v.9 and calculated as the ratio $N_{positive}/N_{total}$ pixels in 10 fields of view (1000X1000 pixel each) per sample relative to the mean of the untreated samples as baseline.

PCR and RT-PCR

PCR detection of the LSL cassette and Cre-mediated recombination in the targeted *Trp53* allele was done as described [15]. For reverse-transcription real-time PCR (RT-qPCR) RNA was isolated from cells or tissue samples using the RNeasy Mini Kit (Qiagen) and cDNA was generated with the SuperScript VILO cDNA Synthesis Kit (Invitrogen). Gene expression was analyzed on a LightCycler 480 (Roche) using SYBR Green (Thermo Fisher Scientific) and primers specific for mouse *Trp53*, *Cdkn1a/p21*, *Ccng1*, *Bbc3/Puma*, *β-Actin/Actb* [50]. Data were evaluated by the ΔΔCt method using β-actin gene expression for normalization.

Chromatin immunoprecipitation (ChIP)

AML cells were treated and fixed after 48 h with freshly prepared 18.5% (w/v) paraformaldehyde (PFA) for 10 min at RT, aiming at a final concentration of 0.88% (v/v) PFA. Crosslinking of DNA and proteins was terminated

by quenching unreacted PFA by addition of glycine to 125 mM end concentration and further incubation for 5 min at RT. Cells were pelleted by centrifugation at 300 x g for 10 min at 4 °C, washed twice with ice-cold PBS and lysed at a concentration of 2×10^7 cells ml^{-1} in SDS lysis buffer containing protease inhibitor. 250 µl lysate per tube was sonicated to shear DNA to a fragment size of 200–1000 bp, using the Sonicator Bioruptor Twin UCD-400 (Diagenode) for 5 cycles of 30 s ON/ 30 s OFF. After sonication, cell debris was pelleted by centrifugation for 10 min at 10,000 x g at 20 °C. Supernatant containing the sheared chromatin was aliquoted á 100 µl and either frozen at − 80 °C for later use or directly processed. For each antibody, one 100 µl aliquot was used and diluted 1:10 with dilution buffer. Pre-clearing was performed for 1 h at 4 °C using 50 µl blocked Protein G-coupled Sepharose beads (GE Healthcare, 1:1 slurry with 20% EtOH) per sample. Supernatant of pelleted beads (3000 x g, 1 min, 4 °C) was transferred into a new tube and 1% was removed as input DNA and stored at 4 °C. Samples were rotated over night at 4 °C with 2.5 µg antibody: p53 (FL393, Santa Cruz sc-6243) or isotype control (E5Y6Q, Cell Signaling #61656). For precipitation, protein-DNA complexes were bound to blocked beads (50 µl per sample) for 4 h at 4 °C. Beads were washed once with each Low Salt, High Salt and LiCl Immune Complex washing buffers and twice with TE buffer. Crosslinking was reverted by incubating immunoprecipitated samples and inputs at 99 °C for 10 min with 100 µl of 10% (w/v) Chelex 100 solution. Proteins were digested with proteinase K for 30 min at 55 °C and this enzyme was subsequently inactivated at 99 °C for 10 min. DNA was eluted in two steps with ddH_2O, first with 55 µl and then with 100 µl each time by centrifugation (1 min at 12,000 x g). Analysis of bound DNA fragments were performed using qPCR with 1 µl DNA per reaction using primers specific for p53 response elements in the *Cdkn1a/p21*, *Bax* and *Bbc3/Puma* genes.

Statistical analysis

For statistical analysis the GraphPad Prism 8 software was used. Graphs show mean values obtained with n technical or biological replicates, and error bars in all figures represent standard deviation (SD), unless indicated otherwise. Two groups were tested for statistically significant differences by a two-sided unpaired t-test or, if not normally distributed, by a Mann-Whitney test. Multiple groups were tested by 1way ANOVA in conjunction with a Dunnett's multiple comparisons test. *P*-values of 1way ANOVA and selected pairwise comparisons are reported in the respective figures. Three or more groups that have been split on two independent variables (here treatment and genotype) were analyzed by 2way ANOVA in conjunction with Sidak's multiple comparisons test. *P*-values for the interaction effect between the two independent variables and *P*-values of selected pairwise comparisons are reported in the figures. Survival data were analyzed with pairwise Log-rank (Mantel-Cox) tests. A p-value < 0.05 was used as level of significance.

Results

Leukemia model for partial p53 reactivation

To model the therapeutic effect of partial p53 reactivation, we have used a previously described genetic Cre-mediated recombination approach to activate a conditional p53 allele in p53-deficient tumor cells [22]. In contrast to earlier studies based on restoration of wild-type p53 [19, 21, 22], we have used a conditional knock-in allele for the p53 partial loss-of-function variant E177R ($Trp53^{LSL\text{-}E177R}$) in combination with the $Rosa26^{CreERT2}$ transgene, which constitutively expresses tamoxifen-regulated $CreER^{T2}$ [15, 22] (Fig. 1a). The inducible $CreER^{T2}$ recombinase can be activated at will by tamoxifen in vivo, or 4-hydroxytamoxifen (4OHT) in vitro, to excise the lox-stop-lox (LSL) cassette that silences expression of the $Trp53^{LSL\text{-}E177R}$ locus, thus triggering expression of the E177R protein (Fig. 1b). We transduced fetal liver cells from $Trp53^{LSL\text{-}E177R;LSL\text{-}E177R}$;$Rosa26^{CreERT2}$ mice with two bicistronic retroviral constructs – one expressing $Nras^{G12D}$ and firefly luciferase, the second *AML1/ETO9a* and EGFP, and transplanted them into lethally irradiated recipient mice as previously described [46] (Fig. 1a). The mice developed acute myeloid leukemia within 1–2 months. As a control for p53-independent toxicity of tamoxifen and DNA damage induced by Cre, we simultaneously generated $CreER^{T2}$-expressing AML with a constitutive p53 knock-out (KO).

Partial p53 reactivation inhibits leukemia proliferation and viability

p53-deficient leukemia cells were explanted and further propagated ex vivo. In LSL-E177R;$CreER^{T2}$ (short: LSL) leukemia cells, 4OHT induced excision of the lox-stop-lox (LSL) cassette and resulted in expression of E177R at the mRNA and protein level (Fig. 1c-e). This was accompanied by significantly enhanced expression of p53 target genes such as the cyclin-dependent kinase inhibitor *p21/Cdkn1a.* Of note, we also observed significant induction of several pro-apoptotic target genes including *Bax, Bbc3/Puma* and *Pmaip1/Noxa* (Fig. 1e). As E177R has previously been reported to be unable to bind and transactivate pro-apoptotic target genes [15], we also analyzed binding of E177R to chromatin (Fig. 1f). We not only detected significant levels of E177R binding to the *p21/Cdkn1a* promoter, but also to the *Bax* promoter (Fig. 1f). Moreover, there was also a trend for binding to the *Bbc3/*

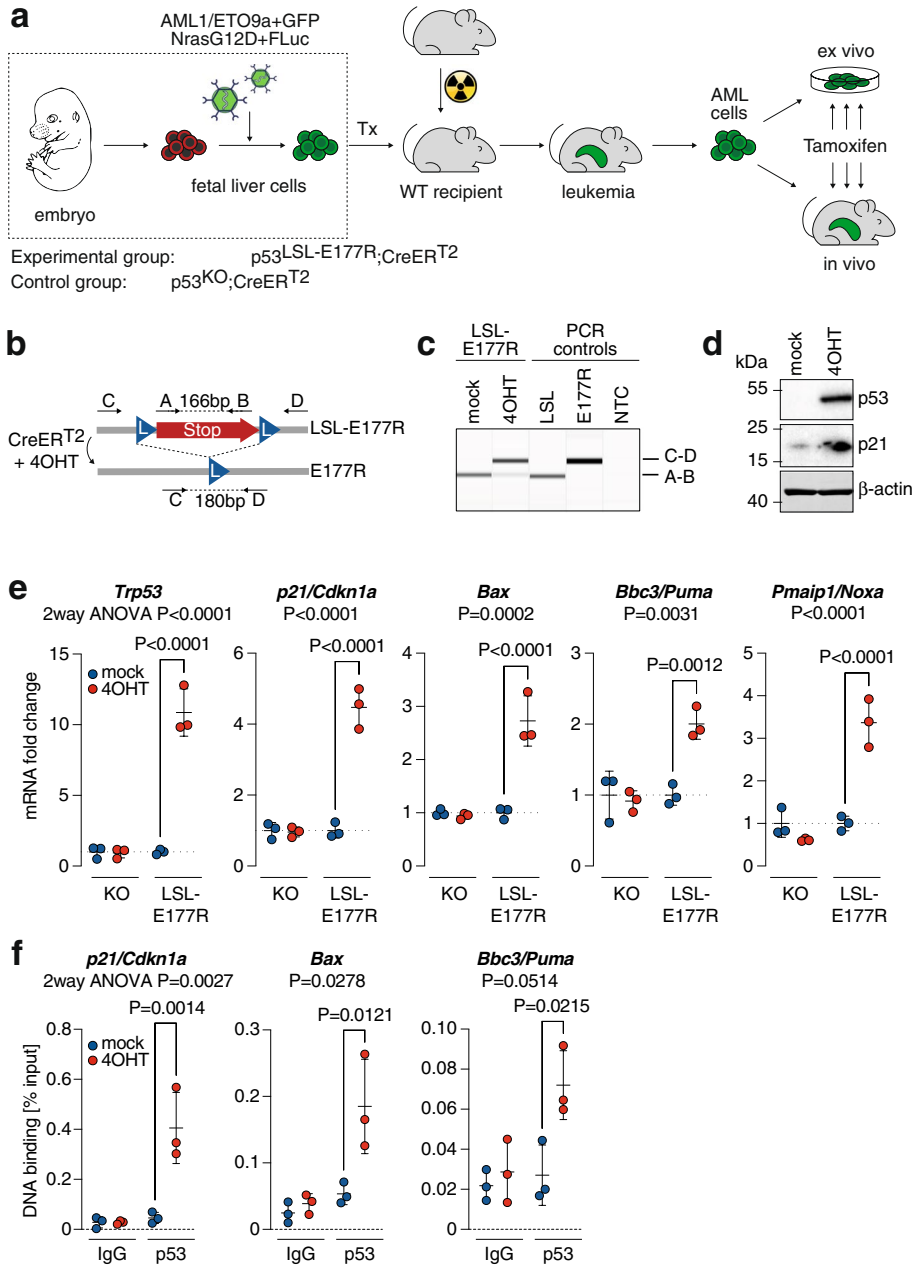

Fig. 1 Acute myeloid leukemia model with inducible reactivation of the partial LOF variant p53^{E177R}. **a** Experimental outline for in vivo generation of AML by retroviral transduction of fetal liver cells from embryos expressing CreER^{T2} together with constitutive p53 knockout (KO) or Cre-inducible partial LOF p53 variant E177R (LSL-E177R). Leukemia, that developed after transplantation of transduced FLCs into irradiated wild-type recipient mice, was further propagated ex vivo for cell culture studies or transplanted into secondary recipients for in vivo reactivation experiments. **b** Scheme depicting CreER^{T2}-mediated excision of the floxed stop cassette (LSL), which silences p53 expression in the LSL-E177R allele. Shown are primers A-D used for genotyping and validating Cre-mediated recombination of the *Trp53* gene locus. **c** PCR genotyping: switch from the A-B to C-D PCR product reveals efficient recombination in *Trp53*$^{LSL-E177R/LSL-E177R}$; *Rosa26*^{CreERT2} AML cells upon 48 h treatment with 1 µM 4OHT. **d** Immunoblot demonstrating induction of p53 and p21/Cdkn1a protein expression upon 4OHT treatment of LSL-E177R; CreER^{T2} (short: LSL) AML cells. β-actin is shown as a loading control. **e** Quantitative reverse transcription PCR for *Trp53* and p53 target gene induction in LSL-E177R; CreER^{T2} and KO; CreER^{T2} AML cells 48 h after treatment with 4OHT. Data were normalized to *Actb* and mock treatment. **f** Chromatin immunoprecipitation analysis of p53 at the indicated target gene promoters 48 h after 4OHT or mock treatment. Chromatin samples were immunoprecipitated with α-p53 antibody (FL393) or IgG as background control. Shown is DNA binding as % input chromatin. **e**-**f** Shown are mean ± SD; datapoints represent biological replicates ($n = 3$); reported are 2way ANOVA *P*-values for the interaction between the two independent variables treatment and genotype and *P*-values for indicated pairwise comparisons (Sidak's multiple comparisons test)

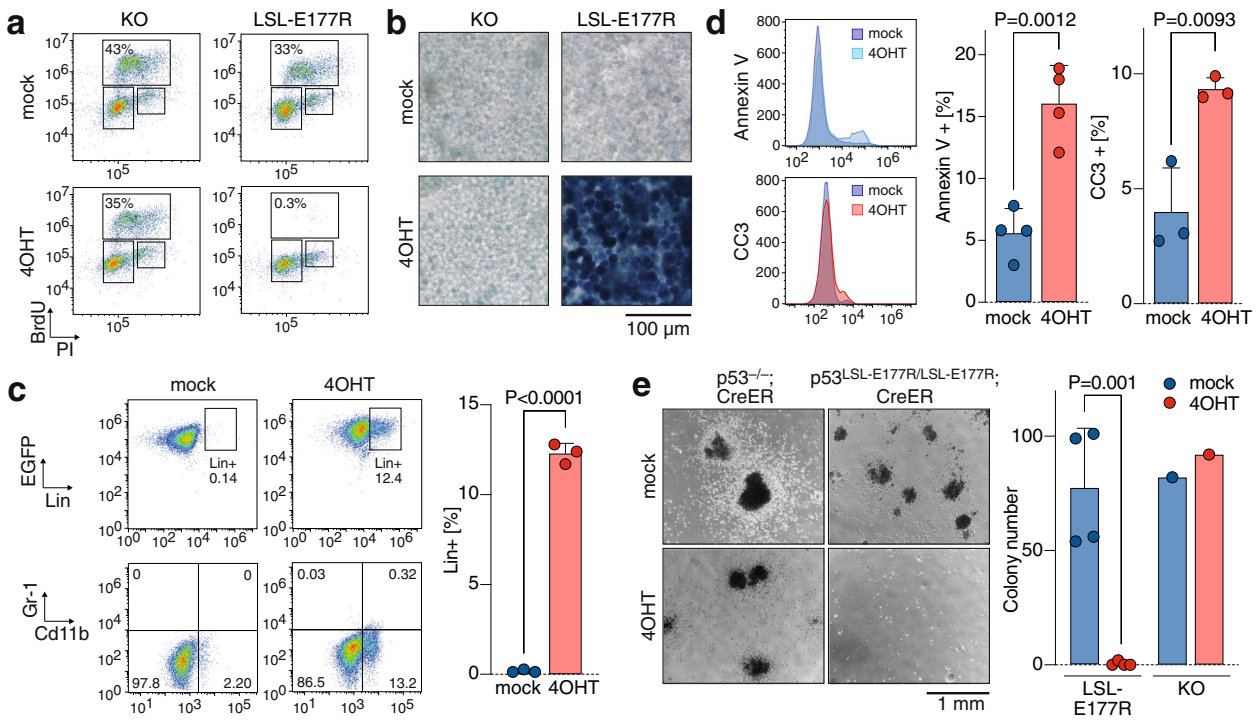

Fig. 2 In vitro response of p53-deficient AML to E177R activation. **a** Flow cytometry of BrdU and propidium iodide (PI)-stained LSL-E177R; CreER^{T2} (LSL) AML cells 72 h after indicated treatment. KO; CreER^{T2} (KO) AML cells are shown as controls. The percentage of cells in S phase is indicated. **b** Senescence-associated β-galactosidase staining of LSL and KO AML cells 1 week after indicated treatment. **c** Flow cytometry of LSL AML cells stained for differentiation markers (Lin, CD11b, Gr-1) 48 h after indicated treatment. **d** Flow cytometry of LSL AML cells stained for the apoptosis markers annexin V and cleaved caspase-3 (CC3) 48 h after indicated treatment. **e** Clonogenic growth assay of AML cells with indicated genotype and treatment grown in MethoCult medium for 1 week. In all experiments, cells were treated with 1 µM 4OHT or solvent (ethanol) as the mock control. All quantification bar graphs show mean ± SD; datapoints represent biological replicates; reported are *P*-values of a two-tailed unpaired t-test

Puma promoter that reached statistical significance only in a pairwise comparison (Fig. 1f). Notably, no target gene activation was observed in control KO;CreER^{T2} (short: KO) leukemia cells (Fig. 1e).

Consistent with previous reports demonstrating that E177R is proficient in regulation of cell cycle and senescence [15], activation of E177R inhibited cell cycle progression, resulting in a strongly reduced number of cells in S phase, which was not observed upon tamoxifen treatment of control KO cells (Fig. 2a). At later time points, we observed a massive accumulation of senescent cells marked by expression of senescence-associated beta-galactosidase selectively in tamoxifen-treated LSL but not KO cells (Fig. 2b). Moreover, as induction of differentiation is a recognized tumor-suppressive mechanism exerted by wild-type p53 [21, 54], we tested for signs of differentiation. We observed an increase of the lineage-positive population after 7 days of 4OHT treatment, in particular an enrichment of the population of CD11b-positive cells indicating myeloid differentiation (Fig. 2c). Consistent with robust transactivation of pro-apoptotic target genes (Fig. 1e, f), we also noticed a significant drop in viability of LSL leukemia cells after 4OHT treatment and flow cytometry revealed induction of the apoptosis markers annexin V and cleaved-caspase 3 after expression of E177R (Fig. 2d). Importantly, activation of E177R abolished the clonogenicity of leukemia cells in 3D culture, whereas KO cells remained unaffected excluding p53-independent toxicity of 4OHT or Cre as a cause (Fig. 2e). Together, these experiments demonstrate that genetic reactivation of E177R induces multiple tumor-suppressive programs in AML cells that induce cell cycle withdrawal or cell death and prevent clonogenic expansion.

Partial p53 reactivation induces leukemia regression

Encouraged by the in vitro data, we transplanted LSL and KO AML cells (both containing CreER^{T2}) into sublethally irradiated recipient mice and monitored transplant engraftment, leukemia progression and therapy response by bioluminescence imaging (BLI) of the firefly luciferase co-expressed with *Nras*^{G12D}

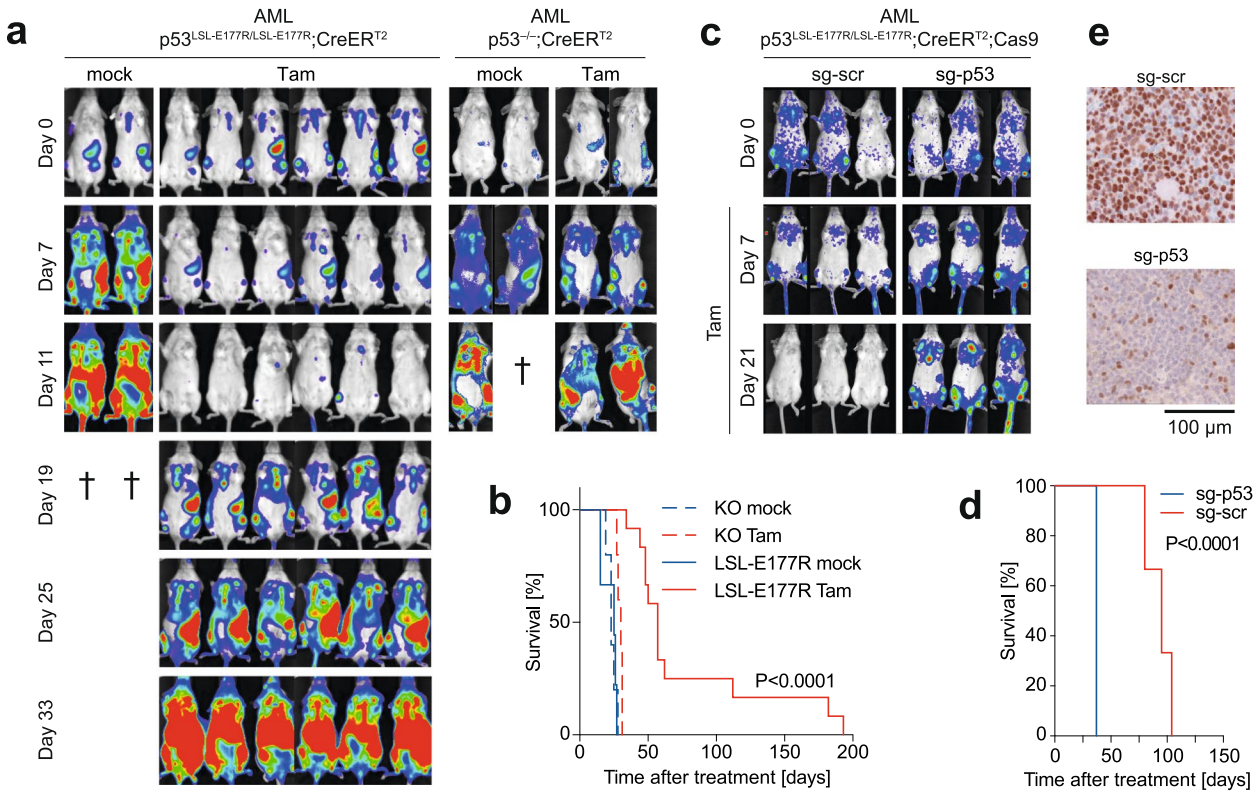

Fig. 3 E177R activation induces regression of p53-deficient AML in vivo. **a**-**b** 10^6 AML cells of indicated genotype were transplanted into sublethally irradiated 129X1 albino x B6 albino (F1 hybrid) mice. After engraftment was confirmed by bioluminescence imaging (BLI), mice were treated 1 week with daily i.p. injections of either vehicle (corn oil) or 1 mg tamoxifen. Mice were euthanized when humane endpoint criteria were reached. **a** BLI of representative mice. **b** Kaplan-Meier survival graph. Log-rank (Mantel-Cox) test for LSL mock vs. Tam. **c**-**d** 10^6 LSL-Cas9 AML cells transduced ex vivo with lentivirus encoding either *Trp53*-directed sgRNA (sg-p53) or scrambled control sgRNA (sg-scr) were transplanted into mice as in **a** and treated 1 week with daily i.p. injections of 1 mg tamoxifen. Mice were euthanized when humane endpoint criteria were reached. **c** BLI of both cohorts. **d** Kaplan-Meier survival graph. Log-rank (Mantel-Cox) test. **e** Immunohistochemistry for p53 of relapsed leukemia samples from both cohorts

(Fig. 3 a). After detection of bioluminescence in tubular bones, sternum and spleen as a sign of successful leukemia engraftment, each cohort was randomly subdivided into two groups which were injected for 1 week daily with either tamoxifen (Tam) or solvent (mock) as control. As revealed by BLI and monitoring of clinical symptoms, leukemia quickly progressed in both mock-treated genotypes (median survival for LSL 25 days, for KO 23 days) (Fig. 3b). When the LSL group was treated with tamoxifen a strong clinical response was observed: BLI showed a gradual decrease of luciferase signal to almost background levels within 2 weeks of treatment (Fig. 3a). Median survival was extended more than twice in comparison to the control group and reached 57 days, 3/12 mice survived for > 100 days and 2 for almost 200 days (Fig. 3b). Importantly, tamoxifen administration had only minor effect on survival of mice with KO leukemia, which continued to progress under treatment (Fig. 3a), and provided only a subtle survival advantage (median survival 30 days, Fig. 3b), underscoring the role of E177R as the driver of the therapeutic response.

To confirm that the therapy response is indeed dependent on E177R expression, we generated an isogenic LSL-E177R;CreER^{T2} AML cell clone with stable Cas9 expression and subsequently transduced this clone with lentiviruses expressing either a *Trp53*-targeting (sg-p53) or a non-targeting scrambled sgRNA (sg-scr). Both sg-p53 and sg-scr AML cell types were transplanted into sublethally irradiated recipient mice and, following successful engraftment, treated with tamoxifen as described above. As indicated by BLI and survival analysis, sg-p53 AML did not respond to tamoxifen, whereas the same treatment promoted regression of sg-scr leukemia and resulted in a strong survival benefit (median survival 37 and 95 days, respectively) (Fig. 3c and d). Immunohistochemistry confirmed the absence of p53 protein in sg-p53 AML after tamoxifen administration, whereas sg-scr leukemia samples collected after disease relapse were

strongly positive for p53 protein (Fig. 3e). Together, these results indicate that E177R is mediating the reactivation response and strongly suggest that even a partial restoration of p53 activity can provide a significant therapeutic effect in vivo.

The remarkable efficiency of reactivation therapy prompted us to investigate the mechanisms that underlie the E177R-mediated response. Using immunohistochemistry, we analyzed tissue samples collected at different time-points after therapy start. As expected, we observed fast accumulation of p53 protein in LSL- tumors after the start of daily tamoxifen injections (Fig. 4a). Interestingly, all relapsed tumors retained a high expression level of E177R protein (Fig. 3e), indicating that relapse is not driven by incomplete Cre-mediated E177R activation or secondary loss of E177R expression. It rather suggests that some leukemia cells tolerate the residual tumor suppressive activity of E177R and eventually adapt to its presence. Coherent with the loss of the luciferase signal in BLI, E177R induction led to a gradual elimination of GFP-positive leukemia cells (Fig. 4a). Consistent with E177R being proficient in cell cycle inhibition and senescence induction, we detected a marked drop in proliferation in tamoxifen-treated leukemia, as indicated by reduced number of BrdU-positive cells (Fig. 4a). In parallel, we observed a significant accumulation of senescent cells (Fig. 4a and b). However, while cell cycle arrest and senescence can decelerate or even stop tumor growth, these processes did not fully explain the rapid removal of leukemia cells, which became detectable as early as 3 days and was clearly evident 7 days after the first tamoxifen administration (Fig. 4a). As we had observed induction of apoptosis following E177R induction in vitro, we therefore also analyzed apoptosis levels immunohistochemically in tissue samples by TUNEL assay and observed a significant increase in tamoxifen-treated, but not in mock-treated, tumors (Fig. 4a and c). Thus, similar to the in vitro results, in vivo induction of E177R also triggered a broad spectrum of tumor suppressive programs, including cell cycle arrest, senescence and apoptosis.

Restoration of wild-type p53 in liver cancer was shown to trigger an infiltration by multiple components of the immune system which contributed to clearance of senescent tumor cells and accelerated cancer regression [21]. Using CD3 as a surrogate marker, we observed significantly increased staining at day 3 in tamoxifen-, but not mock-treated tumors (Fig. 4a and d), suggesting that immune cells might contribute to E177R-mediated leukemia regression.

Partial p53 reactivation induces regression of Myc-driven Burkitt-like lymphoma

Inspired by the results in the AML model, we decided to test whether partial restoration of p53 function is an effective treatment in other hematological malignancies such as lymphoma. We first studied EμMyc-driven B cell lymphoma, which mimics the t (8;14)(q24;q32) translocation in human Burkitt lymphoma and which is facilitated by the E177R mutation [15, 48]. We crossed male *EμMyc* mice with female *Trp53*$^{\text{LSL-E177R/+}}$;*Rosa26*$^{\text{CreERT2}}$ mice to generate littermates that undergo LOH and develop p53-deficient LSL-E177R lymphomas with and without expression of CreER^{T2}. These p53-deficient lymphoma cells were transplanted into immunocompetent recipient mice. After successful engraftment of the lymphoma, detected by palpable lymph nodes, all animals were treated with tamoxifen for 7 consecutive days (Fig. 5a). In the group of mice with CreER^{T2}, tamoxifen treatment activated E177R and triggered a pronounced therapeutic response, as suggested by a significantly extended survival compared to tamoxifen-treated mice with LSL-lymphomas lacking CreER^{T2} (median survival 26 vs. 16 days, Log-rank (Mantel-Cox) test $P < 0.0001$; Fig. 5a). Excluding a confounding effect of CreER^{T2}, no difference in survival was observed in mice lacking an inducible p53 allele (Fig. 5b). Although tamoxifen also functions as an antiestrogen, we observed no gender-dependent differences in the p53 reactivation response (Supplemental Fig. S1).

Expression of E177R protein was readily detected by immunohistochemistry in tumors 2 days after the therapy start accompanied by strong inhibition of cell proliferation, evident from the massive reduction in BrdU-positive cells (Fig. 5c and d). Similar as in the AML model, we again detected a massive increase in apoptosis, which culminated at 2 days after therapy start and then decreased to background levels (Fig. 5c and e). Notably, p53-deficient lymphomas are highly invasive and infiltrate into various nonlymphoid organs as evidenced by periportal invasion and spreading of lymphoma cell clusters throughout the liver parenchyma [55]. Interestingly,

(See figure on next page.)

Fig. 4 In vivo response of p53-deficient AML to E177R activation. **a** Mice transplanted with LSL AML cells were sacrificed before and day 1, 3, 7 and 11 after start of 1 week of daily treatment with Tam or corn oil (mock). Samples were analyzed by immunohistochemistry for p53$^{\text{E177R}}$, GFP (as a marker of AML cells), BrdU (proliferation), senescence-associated β-galactosidase (SA β-gal), apoptosis (TUNEL) and CD3 as a marker of immune infiltration. Arrowheads indicate senescent cells. **b**-**d** Quantification of immunohistochemistry analysis. **b** Senescence-associated β-galactosidase. **c** Apoptosis (TUNEL). **d** Immune infiltrate (CD3). All bar graphs show the mean positivity index ±SD; datapoints represent individual fields of view (1000X1000 pixel each) from $n = 2$ mice sacrificed at each time point; reported are *P*-values of 1way ANOVA and indicated pairwise comparisons (Dunnett's multiple comparisons test)

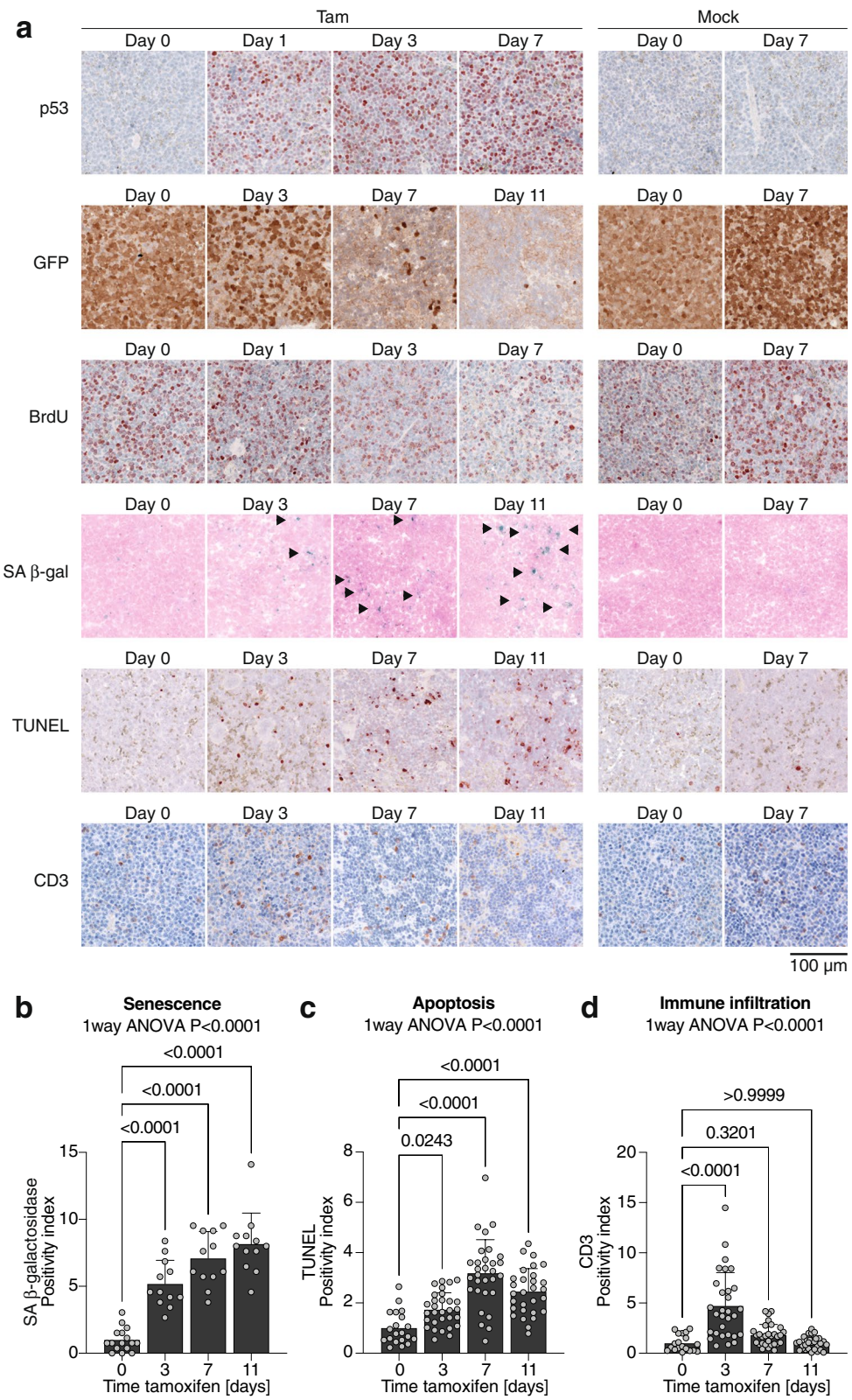

Fig. 4 (See legend on previous page.)

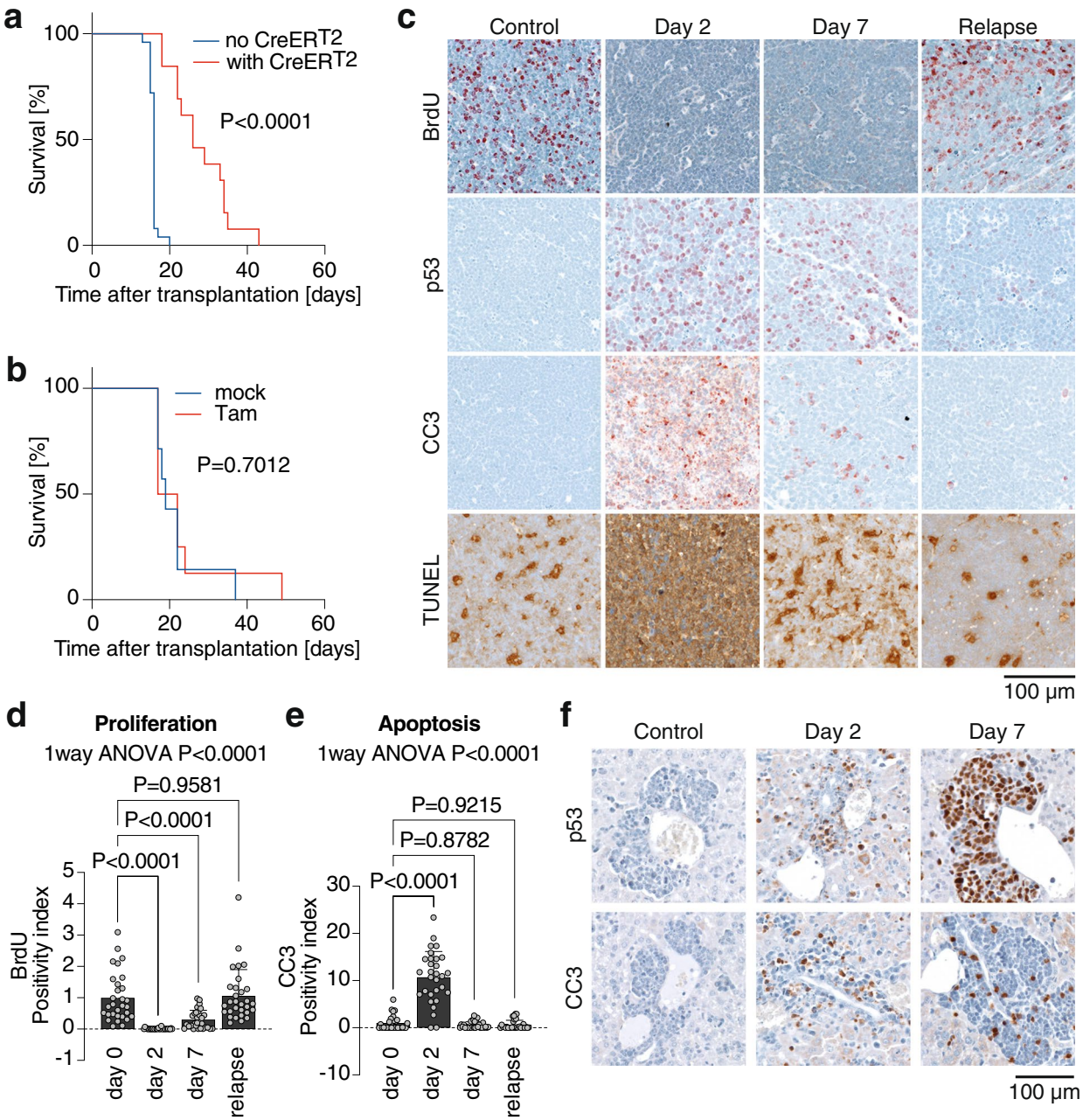

Fig. 5 E177R activation induces regression of p53-deficient Burkitt-like B cell lymphomas. **a** EμMyc; *Trp53*$^{LSL\text{-}E177R/-}$ lymphomas with ($n=13$) or without ($n=25$) the *Rosa26*^{CreERT2} transgene were transplanted into immunocompetent 129/B6 F1 hybrid mice and, after confirmation of disease onset, treated 1 week with daily i.p. injections of 1 mg tamoxifen. Mice were euthanized when humane endpoint criteria were reached. Shown is the Kaplan-Meier survival graph with Log-rank (Mantel-Cox) test. **b** EμMyc; *Rosa26*$^{CreERT2/+}$ lymphomas were transplanted as in **a** and treated 1 week with daily i.p. injections of either corn oil (mock; $n=7$) or 1 mg tamoxifen (Tam; $n=8$). Shown is the Kaplan-Meier survival graph with Log-rank (Mantel-Cox) test. **c**-**f** Mice transplanted with EμMyc; *Trp53*$^{LSL\text{-}E177R/-}$; *Rosa26*^{CreERT2} lymphomas were sacrificed before, day 2 and 7 after start of tamoxifen (Tam) treatment or upon relapse. Samples were analyzed by immunohistochemistry for BrdU (proliferation), p53 and apoptosis (cleaved caspase-3 CC3, TUNEL). **c** Representative images. **d**-**e** Quantification of immunohistochemistry. **d** Proliferation (BrdU). **e** Apoptosis (cleaved caspase-3, CC3). All bar graphs show the mean positivity index ±SD; datapoints represent individual fields of view (1000X1000 pixel each) from $n=3$ mice sacrificed at each time point; reported are *P*-values of 1way ANOVA and indicated pairwise comparisons (Dunnett's multiple comparisons test). **f** Representative images of hepatic lymphoma infiltrates in the periportal space stained for p53 and apoptosis (cleaved caspase-3, CC3) at indicated time points after Tam treatment

we observed robust E177R expression and apoptosis induction also in periportal lymphoma infiltrates (Fig. 5f), suggesting that partial reactivation is equally effective in a metastatic setting.

At later time-points, the number of p53-positive cells dropped and relapsed tumors were mostly negative for p53 staining with only a few remaining small clusters of p53-positive cells (Fig. 5c). This suggests that recombination in this model is either incomplete or recombined LSL-E177R becomes inactivated by, for example, LOH, so that residual or emerging p53-deficient lymphoma cells escape and mediate relapse.

Partial p53 reactivation induces regression of spontaneous T-cell lymphomas in p53-null mice

As a second lymphoma model, we decided to use thymic T-cell lymphoma that accounts for the majority of all cancers detected in p53-null mice and spontaneously develops early within the first 6 months of age [49, 56]. We generated *Trp53*$^{\text{LSL-E177R/LSL-E177R}}$ mice which co-expressed the *Rosa26*$^{\text{CreERT2}}$ transgene (short: p53$^{\text{LSL/LSL}}$;CreER$^{\text{T2}}$). We used Cre-negative mice that cannot induce E177R expression upon tamoxifen administration as a constitutive p53-null control group (short: p53$^{\text{LSL/LSL}}$). In our previous experiments, we estimated the median survival of p53-deficient mice to 5–6 months and therefore expected that the majority of animals should have developed tumors by 4 months of age. As soon as animals reached 4 months of age, both groups were treated 1 week daily with tamoxifen and monitored for survival. This approach allowed us to avoid a potential bias caused by p53-independent effects of tamoxifen. If re-expression of E177R can block or slow down progression of such tumors, it should result in enhanced survival. Indeed, we observed a significantly longer median survival in the E177R reactivation group (64 vs. 37 days survival after therapy end, Fig. 6a).

From this experiment, however, we could not conclude whether re-expression of E177R prevented tumor formation, limited cancer progression or induced regression of established tumors. To address this question, we examined p53$^{\text{LSL/LSL}}$ animals with and without CreER$^{\text{T2}}$ by MRI. Included were 4-months old or younger mice with clinical signs of thymoma (breath shortening, hunchback posture, weight loss). Animals with thymus enlargement were treated with tamoxifen as described above and monitored by MRI for up to 4 weeks. At the start of therapy both cohorts had a similar average tumor volume (Fig. 6b). In conformity with survival data, imaging showed that all p53$^{\text{LSL/LSL}}$ animals without Cre showed progressive tumor growth under tamoxifen (Fig. 6b-d). In stark contrast, we observed a clear reduction of thymus size in 7 of 9 p53$^{\text{LSL/LSL}}$ mice with Cre 1–2 weeks after E177R activation (Fig. 6b-d). The response to tamoxifen was similar in mice of both sexes (Supplemental Fig. S2). Moreover, all control animals reached the humane endpoint and had to be sacrificed within 2 weeks after therapy start whereas 7/9 mice with E177R activation survived for more than 4 weeks. Thus, E177R expression elicited in B- and T-cell lymphoma models a similar therapeutic response as in AML, indicating that even partial restoration of p53 function is able to induce regression in different hematopoietic cancers.

Of note, after initial remission thymic lymphomas regrew in virtually all mice. Nevertheless, many of these animals did not die of thymic lymphoma but were sacrificed because of other cancers, mostly sarcomas in varying locations and some splenic B cell lymphomas (Fig. 6e and f). These were not detected as the major tumor before treatment, but apparently continued to grow despite E177R activation, suggesting that not all types of cancer might be equally vulnerable to partial p53 activation.

Discussion

Previous studies have indicated that many p53-deficient tumors regress when p53 is restored, implying that they are strongly addicted to the absence of p53 activity

(See figure on next page.)

Fig. 6 E177R activation induces regression of thymic lymphomas in p53-deficient mice. *Trp53*$^{\text{LSL-E177R/LSL-E177R}}$ mice (p53$^{\text{LSL/LSL}}$) with the *Rosa26*$^{\text{CreERT2}}$ (CreER$^{\text{T2}}$) transgene ($n=17$) were treated 1 week with daily i.p. injections of 1 mg tamoxifen at 4 months of age and euthanized when humane endpoint criteria were reached. p53$^{\text{LSL/LSL}}$ mice (without CreER$^{\text{T2}}$) treated with tamoxifen served as controls ($n=22$). **a** Kaplan-Meier survival graph with Log-rank (Mantel-Cox) test. **b**-**d** Individual mice (p53$^{\text{LSL/LSL}}$; CreER$^{\text{T2}}$ (red): $n=9$; p53$^{\text{LSL/LSL}}$ (blue): $n=8$) that were diagnosed with thymic lymphoma by MRI received tamoxifen treatment and were re-examined by MRI 7, 14, and 28 days after treatment start. **b** Shown is the fold-change in tumor volume (determined by MRI) relative to pre-treatment for individual animals. Insert shows the mean absolute tumor volume ± SD in both cohorts at the start of treatment; data points represent individual mice; two-tailed unpaired t-test. **c** Shown is the maximum response (fold increase in tumor volume) in individual mice. Reported is the *P*-value of a two-tailed Mann-Whitney test comparing tamoxifen treatment responses of p53$^{\text{LSL/LSL}}$; CreER$^{\text{T2}}$ (red) and p53$^{\text{LSL/LSL}}$ (blue) mice. **d** Representative MRI results from one mouse of each cohort. The p53$^{\text{LSL/LSL}}$ mouse without CreER$^{\text{T2}}$ (blue) progressed under treatment and reached the endpoint before day 14. The p53$^{\text{LSL/LSL}}$ mouse with CreER$^{\text{T2}}$ (red) showed tumor regression until day 14 and presented with relapse on day 28. Shown are tumor sections in all 3 dimensions; tumors are highlighted in color. **e**-**f** Cancer types detected in both cohorts after treatment when the animals reached the humane endpoint criteria. **e** Fraction of thymic lymphomas versus non-thymic tumor types (including mostly sarcomas and splenic B cell lymphomas). **f** Representative histological images of non-regressed undifferentiated sarcomas in $n=6$ different animals

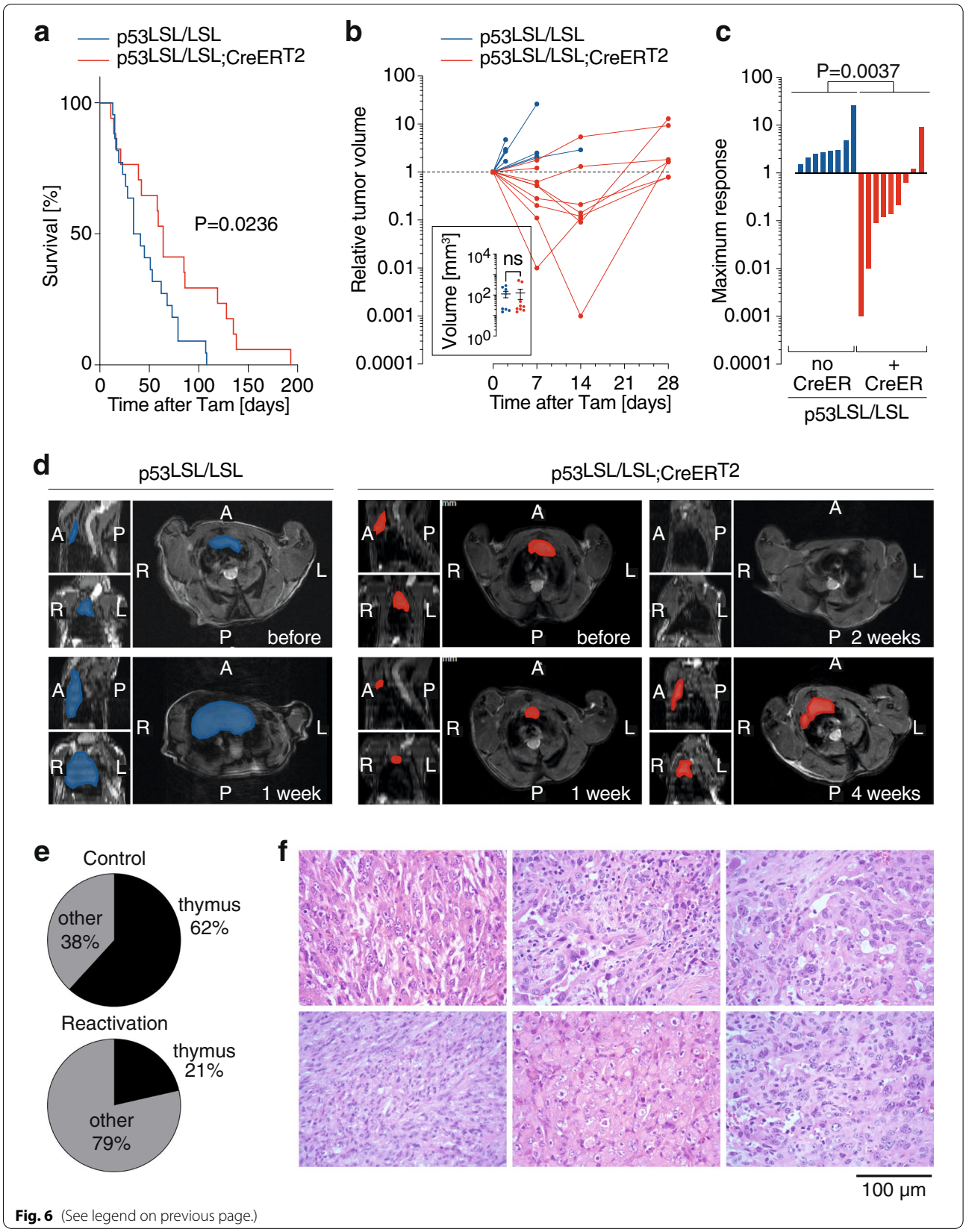

Fig. 6 (See legend on previous page.)

[19–22, 24]. However, it has remained unclear how much p53 activity is required to trigger tumor regression [18]. Given the yet limited pharmacological abilities to fully reactivate a p53 mutant [25, 26], we aimed to analyze whether partial p53 reactivation may suffice to induce a therapeutic effect. To reproducibly reactivate p53 to a defined suboptimal degree, we chose to genetically limit p53 activity using the previously well-characterized partial LOF variant E177R [15]. This mutation does not affect any DNA contacting residues and maintains a normally folded DNA binding domain [41]. Nevertheless, it is impaired in DNA binding because it fails to form a strong intermolecular salt-bridge which is crucial to stabilize the tetrameric protein complex on DNA [43]. Previous DNA binding studies in vitro and in vivo have characterized the DNA binding defect as a global reduction in DNA binding across the entire target gene spectrum [44, 45]. By limiting global DNA binding in a genetically fixed manner, the E177R mutation is suitable to model the consequences of an incompletely reactivated p53 mutant.

Even though the E177R mutation reduced DNA binding globally, we observed transactivation of the typical p53 target genes (Fig. 1e) and induction of a broad range of effector programs including cell cycle arrest, senescence, differentiation and apoptosis (Fig. 2). While transactivation of antiproliferative target genes like *p21/Cdkn1a* is in line with the described phenotype of E177R knock-in mice and explains induction of cell cycle arrest, senescence and differentiation [15], activation pro-apoptotic target genes was rather unexpected, because E177R and several other related cooperativity mutants are generally characterized by an apoptosis defect [43, 57–59]. However, the ability of p53 to induce apoptosis is highly context-dependent and modulated by the extent and dynamics of p53 protein accumulation as well as the intrinsic apoptosis threshold of the cell and its level of mitochondrial priming [60–64]. It is therefore conceivable that sustained high-level expression of a DNA-binding impaired p53 mutant can trigger apoptosis especially in cell types with an intrinsically low apoptosis threshold [65, 66]. In line, massive constitutive stabilization of the E177R mutant protein by knockout of Mdm2 was shown to trigger lethal apoptosis in highly proliferative embryonic tissues [65], which have a lower apoptosis threshold than most adult tissues due to Myc-mediated mitochondrial priming [65, 66]. Similarly, tumors in E177R mice commonly display constitutive stabilization of the E177R mutant protein, and DNA damage in such tumors was reported to induce pro-apoptotic p53 target genes and render them sensitive to chemotherapy [47]. In all our leukemia and lymphoma models, the E177R protein was readily detectable by immunohistochemistry (Figs. 3e, 4a, 5f), showing a staining pattern similar to human tumors with a massively stabilized mutant p53 protein. Moreover, p53-deficient leukemias and lymphomas commonly upregulate p19Arf [20, 47], which can sequester Mdm2, thereby contribute to the massive E177R accumulation, overcome the apoptosis-deficiency and enable tumor cell killing by E177R.

In vivo, additional non-cell-autonomous p53 effects might contribute to eradication of tumor cells [21, 67, 68]. In liver carcinomas, for example, wild-type p53 restoration triggers infiltration by innate immune cells like macrophages, neutrophils and lymphocytes that support clearance of senescent tumor cells [21]. While we have not detected changes in macrophages, we have observed lymphocytic infiltration upon E177R activation (Fig. 4), which makes it tempting to speculate that immune infiltration induced by p53 in a non-cell-autonomous manner might contribute to tumor regression in vivo. In summary, the presented data indicate that E177R is directly capable of inducing apoptosis in p53-deficient leukemia and lymphoma cells and provide an explanation for the observed cancer regression. Whether and how immune cells contribute remains to be investigated.

We observed cancer regression not only in AML but also in lymphoma models, including thymic T cell lymphomas that spontaneously develop in p53-deficient mice. While non-reactivated mice mostly succumbed to thymic lymphoma, reactivated mice at the time of sacrifice more often presented with other types of cancer, often sarcomas (Fig. 6e and f), suggesting that lymphomas are more vulnerable to p53 reactivation than other cancer entities. A differential sensitivity of sarcomas and lymphomas was also reported upon restoration of wild-type p53, where restoration in lymphomas caused widespread apoptosis, whereas sarcomas showed a delayed anti-proliferative response with features of senescence [22]. The higher sensitivity of hematopoietic cancers is not entirely unexpected as already the normal bone marrow displays an exquisite vulnerability to elevated p53 activity which is at least partially explained by mitochondrial priming of the hematopoietic compartment [61, 66, 69–72]. Moreover, this is in line with clinical studies on p53/mutp53-reactivating compounds like Mdm2-inhibitors or eprenetapopt (APR-246), which have reported clinical responses mostly in patients with hematological cancers [37, 38, 73].

Even though most animals demonstrated strong responses to partial reactivation, none of the animals was cured and all relapsed eventually. The cause of relapse differed between the different models. Relapsed EμMyc-driven lymphomas showed a high percentage of p53-negative tumor cells (Fig. 5c), suggesting that not all lymphoma cells had recombined the LSL-E177R

allele and therefore escaped due to a technically inefficient reactivation. An alternative explanation would be a secondary loss or inactivation of the E177R mutant, for example, by LOH. In contrast, relapsed AML mice showed homogeneous high-level expression of the E177R mutant, indicating that some tumor cells eventually adapt and tolerate E177R expression. Of note, these observations are not unique to partial p53 reactivation and similar findings have been reported in the previous studies with wild-type p53 restoration. All EμMyc lymphomas with tamoxifen-inducible p53ER^{TAM} activity relapsed after reactivation, losing either p53ER^{TAM} expression or deleting its upstream activator p19ARF [19]. Responses to partial reactivation are therefore mostly transient, calling for synergistic approaches such as DNA damaging chemotherapeutics that might help to boost p53 activity to obtain longer-lasting remissions. In AML, even a transient response might be efficient, by inducing the clinical remission needed for a bone marrow transplant as the final curative treatment.

Tamoxifen, used to induce E177R-mediated tumor regression in our study, is an estrogen receptor (ER) antagonist. As estrogens vary between sexes and interfere with the p53 pathway [74], the anti-estrogenic tamoxifen activity might have contributed to the p53 reactivation response in a sex-dependent manner. In the AML model, both the LSL and KO leukemia cells were derived from female embryos and 86% of all recipient mice were also female. The improvement in survival upon tamoxifen treatment of LSL-E177R AML mice remained highly significant when excluding male mice from the survival analysis (Supplemental Fig. S3). A gender-effect as the cause for the differential in vitro and in vivo response to tamoxifen treatment can therefore be excluded. However, due to the small number of male recipient mice, we could not analyze whether the reactivation response is different in male AML mice. Both lymphoma models comprised comparable numbers of male and female mice and the reactivation responses were similar in both sexes (Supplemental Fig. S1 and S2). In the transplanted Myc lymphomas, reactivation was also independent of the sex of the lymphoma donor (Supplemental Fig. S1). Together, these analyses indicate no confounding sex-dependent effects in the hematopoietic cancer models studied here. This is in line with the clinical use of tamoxifen primarily for the treatment of hormone-dependent ER+ breast and endometrial cancer. In other ER-negative cancer types, anti-tumor effects of tamoxifen require doses 4–8 fold higher than necessary for ER inhibition [75], suggesting that these effects are hormone-independent.

Of note, tumor cells can not only become addicted to the loss of wild-type p53 activity, they can also become dependent on neomorphic GOF properties of the p53 mutant. Refolding a GOF mutant would therefore not only restore some degree of wild-type function but simultaneously deprive tumor cells of survival-promoting GOF effects. As such, it has been demonstrated that loss of GOF activities by therapeutic ablation of the mutant protein can be sufficient to induce cancer regression, even in the absence of any restoration of wild-type function [76, 77]. By switching p53-null tumor cells to E177R, we can exclude that the responses observed in our cancer models are mediated by a loss of GOF properties. However, it is reasonable to assume that an additional loss of GOF would synergize with restoration of wild-type function and could further enhance the extent and duration of tumor regression. It is therefore expected that a partial p53 reactivation would be even more effective in tumors bearing GOF missense mutants rather than pure LOF mutants.

Conclusions

We demonstrate that a p53 variant, which has partially lost the activity of wild-type p53 and by itself increases cancer susceptibility and promotes oncogene-driven development of leukemia and lymphoma, induces cancer regression in vivo when introduced into p53-deficient leukemia and lymphomas. This not only provides compelling evidence that p53 mutants function in a highly context-dependent manner, being pro-tumorigenic in one setting and tumor suppressive in another, it also highlights how sensitive cancer cells respond to changes in p53 activity and that changes in activity are more important than the absolute activity level. Even a slight increase in p53 activity resulting from switching a p53-null into a partially active p53 allele can suffice to induce tumor regression. As such, our findings will encourage ongoing research into mutant p53-reactivating drugs by providing genetic proof-of-principle evidence that incomplete reactivation of p53 mutants can elicit a beneficial therapeutic response.

Abbreviations

LOF: Loss of function; GOF: Gain of function; MDS: Myelodysplastic syndrome; AML: Acute myeloid leukemia; GSH: Glutathione; Tam: Tamoxifen; 4OHT: 4-hydroxy-tamoxifen; LSL: loxpP-stop-loxP; MRI: Magnetic resonance imaging; BLI: Bioluminescence imaging; LOH: Loss of heterozygosity; BrdU: Bromodeoxyuridine; GFP: Green fluorescent protein; RT: Room temperature; PBS: Phosphate buffered saline.

Supplementary Information

The online version contains supplementary material available at https://doi.org/10.1186/s13046-022-02269-6.

Additional file 1.

Acknowledgements
Authors thank Sigrid Bischofsberger, Antje Grzeschiczek, Angela Mühling, Björn Geißert, Marlen Lahmann and employees of the animal facility of Marburg University for technical and experimental support. We acknowledge support by the Medical Core Facilities (Flow Cytometry: Gavin Giel, Cornelia Brendel; Small animal MRI: Andreas Mahnken; X-ray: Ulrike Schötz).

Authors' contributions
BK and LM performed experiments in the AML mouse model; OT and NA carried out the experiments in the lymphoma model; AMK performed magnetic resonance imaging; CUK analyzed and evaluated the histopathology results; NM performed molecular biology experiments and assisted with animal experiments; MN performed molecular biology experiments in the AML model; SE supervised animal experiments; OT and TS conceived the study, and participated in its design and coordination and drafted the manuscript. All authors reviewed and edited the draft and approved the final manuscript.

Funding
Open Access funding enabled and organized by Projekt DEAL. This work was supported by grants from Deutsche Krebshilfe (111250, 70112623 to TS and 111444 to OT), Deutsche José Carreras Leukämie Stiftung e.V. (09 R/2018 to OT and TS), Deutsche Forschungsgemeinschaft (TRR81/3 109546710 Project A10 to TS, TI 1028/2–1 to OT, STI 182/13–1 to TS, GRK2573), German Center for Lung Research (DZL) to TS, BMBF (031 L0063 to TS), von Behring-Röntgen Stiftung (65–0004 and 66-LV06 to TS).

Availability of data and materials
All data generated or analyzed during the present study are included in this published article.

Declarations

Ethics approval and consent to participate
The animal experiments were performed under the approval of the local authority Regierungspräsidium Gießen.

Consent for publication
All authors have agreed to publish this manuscript.

Competing interests
The authors declare that they have no competing interests.

Author details
[1]Institute of Molecular Oncology, Universities of Giessen and Marburg Lung Center (UGMLC), Philipps-University, Marburg, Germany. [2]Clinic of Diagnostic and Interventional Radiology, Core Facility 7T-small animal MRI, Philipps-University, Marburg, Germany. [3]Institute for Pathology, University Hospital Marburg, Philipps-University, Marburg, Germany. [4]German Center for Lung Research (DZL), Philipps-University, Marburg, Germany. [5]Genomics Core Facility, Philipps-University, Marburg, Germany.

Received: 15 September 2021 Accepted: 20 January 2022
Published online: 02 March 2022

References

1. Boutelle AM, Attardi LD. p53 and tumor suppression: it takes a network. Trends Cell Biol. 2021;31(4):298–310.
2. Kastenhuber ER, Lowe SW. Putting p53 in context. Cell. 2017;170(6):1062–78.
3. Kaiser AM, Attardi LD. Deconstructing networks of p53-mediated tumor suppression in vivo. Cell Death Differ. 2018;25(1):93–103.
4. Wade M, Li YC, Wahl GM. MDM2, MDMX and p53 in oncogenesis and cancer therapy. Nat Rev Cancer. 2013;13(2):83–96.
5. Donehower LA, Soussi T, Korkut A, Liu Y, Schultz A, Cardenas M, et al. Integrated analysis of TP53 gene and Pathway alterations in the Cancer genome atlas. Cell Rep. 2019;28(5):1370–1384 e1375.
6. Leroy B, Anderson M, Soussi T. TP53 mutations in human cancer: database reassessment and prospects for the next decade. Hum Mutat. 2014;35(6):672–88.
7. Brosh R, Rotter V. When mutants gain new powers: news from the mutant p53 field. Nat Rev Cancer. 2009;9(10):701–13.
8. Muller PA, Vousden KH. Mutant p53 in cancer: new functions and therapeutic opportunities. Cancer Cell. 2014;25(3):304–17.
9. Freed-Pastor WA, Prives C. Mutant p53: one name, many proteins. Genes Dev. 2012;26(12):1268–86.
10. Stiewe T, Haran TE. How mutations shape p53 interactions with the genome to promote tumorigenesis and drug resistance. Drug Resist Updat. 2018;38:27–43.
11. Frebourg T, Kassel J, Lam KT, Gryka MA, Barbier N, Andersen TI, et al. Germ-line mutations of the p53 tumor suppressor gene in patients with high risk for cancer inactivate the p53 protein. Proc Natl Acad Sci U S A. 1992;89(14):6413–7.
12. Monti P, Ciribilli Y, Jordan J, Menichini P, Umbach DM, Resnick MA, et al. Transcriptional functionality of germ line p53 mutants influences cancer phenotype. Clin Cancer Res. 2007;13(13):3789–95.
13. Liu G, Parant JM, Lang G, Chau P, Chavez-Reyes A, El-Naggar AK, et al. Chromosome stability, in the absence of apoptosis, is critical for suppression of tumorigenesis in Trp53 mutant mice. Nat Genet. 2004;36(1):63–8.
14. Wang Y, Suh YA, Fuller MY, Jackson JG, Xiong S, Terzian T, et al. Restoring expression of wild-type p53 suppresses tumor growth but does not cause tumor regression in mice with a p53 missense mutation. J Clin Invest. 2011;121(3):893–904.
15. Timofeev O, Schlereth K, Wanzel M, Braun A, Nieswandt B, Pagenstecher A, et al. p53 DNA binding cooperativity is essential for apoptosis and tumor suppression in vivo. Cell Rep. 2013;3(5):1512–25.
16. Kang JG, Lago CU, Lee JE, Park JH, Donnelly MP, Starost MF, et al. A mouse homolog of a human TP53 germline mutation reveals a Lipolytic activity of p53. Cell Rep. 2020;30(3):783–792 e785.
17. Hemann MT, Fridman JS, Zilfou JT, Hernando E, Paddison PJ, Cordon-Cardo C, et al. An epi-allelic series of p53 hypomorphs created by stable RNAi produces distinct tumor phenotypes in vivo. Nat Genet. 2003;33(3):396–400.
18. Lozano G. Restoring p53 in cancer: the promises and the challenges. J Mol Cell Biol. 2019;11(7):15–619.
19. Martins CP, Brown-Swigart L, Evan GI. Modeling the therapeutic efficacy of p53 restoration in tumors. Cell. 2006;127(7):1323–34.
20. Klimovich B, Mutlu S, Schneikert J, Elmshauser S, Klimovich M, Nist A, et al. Loss of p53 function at late stages of tumorigenesis confers ARF-dependent vulnerability to p53 reactivation therapy. Proc Natl Acad Sci U S A. 2019;116(44):22288–93.
21. Xue W, Zender L, Miething C, Dickins RA, Hernando E, Krizhanovsky V, et al. Senescence and tumour clearance is triggered by p53 restoration in murine liver carcinomas. Nature. 2007;445(7128):656–60.
22. Ventura A, Kirsch DG, McLaughlin ME, Tuveson DA, Grimm J, Lintault L, et al. Restoration of p53 function leads to tumour regression in vivo. Nature. 2007;445(7128):661–5.
23. Junttila MR, Karnezis AN, Garcia D, Madriles F, Kortlever RM, Rostker F, et al. Selective activation of p53-mediated tumour suppression in high-grade tumours. Nature. 2010;468(7323):567–71.
24. Feldser DM, Kostova KK, Winslow MM, Taylor SE, Cashman C, Whittaker CA, et al. Stage-specific sensitivity to p53 restoration during lung cancer progression. Nature. 2010;468(7323):572–5.
25. Bykov VJN, Eriksson SE, Bianchi J, Wiman KG. Targeting mutant p53 for efficient cancer therapy. Nat Rev Cancer. 2018;18(2):89–102.
26. Sabapathy K, Lane DP. Therapeutic targeting of p53: all mutants are equal, but some mutants are more equal than others. Nat Rev Clin Oncol. 2018;15(1):13–30.
27. Joerger AC, Fersht AR. Structural biology of the tumor suppressor p53. Annu Rev Biochem. 2008;77:557–82.
28. Bullock AN, Fersht AR. Rescuing the function of mutant p53. Nat Rev Cancer. 2001;1(1):68–76.
29. Joerger AC, Fersht AR. The tumor suppressor p53: from structures to drug discovery. Cold Spring Harb Perspect Biol. 2010;2(6):a000919.
30. Joerger AC, Fersht AR. The p53 Pathway: Origins, Inactivation in Cancer, and Emerging Therapeutic Approaches. Annu Rev Biochem. 2016;85:375–404.

31. Joerger AC, Bauer MR, Wilcken R, Baud MG, Harbrecht H, Exner TE, et al. Exploiting transient protein states for the Design of Small-Molecule Stabilizers of mutant p53. Structure. 2015;23(12):2246–55.
32. Blanden AR, Yu X, Wolfe AJ, Gilleran JA, Augeri DJ, O'Dell RS, et al. Synthetic metallochaperone ZMC1 rescues mutant p53 conformation by transporting zinc into cells as an ionophore. Mol Pharmacol. 2015;87(5):825–31.
33. Chen S, Wu JL, Liang Y, Tang YG, Song HX, Wu LL, et al. Arsenic trioxide rescues structural p53 mutations through a cryptic allosteric site. Cancer Cell. 2021;39(2):225–239 e228.
34. Lambert JM, Gorzov P, Veprintsev DB, Soderqvist M, Segerback D, Bergman J, et al. PRIMA-1 reactivates mutant p53 by covalent binding to the core domain. Cancer Cell. 2009;15(5):376–88.
35. Bykov VJ, Issaeva N, Shilov A, Hultcrantz M, Pugacheva E, Chumakov P, et al. Restoration of the tumor suppressor function to mutant p53 by a low-molecular-weight compound. Nat Med. 2002;8(3):282–8.
36. Zhang Q, Bykov VJN, Wiman KG, Zawacka-Pankau J. APR-246 reactivates mutant p53 by targeting cysteines 124 and 277. Cell Death Dis. 2018;9(5):439.
37. Sallman DA, DeZern AE, Garcia-Manero G, Steensma DP, Roboz GJ, Sekeres MA, et al. Eprenetapopt (APR-246) and Azacitidine in TP53-mutant myelodysplastic syndromes. J Clin Oncol. 2021;39(14):1584–94.
38. Cluzeau T, Sebert M, Rahme R, Cuzzubbo S, Lehmann-Che J, Madelaine I, et al. Eprenetapopt plus Azacitidine in TP53-mutated myelodysplastic syndromes and acute myeloid leukemia: a phase II study by the Groupe francophone des Myelodysplasies (GFM). J Clin Oncol. 2021;39(14):1575–83.
39. Ceder S, Eriksson SE, Cheteh EH, Dawar S, Corrales Benitez M, Bykov VJN, et al. A thiol-bound drug reservoir enhances APR-246-induced mutant p53 tumor cell death. EMBO Mol Med. 2021;13(2):e10852.
40. Liu DS, Duong CP, Haupt S, Montgomery KG, House CM, Azar WJ, et al. Inhibiting the system xC(−)/glutathione axis selectively targets cancers with mutant-p53 accumulation. Nat Commun. 2017;8:14844.
41. Dehner A, Klein C, Hansen S, Muller L, Buchner J, Schwaiger M, et al. Cooperative binding of p53 to DNA: regulation by protein-protein interactions through a double salt bridge. Angew Chem Int Ed Engl. 2005;44(33):5247–51.
42. Kitayner M, Rozenberg H, Rohs R, Suad O, Rabinovich D, Honig B, et al. Diversity in DNA recognition by p53 revealed by crystal structures with Hoogsteen base pairs. Nat Struct Mol Biol. 2010;17(4):423–9.
43. Timofeev O, Stiewe T. Rely on each other: DNA binding cooperativity shapes p53 functions in tumor suppression and cancer therapy. Cancers (Basel). 2021;13(10):2422.
44. Schlereth K, Beinoraviciute-Kellner R, Zeitlinger MK, Bretz AC, Sauer M, Charles JP, et al. DNA binding cooperativity of p53 modulates the decision between cell-cycle arrest and apoptosis. Mol Cell. 2010;38(3):356–68.
45. Schlereth K, Heyl C, Krampitz AM, Mernberger M, Finkernagel F, Scharfe M, et al. Characterization of the p53 cistrome--DNA binding cooperativity dissects p53's tumor suppressor functions. Plos Genet. 2013;9(8):e1003726.
46. Zuber J, Radtke I, Pardee TS, Zhao Z, Rappaport AR, Luo W, et al. Mouse models of human AML accurately predict chemotherapy response. Genes Dev. 2009;23(7):877–89.
47. Klimovich B, Merle N, Neumann M, Elmshäuser S, Nist A, Mernberger M, et al. p53 partial loss-of-function mutations sensitize to chemotherapy. Oncogene. 2021. https://doi.org/10.1038/s41388-021-02141-5.
48. Adams JM, Harris AW, Pinkert CA, Corcoran LM, Alexander WS, Cory S, et al. The c-myc oncogene driven by immunoglobulin enhancers induces lymphoid malignancy in transgenic mice. Nature. 1985;318(6046):533–8.
49. Donehower LA, Harvey M, Slagle BL, McArthur MJ, Montgomery CA Jr, Butel JS, et al. Mice deficient for p53 are developmentally normal but susceptible to spontaneous tumours. Nature. 1992;356(6366):215–21.
50. Timofeev O, Klimovich B, Schneikert J, Wanzel M, Pavlakis E, Noll J, et al. Residual apoptotic activity of a tumorigenic p53 mutant improves cancer therapy responses. EMBO J. 2019;38(20):e102096.
51. Timofeev O, Koch L, Niederau C, Tscherne A, Schneikert J, Klimovich M, et al. Phosphorylation control of p53 DNA-binding cooperativity balances tumorigenesis and aging. Cancer Res. 2020;80(23):5231–44.
52. Reimer J, Knoss S, Labuhn M, Charpentier EM, Gohring G, Schlegelberger B, et al. CRISPR-Cas9-induced t (11;19)/MLL-ENL translocations initiate leukemia in human hematopoietic progenitor cells in vivo. Haematologica. 2017;102(9):1558–66.
53. Brinkman EK, Chen T, Amendola M, van Steensel B. Easy quantitative assessment of genome editing by sequence trace decomposition. Nucleic Acids Res. 2014;42(22):e168.
54. Stiewe T. The p53 family in differentiation and tumorigenesis. Nat Rev Cancer. 2007;7(3):165–8.
55. Schmitt CA, McCurrach ME, de Stanchina E, Wallace-Brodeur RR, Lowe SW. INK4a/ARF mutations accelerate lymphomagenesis and promote chemoresistance by disabling p53. Genes Dev. 1999;13(20):2670–7.
56. Jacks T, Remington L, Williams BO, Schmitt EM, Halachmi S, Bronson RT, et al. Tumor spectrum analysis in p53-mutant mice. Curr Biol. 1994;4(1):1–7.
57. Ludwig RL, Bates S, Vousden KH. Differential activation of target cellular promoters by p53 mutants with impaired apoptotic function. Mol Cell Biol. 1996;16(9):4952–60.
58. Rowan S, Ludwig RL, Haupt Y, Bates S, Lu X, Oren M, et al. Specific loss of apoptotic but not cell-cycle arrest function in a human tumor derived p53 mutant. EMBO J. 1996;15(4):827–38.
59. Ryan KM, Vousden KH. Characterization of structural p53 mutants which show selective defects in apoptosis but not cell cycle arrest. Mol Cell Biol. 1998;18(7):3692–8.
60. Purvis JE, Karhohs KW, Mock C, Batchelor E, Loewer A, Lahav G. p53 dynamics control cell fate. Science. 2012;336(6087):1440–4.
61. Le Pen J, Laurent M, Sarosiek K, Vuillier C, Gautier F, Montessuit S, et al. Constitutive p53 heightens mitochondrial apoptotic priming and favors cell death induction by BH3 mimetic inhibitors of BCL-xL. Cell Death Dis. 2016;7:e2083.
62. Kracikova M, Akiri G, George A, Sachidanandam R, Aaronson SA. A threshold mechanism mediates p53 cell fate decision between growth arrest and apoptosis. Cell Death Differ. 2013;20(4):576–88.
63. Chen X, Ko LJ, Jayaraman L, Prives C. p53 levels, functional domains, and DNA damage determine the extent of the apoptotic response of tumor cells. Genes Dev. 1996;10(19):2438–51.
64. Sanchez-Rivera FJ, Ryan J, Soto-Feliciano YM, Clare Beytagh M, Xuan L, Feldser DM, et al. Mitochondrial apoptotic priming is a key determinant of cell fate upon p53 restoration. Proc Natl Acad Sci U S A. 2021;118(23):e2019740118.
65. Klimovich B, Stiewe T, Timofeev O. Inactivation of Mdm2 restores apoptosis proficiency of cooperativity mutant p53 in vivo. Cell Cycle. 2020;19(1):109–23.
66. Sarosiek KA, Fraser C, Muthalagu N, Bhola PD, Chang W, McBrayer SK, et al. Developmental regulation of mitochondrial apoptosis by c-Myc governs age- and tissue-specific sensitivity to Cancer therapeutics. Cancer Cell. 2017;31(1):142–56.
67. Pavlakis E, Stiewe T. p53's extended reach: the mutant p53 Secretome. Biomolecules. 2020;10(2):307–31.
68. Yoon KW, Byun S, Kwon E, Hwang SY, Chu K, Hiraki M, et al. Control of signaling-mediated clearance of apoptotic cells by the tumor suppressor p53. Science. 2015;349(6247):1261669.
69. Ringshausen I, O'Shea CC, Finch AJ, Swigart LB, Evan GI. Mdm2 is critically and continuously required to suppress lethal p53 activity in vivo. Cancer Cell. 2006;10(6):501–14.
70. Abbas HA, Maccio DR, Coskun S, Jackson JG, Hazen AL, Sills TM, et al. Mdm2 is required for survival of hematopoietic stem cells/progenitors via dampening of ROS-induced p53 activity. Cell Stem Cell. 2010;7(5):606–17.
71. Mendrysa SM, O'Leary KA, McElwee MK, Michalowski J, Eisenman RN, Powell DA, et al. Tumor suppression and normal aging in mice with constitutively high p53 activity. Genes Dev. 2006;20(1):16–21.
72. Terzian T, Wang Y, Van Pelt CS, Box NF, Travis EL, Lozano G. Haploinsufficiency of Mdm2 and Mdm4 in tumorigenesis and development. Mol Cell Biol. 2007;27(15):5479–85.
73. Konopleva M, Martinelli G, Daver N, Papayannidis C, Wei A, Higgins B, et al. MDM2 inhibition: an important step forward in cancer therapy. Leukemia. 2020;34(11):2858–74.
74. Konduri SD, Medisetty R, Liu W, Kaipparettu BA, Srivastava P, Brauch H, et al. Mechanisms of estrogen receptor antagonism toward p53 and

its implications in breast cancer therapeutic response and stem cell regulation. Proc Natl Acad Sci. 2010;107(34):15081–6.
75. Gelmann EP. Tamoxifen for the treatment of malignancies other than breast and endometrial carcinoma. Semin Oncol. 1997;24(1 Suppl 1):S1-65-S61-70.
76. Alexandrova EM, Yallowitz AR, Li D, Xu S, Schulz R, Proia DA, et al. Improving survival by exploiting tumour dependence on stabilized mutant p53 for treatment. Nature. 2015;523(7560):352–6.
77. Schulz-Heddergott R, Stark N, Edmunds SJ, Li J, Conradi LC, Bohnenberger H, et al. Therapeutic ablation of gain-of-function mutant p53 in colorectal Cancer inhibits Stat3-mediated tumor growth and invasion. Cancer Cell. 2018;34(2):298–314 e297.

Publisher's Note

Supplemental Information

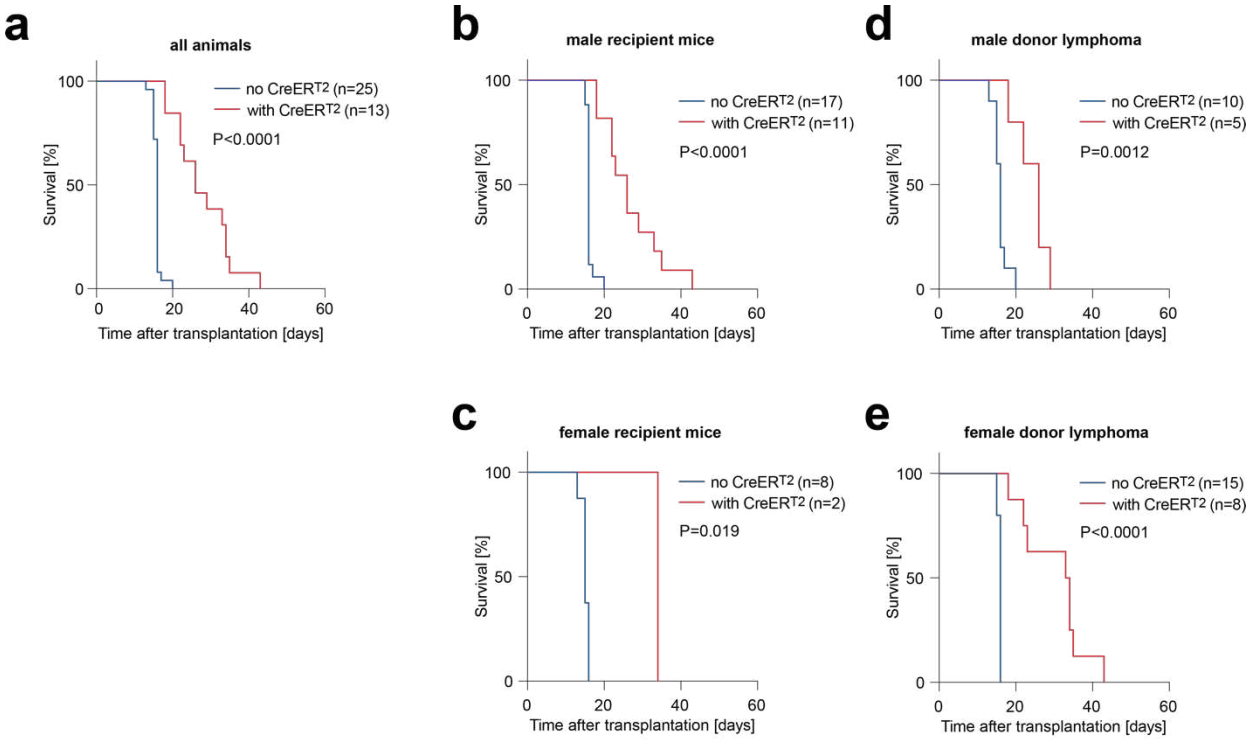

Supplemental Fig. S1. EμMyc; *Trp53*$^{LSL\text{-}E177R/-}$ lymphomas with (n=13) or without (n=25) the *Rosa26*^{CreERT2} transgene were transplanted into immunocompetent 129/B6 F1 hybrid mice and, after confirmation of disease onset, treated 1 week with daily i.p. injections of 1 mg tamoxifen. Mice were euthanized when humane endpoint criteria were reached. Shown are Kaplan-Meier survival graphs with P-values of the Log-rank (Mantel-Cox) test. **a** all animals in the study. **b** only male recipient mice. **c** only female recipient mice. **d** only animals transplanted with lymphoma cells from male donor mice. **e** only animals transplanted with lymphoma cells from female donor mice.

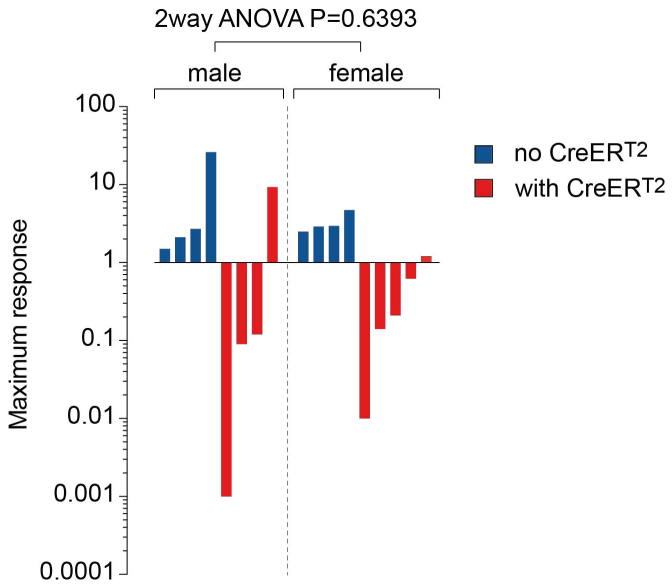

Supplemental Fig. S2 *Trp53*$^{LSL\text{-}E177R/LSL\text{-}E177R}$ mice (p53$^{LSL/LSL}$) with or without the *Rosa26*^{CreERT2} (CreER^{T2}) transgene that were diagnosed with thymic lymphoma by MRI were treated 1 week with daily i.p. injections of 1 mg tamoxifen and were re-examined by MRI 7, 14, and 28 days after treatment start. Shown is the maximum response (fold increase in tumor volume) in individual male and female mice. Reported is the P-value of of a 2way ANOVA analysis for the interaction between sex and genotype/reactivation.

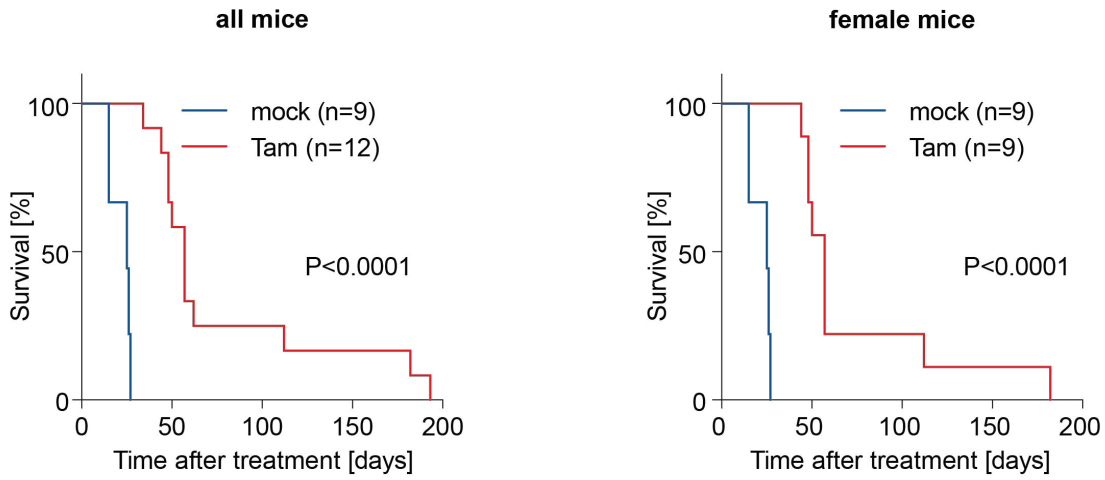

Supplemental Fig. S3 Female LSL-E177R; CreER^{T2} (LSL) AML cells were transplanted into sublethally irradiated 129X1 albino x B6 albino (F1 hybrid) mice. After engraftment was confirmed by bioluminescence imaging (BLI), mice were treated 1 week with daily i.p. injections of either vehicle (corn oil) or 1 mg tamoxifen. Mice were euthanized when humane endpoint criteria were reached. Shown are Kaplan-Meier survival graphs for all (left) and female-only recipient mice (right). Reported are P-values of the Log-rank (Mantel-Cox) test for mock vs. Tam.

Molecular Cancer

RESEARCH

Open Access

Monitoring autochthonous lung tumors induced by somatic CRISPR gene editing in mice using a secreted luciferase

Nastasja Merle[1], Sabrina Elmshäuser[1], Florian Strassheimer[1], Michael Wanzel[1], Alexander M. König[2], Julianne Funk[1], Michelle Neumann[1], Katharina Kochhan[1], Frederik Helmprobst[3], Axel Pagenstecher[3], Andrea Nist[4], Marco Mernberger[1], André Schneider[5], Thomas Braun[5], Tilman Borggrefe[6], Rajkumar Savai[7,8], Oleg Timofeev[1] and Thorsten Stiewe[1,4,8*]

Abstract

Background: In vivo gene editing of somatic cells with CRISPR nucleases has facilitated the generation of autochthonous mouse tumors, which are initiated by genetic alterations relevant to the human disease and progress along a natural timeline as in patients. However, the long and variable, orthotopic tumor growth in inner organs requires sophisticated, time-consuming and resource-intensive imaging for longitudinal disease monitoring and impedes the use of autochthonous tumor models for preclinical studies.

Methods: To facilitate a more widespread use, we have generated a reporter mouse that expresses a Cre-inducible luciferase from *Gaussia princeps* (GLuc), which is secreted by cells in an energy-consuming process and can be measured quantitatively in the blood as a marker for the viable tumor load. In addition, we have developed a flexible, complementary toolkit to rapidly assemble recombinant adenoviruses (AVs) for delivering Cre recombinase together with CRISPR nucleases targeting cancer driver genes.

Results: We demonstrate that intratracheal infection of GLuc reporter mice with CRISPR-AVs efficiently induces lung tumors driven by mutations in the targeted cancer genes and simultaneously activates the GLuc transgene, resulting in GLuc secretion into the blood by the growing tumor. GLuc blood levels are easily and robustly quantified in small-volume blood samples with inexpensive equipment, enable tumor detection already several months before the humane study endpoint and precisely mirror the kinetics of tumor development specified by the inducing gene combination.

Conclusions: Our study establishes blood-based GLuc monitoring as an inexpensive, rapid, high-throughput and animal-friendly method to longitudinally monitor autochthonous tumor growth in preclinical studies.

Keywords: Autochthonous mouse tumor, Lung cancer, Orthotopic tumor, Luciferase, CRISPR, Adenovirus

Background

Cancer is caused by mutations in tumor suppressors and proto-oncogenes, most of which are acquired by somatic cells during life-time. The identity and combination of the affected genes defines genetic cancer subtypes with distinct morphology, aggressiveness, metastatic potential, clinical prognosis and, probably most importantly,

*Correspondence: stiewe@uni-marburg.de

[1] Institute of Molecular Oncology, Universities of Giessen and Marburg Lung Center (UGMLC), Member of the German Center for Lung Research (DZL), Philipps-University, Marburg, Germany
Full list of author information is available at the end of the article

with different therapeutic vulnerabilities. In lung cancer, for example, small cell lung cancer (SCLC) almost universally displays combinations of inactivating mutations in the tumor suppressor gene *TP53* and one or more of the *RB* family pocket proteins [1]. In contrast, non-small cell lung cancer (NSCLC) is characterized by activating mutations affecting proto-oncogenic receptor tyrosine kinases or downstream signal transducers, offering personalized therapy options with oncogene-targeted drugs such as tyrosine or MAP kinase inhibitors [2]. The value of animal models for preclinical therapy studies therefore critically depends on how accurately mouse tumors resemble the complex and diverse genetics of human tumors [3].

Among the broad spectrum of animal cancer models, xenograft models based on patient-derived primary tumor tissues or human cancer cell lines obviously model the genetics of human tumors most precisely and have become especially popular for therapy studies, as tumors often grow rapidly within a few weeks. When grafted on the flank of mice, tumor growth is directly visible and measurable with calipers which facilitates the establishment of large animal cohorts with tumors of similar stage. However, being transplanted and grown in an immunocompromised host, xenografts fail to develop the characteristic tumor microenvironment (TME) that is shaped by stage-specific, reciprocal interactions with stromal and immune cells [4–7]. As the TME promotes metastatic tumor progression, protects tumors from drugs and immune attack, and presents itself numerous therapeutic targets, immunodeficient xenograft models have limited value for the preclinical evaluation of many TME-targeted treatments including, for example, immune checkpoint inhibitors [5–7].

At the other end of the spectrum are non-transplanted, autochthonous tumors developing orthotopically from single normal cells that were transformed in situ by engineered mutations. In such genetically engineered mouse models (GEMM) tumorigenic mutations are most commonly introduced into the germline of mice, with various conditional approaches allowing for temporal and spatial expression control. In a laborious and time-consuming process, multiple different germline alleles are combined by cross-breeding to obtain experimental animals with the desired complex genotype. In the course, a majority of mice are sacrificed because of an unwanted genotype, which is constantly raising major ethical concerns. More recent advances with in situ mutagenesis of somatic cells using CRISPR technologies have allowed to directly introduce multiple defined tumorigenic mutations into living mice [8–10]. Circumventing germline modifications, somatic gene editing avoids the ethical problems of inefficient breeding schemes and, at the same time, models the natural course of tumorigenesis originating from a single, somatically mutated cell even better.

A technical hurdle of in vivo mutagenesis remains the efficient delivery of the gene editing machinery. Currently, gene transfer by viral vectors such as lentiviruses, adenoviruses (AV) or adeno-associated viruses is most efficient in many models, but limited by the large size of expression cassettes for CRISPR nucleases such as SpCas9, sgRNAs and accessory proteins like Cre, which together exceed the cargo packaging capacity of many common vectors [9]. This problem can be circumvented by split-approaches that separate the effectors into different vectors [11], by switching to naturally shorter or size-optimized CRISPR enzymes [12], by newer vector generations with higher cargo capacity [13] or by providing some of the CRISPR components, such as Cas9, via a conditional, Cre-inducible, germline transgene [14]. For example, adenovirus- or AAV-mediated transfer of CRISPR effectors targeting various tumor suppressor genes was successfully applied to engineer SCLC in mice, showing that co-mutations in the RB-family members *Rbl1* and *Rbl2* [15], the lysine demethylase *Kdm5a/Rbp2* [16] or Notch receptors *Notch1* and *Notch2* [17] enhance SCLC development initiated by combined *Trp53* and *Rb1* mutations.

Because genetically-altered cells progress in situ through different stages of tumorigenesis, involving the accumulation of secondary cooperating mutations and development of immune escape strategies, tumor growth is typically much slower, more variable in time and between animals, and consequently experimentally less predictable. Therapy studies using autochthonous tumors therefore require tools for longitudinal monitoring to identify mice with tumors of an appropriate stage and enroll them into the treatment protocol at the optimal time point.

Multiple methods for longitudinal tumor monitoring in animals have been developed, most of which rely on imaging technologies such as computed tomography, magnetic resonance imaging, positron-emission tomography, single-photon emission computed tomography, ultrasonography and optical imaging of bioluminescence or fluorescence [18]. Notably, these sophisticated technologies do not only require expensive equipment and a highly trained staff, imaging is also time-consuming and requires anesthesia for immobilization of the animal. In addition, contrast agents, radioactive or fluorescent tracers or luminescence substrates are often administered systemically to improve sensitivity or signal specificity. All these factors not only considerably increase the complexity of the experiment, but also contribute significantly to animal burden and therefore strongly limit the examination frequency.

An alternative tumor monitoring method uses secreted luciferases that are released by cells into the environment and which exhibit higher luminescence activity and stability than conventional luciferases [19]. Similar to clinical tumor markers, such as prostate-specific antigen, which are routinely used in patients for cancer screening or therapy monitoring, xenograft growth induced by transplanted tumor cells expressing a secreted luciferase from the marine copepod *Gaussia princeps* (GLuc) can be quantitatively monitored based on GLuc activity levels determined ex vivo in small-volume blood or urine samples [20–26]. Importantly, as GLuc secretion is an active energy-consuming process and the half-life of GLuc in circulation is only approximately 10 min [21], GLuc activity in the blood is specifically measuring the amount of viable tumor cells in the organism, thereby excluding both necrotic cells and stromal cells that contribute to the tumor volume measured by morphological imaging techniques [27]. While secreted luciferases have become increasingly powerful for monitoring transplanted tumors, it has so far not been possible to exploit their scientific and animal welfare advantages for monitoring the growth of non-transplanted, autochthonous tumors in germline or somatic GEMMs.

Here we describe a flexible and easy-to-use toolkit that combines the induction of genetically-defined autochthonous tumors by adenoviral CRISPR vectors with GLuc as a blood-based tumor marker for longitudinal disease monitoring. For this, we have first generated a reporter knock-in mouse *Gt(ROSA)26Sor*$^{tm2(CAG-GLuc)Thst}$ containing a Cre-inducible GLuc transgene (Fig. 1a). Second, we have established a cloning system for rapid and flexible assembly of adenoviral CRISPR vectors (CRISPR-AVs) expressing both CRISPR effectors (SpCas9 and gene-specific sgRNAs) and Cre recombinase in an adenoviral vector backbone. Using lung cancer as a model, we demonstrate that infection of mouse lungs with such CRISPR-AVs induces tumor-initiating cancer gene mutations and simultaneously labels the incipient cancer cells with GLuc, so that cancer growth can be monitored over time by measurement of GLuc activity as a tumor marker in small-volume blood samples.

Methods

Animal experiments

All mouse experiments were performed according to the German Animal Welfare Law (TierSchG) and were approved by the local authorities (Regierungspräsidium Gießen and Darmstadt). Mice were housed in specific-pathogen free conditions, on a 12-h light/dark cycle and fed with standard housing diet (Altromin) receiving water ad libitum.

Generation of STOCK-*Gt(ROSA)26Sor*$^{tm2(CAG-GLuc)Thst}$ (LSL-GLuc) *reporter mice.* Transgenic mice conditionally overexpressing GLuc luciferase in tumor cells are based on a modified ROSA26 targeting approach replacing the splice acceptor site of pBigT by a CAG promoter [28]. GLuc open reading frame was PCR amplified to introduce NheI and NotI sites, and cloned into the corresponding sites of the pBigT-CAG vector. Thereafter, the generated pBigT-CAG-GLuc cassette was cloned into PacI and AscI sites of the pRosa26-PA construct. The final construct was linearized by KpnI and electroporated into V6.5 F1 hybrid ES cells. Targeted stem cell clones were selected by G418 treatment and subsequently screened by Southern blotting using a 5' external probe combined with EcoRV digestion. Positive ES cell clones were injected into C57BL/6 blastocysts. The resultant chimeras were backcrossed to C57BL/6 mice and maintained on a mixed C57BL/6/129 background.

Other mouse strains used are: 129S2*SvHsdThst*, STOCK-*Gt(ROSA)26Sor*$^{tm1(CAG-cas9*,-EGFP)Fezh}$*/JThst* (LSL-Cas9) [14], B6.129-*Gt(ROSA)26Sor*$^{tm2(ACTB-Luc)Tyj}$/NciThst (LSL-FLuc) [29], B6.129S/Sv-*Kras*^{tm4Tyj}/JThst (LSL-KrasG12D) [30], B6.Cg-Tg(IghMyc)22Bri/JThst (EμMyc) [31], C.129S4-*Rag2*$^{tm1.1Flv}$ *Il2rg*$^{tm1.1Flv}$/JThst (Rag2γ) [32]. For removal of the LSL-cassette and ubiquitous luciferase expression, LSL-GLuc and LSL-FLuc mice were crossed with 129-Tg(Prm-cre)58Og/JThst (Prm-Cre) mice [33] yielding *Gt(ROSA)26Sor*$^{+/GLuc}$ (GLuc) and *Gt(ROSA)26Sor*$^{+/FLuc}$ (FLuc) mice, respectively.

Transplanted lymphoma model. For in vivo labelling of Burkitt-like lymphoma cells with luciferases, EμMyc transgenic males were crossed with heterozygous GLuc females to obtain double transgenic EμMyc;GLuc males that were bred with homozygous FLuc females. Compound transgenic EμMyc;GLuc/FLuc mice were monitored for lymphoma development. Lymphoma cells were isolated from lymph nodes and spleens of terminally sick mice and 10^6 living cells were transplanted via tail vein injection into immunodeficient Rag2γ recipient mice. For chemotherapy of lymphoma, mice received a single i.p. injection of 300 mg/kg cyclophosphamide.

Autochthonous lung cancer models. For induction of lung cancer, mice were intratracheally injected with adenoviral vectors as described previously [34]. Briefly, mice were anesthetized by intraperitoneal injection of ~ 25 mg/kg ketamine and ~ 0.6 mg/kg medetomidine and maintained at 37 °C during anesthesia. Mice were intubated with a 20G catheter (B.Braun) and 1×10^9 PFU/mouse of purified AV (ViraQuest Inc.) was applied in a volume of 50 µl. AVs were diluted in Minimal Essential Medium (MEM, Sigma) and 2 M $CaCl_2$ was added to a final concentration of 10 mM. After complete inhalation, the catheter was removed, mice were

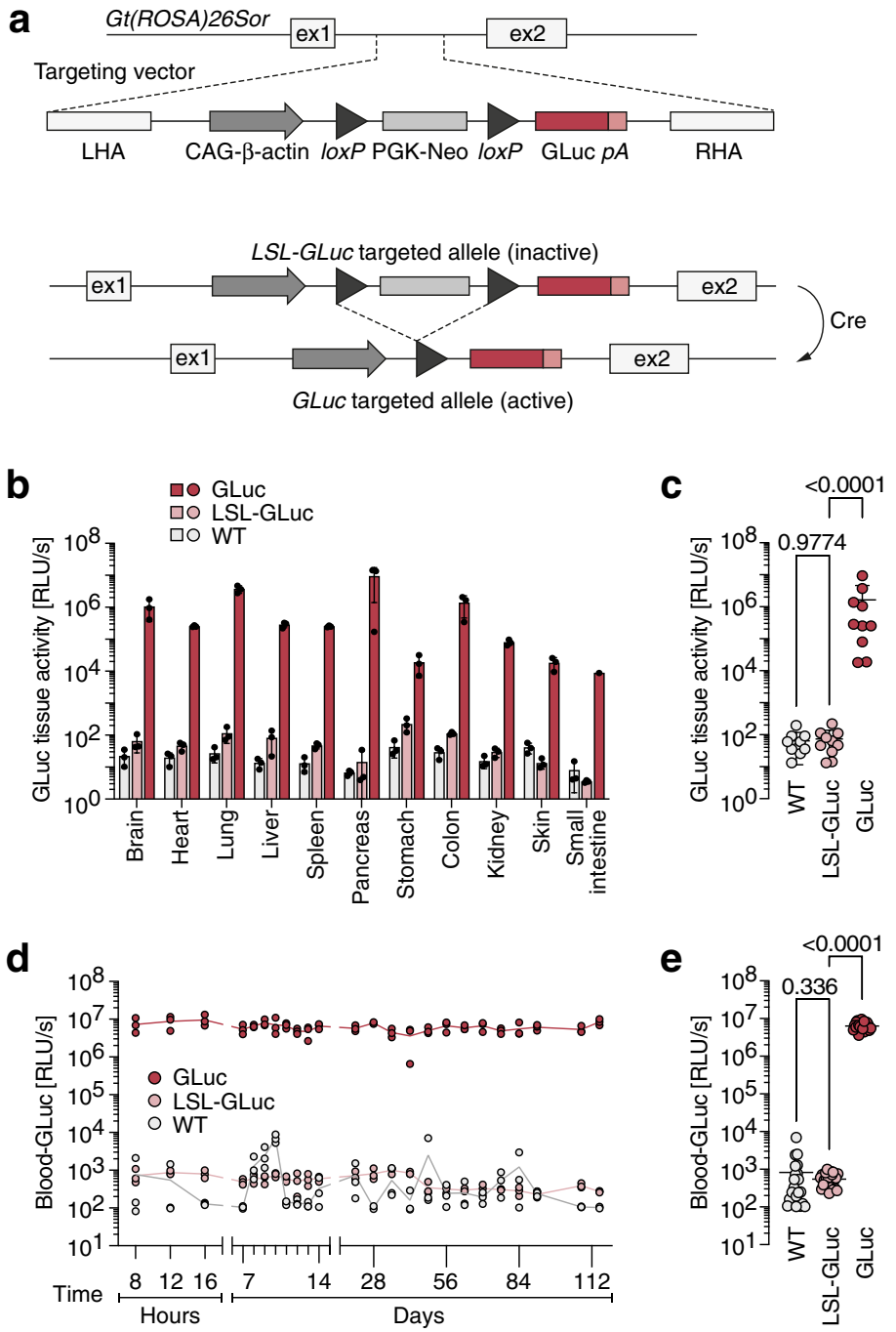

Fig. 1 Conditional GLuc reporter mice. **a** Targeting strategy for *Gt(ROSA)26Sor*$^{tm2(CAG-GLuc)}$ mice: insertion of a GLuc cDNA expression cassette controlled by the cytomegalovirus early enhancer/chicken beta actin (CAG) promoter and a *loxP*-flanked transcriptional stop cassette (LSL) into intron 1 of the *Gt(ROSA)26Sor* gene locus. **b** GLuc activity measured in organ lysates of mice with indicated genotypes ($n = 3$ biological replicates). **c** GLuc tissue activity. Each data point represents one tissue type ($n = 11$ tissues; P-values from Dunnett's multiple comparisons test). **d, e** Level and temporal stability of GLuc activity in blood plasma of mice with indicated genotypes. **d** Time course, $n = 3$ mice per genotype. **e** Time average ± SD with data points representing individual time points ($n = 24$ time points; *P*-values from Dunnett's multiple comparisons test

kept warm and monitored for breathing and recovery. Anesthesia was partially antagonized using ~ 1.5 mg/kg atipamezole and mice were transferred to individually ventilated cages (IVC). For induction of lung adenocarcinoma, a *Kras*$^{+/LSL-G12D}$;*Rosa26*$^{LSL-GLuc/LSL-FLuc}$ mouse and a *Rosa26*$^{LSL-GLuc/LSL-FLuc}$ control were infected with AV-Cre (ViraQuest Inc.). For induction of SCLC, wild-type, *Rosa26*$^{LSL-GLuc}$ or *Rosa26*$^{LSL-Cas9/LSL-GLuc}$ mice were infected with CRISPR-AVs.

Mice were analyzed by MRI and BLI using an IVIS 100 Imaging System (Xenogen), an In Vivo Xtreme II System (Bruker) or 7 T Clinscan 70 /30 USR (Bruker) as previously described [34, 35]. Mice were anesthetized with isoflurane. Bioluminescence was recorded 5 min after intraperitoneal injection of 200 µl D-luciferin (15 mg/ml in PBS, BioVision).

Cell culture

The murine NIH 3T3 cell line was obtained from the American Tissue Collection Center (ATCC), Ad293 cells from Agilent. Primary dermal fibroblasts were isolated from LSL-Cas9 and LSL-GLuc mice: ear biopsies were minced and digested with 1000 U/ml collagenase Ia (Sigma) overnight at 4 °C followed by a 45 min treatment with 0.025% Trypsin solution (Sigma) at 37 °C. Disaggregated tissue was resuspended in 5 ml Dulbecco's Modified Eagle Medium (DMEM, Thermo Fisher) supplemented with 20% fetal bovine serum (FBS, Sigma-Aldrich) and cultured until immortalization. For further experiments, cell lines were cultivated in a humidified atmosphere at 37 °C and 5% CO_2 using DMEM supplemented with 10% FBS, 100 U/ml penicillin and 100 µg/ml streptomycin (Life Technologies).

Generation of a NIH3T3-Cas9 cell line. NIH3T3 cells were infected with the lentivirus lentiCas9-Blast (Addgene #52962) and selected with 20 µg/ml Blasticidin (Invivogen) starting 2 days post infection for 3 days until resistant cell clones were established. Infectious lentiviral particles were produced as previously described [36].

Generation of murine SCLC cell lines. Tumors were excised, washed twice in ice-cold PBS (Thermo Fisher), minced and digested in 2 ml of 0,025% Trypsin/EDTA (Sigma) at 37 °C for 30 min, resuspended in 5 ml of Roswell Park Memorial Institute 1640 Medium (RPMI 1640, Gibco) supplemented with 10% FBS and 100 U/ml penicillin and 100 µg/ml streptomycin. Cells were observed daily and medium was subsequently replaced every 3 days until a stable cell line was established.

Adenoviral CRISPR vectors

Single-guide RNAs (sgRNAs) targeting genes of interest were designed and cloned into the pSpCas9(BB)-2A-Puro vector (Addgene #62988) using Golden Gate Cloning as described [24]. The following sgRNAs were used: *Trp53*: 5'-CAT AAG GTA CCA CCA CGC TG-3', *Rb1*: 5'-GAA CAG ATT TGT CCT TCC CG-3 ', *Rbl2*: 5'-CCC GTG AGT CGA GTT GGT GT-3 ', Control: 5'-GGG CGA GGA GCT GTT CAC CG-3'. The pSpCas9(BB)-2A-Puro gRNA containing plasmids were used as template for PCR amplification of the U6-sgRNA region using Q5® High Fidelity DNA Polymerase (NEB). For directional Golden Gate Assembly of multiple sgRNA amplicons, BbsI restriction sites and unique 4 bp overhangs were added to the primers, the following primers were used: sgRNA1 forward 5'- GGT GAA GGA AGA CTC GGC TGA GGG CCT ATT TCC CAT G-3'; sgRNA1 reverse 5'- GGT GAA GGA AGA CTC CAA AAA AGC ACC GAC TCG G-3', sgRNA2 forward 5'-GGT GAA GGA AGA CGT TTT GAG GGC CTA TTT CCC ATG-3'; sgRNA2 reverse 5'- GGT GAA GGA AGA CGT CCC TCA AAA AAG CAC CGA CTC GG-3', sgRNA3 forward 5'-GGT GAA GGA AGA CTG AGG GCC TAT TTC CCA TGA-3'; sgRNA3 reverse 5'-GGT GAA GGA AGA CGT GCG GAA AAA AGC ACC GAC TCG G-3'. PCR products were cloned into pCR™-Blunt II-TOPO® (TOPO) using the Zero Blunt™ TOPO™ PCR Cloning Kit (Invitrogen). U6-sgRNA cassettes were excised with BbsI (NEB), gel purified using the Wizard® Genomic DNA Purification Kit (Promega) and used for Golden Gate assembly into shuttle plasmids pShuttle.Cre and pShuttle.CC9 containing sgRNA cloning site and expression cassettes for Cre or Cre-T2A-SpCas9. For the generation of shuttle plasmids, the Gateway™ pDONR™221 plasmid (Invitrogen) was modified to include BsaI sites flanked by the attL sites. For pShuttle.Cre, the nls-Cre sequence was PCR amplified from pHR-CMV-nlsCre (Addgene #12265) using primers adding a BbsI site and a unique 4 bp sequence: nlsCre forward 5'-GGT GAA GGA AGA CGT CCG CGT TAC ATA ACT TAC GGT AAA TGG CCC GC-3'; nlsCre reverse 5'- GGT GAA GGA AGA CGA TTC CCT AAT CGC CAT CTT CCA GCA GGC GCA C-3'. The PCR product was cloned into pCR™-Blunt II-TOPO® using the Zero Blunt™ TOPO™ PCR Cloning Kit (Invitrogen). The previously modified Gateway™ pDONR™221 plasmid and the BbsI-digested pCR™-Blunt II-TOPO®-nlsCre plasmid were used for Golden Gate Cloning together with a pre-annealed oligonucleotide containing two BsaI sites for later sgRNA insertion: forward 5'- GGC TAG AGA CCT AGA GCG ATC GCT CGC GGT CTC A-3', reverse 5'- GCG GTG AGA CCG CGA GGC TAG CCT CTA GGT CTC T-3'. For the pShuttle.CC9 plasmid, nlsCre was PCR amplified using the nlsCre forward primer and a reverse primer containing part of a T2A sequence: nlsCre reverse-T2A: 5'- GGT GAA GGA AGA CGT TGT TAG CAG ACT TCC TCT GCC CTC TCC GCT TCC ATC GCC ATC

TTC CAG CAG-3'. SpCas9 was amplified from pX330-U6-Chimeric_BB-CBh-hSpCas9 (Addgene #42230) using the primers: Cas9 forward-T2A 5'- GGT GAA GGA AGA CGA AAC ATG CGG TGA CGT CGA GGA GAA TCC TGG ACC TAT GGA CTA TAA GGA CCA CGA-3', Cas9 reverse 5'- GGT GAA GGA AGA CGA TTC CCC AGC ATG CCT GCT ATT CTC TTC C-3'. Cre-T2A and T2A-Cas9 amplicons were cloned into pCR™-Blunt II-TOPO®, released by BbsI digest and used for Golden Gate Cloning as described for the pShuttle.Cre vector. Shuttle vectors containing sgRNAs were recombined with pAd/PL-Dest vector (Invitrogen) using the Gateway™ LR Clonase™ II Enzyme Mix (Invitrogen).

For generation of infectious adenoviruses (AVs), 10 µg pAd/PL-Dest vector, carrying the desired expression cassettes (sgRNAs, Cre, SpCas9), was linearized using PacI (NEB) to reveal ITR regions. The released adenoviral vector genome was purified using the Wizard® Genomic DNA Purification Kit (Promega) and transfected into 7×10^5 Ad293 cells (Agilent) using Lipofectamine™ 2000 Transfection Reagent (Invitrogen). One day post transfection, medium was changed to DMEM supplemented with 2% FBS. Cells were harvested when showing the desired cytopathic effect and snap frozen in liquid nitrogen. AVs were released by 3 cycles of freeze–thaw and, following pelleting of debris (10 min, 3000 g, 4 °C), used to infect 8×15 cm dishes of 7×10^6 Ad293 cells seeded one day prior to infection. After 3–4 days, high-titer AV was harvested by resuspending and pelleting cells. Cell pellets were resuspended in 5 ml PBS/10% Glycerol (Roth) and AV particles were released by 3 freeze–thaw cycles followed by centrifugation for removal of debris (10 min, 3000 g, 4 °C). For in vitro experiments, cells were incubated with AVs diluted in a low volume of DMEM supplemented with 2% FBS for 1 h before adding complete DMEM (10% FBS, 1% P/S) to full volume. For in vivo experiments, AVs were commercially (ViraQuest Inc.) amplified, purified and titrated for plaque-forming units (PFU).

Luciferase assays

To monitor tumor development by GLuc secretion, 10–20 µl blood was obtained by puncturing the tail vein. Blood was directly mixed with 4 µl of 0.125 IU/ml heparin (Ratiopharm). Plasma was collected by centrifugation (15 min, 1200 g, 4 °C) and, optionally, stored in round-bottom 96-well plates sealed with clear foil at -20 °C. Luciferase activity measurements of plasma samples were performed as previously described for monitoring of transplanted tumors [27]. Briefly, plasma samples were diluted with phosphate-buffered saline (PBS) to match the dynamic range of the Orion II luminometer (Berthold). 5 µl of diluted plasma were transferred to white 96-well plates with V-bottom (Greiner) and measured by automated injection of 50 µl coelenterazine (PJK, Germany, stock diluted 1:200 in PBS). Coelenterazine was prepared as a 10 mM stock in acidified ethanol (10 ml EtOH + 200 µl 6 M HCl). To monitor the time course of tumor development and account for subtle differences in AV infection efficiency, all luminescence values from one mouse were normalized to its baseline luminescence, operationally defined as the mean luminescence during the first 90 days after AV infection. The mean ± 3SD of the baseline luminescence of all mice in the experiment was considered 'background'. Normalized luminescence values exceeding this background level were considered significantly altered. For measuring luciferase activity in tissues, 10–20 mg tissue were lysed with 5 × Cell Culture Lysis Reagent (Promega) and a metal bead for 5 min at 50 Hz in TissueLyser LT (QIAGEN). Lysates were cleared from debris by centrifugation and measured as described for plasma samples.

Western blot

For immunoblotting, cells were lysed in RIPA Lysis Buffer (50 mM Tris–HCl, 150 mM NaCl, 0.1% SDS, 1% Sodium Deoxycholate, 1% Triton X-100) supplemented with protease inhibitor (complete ULTRA tablets EASYpack, Roche). The following antibodies were used: anti-Cas9 (Diagenode #C15200216 1:500), anti-p53 (Bioss #bs8687R, 1:1000), anti-Rb1 (Cell Signaling #9313, 1:1000), anti-p130 (SantaCruz Biotech #sc-317, 1:200), anti-β-actin (AC-15, #ab6276, Abcam, 1:2500). For detection, secondary anti-rabbit or anti-mouse IgG-HRP (GE Healthcare, 1:5000) and SuperSignal ECL Kit (ThermoFisher) were used. Anti-β-actin was detected using an Alexa-488 coupled secondary antibody.

Immunohistochemistry

For immunohistochemistry (IHC), tissue samples were cut as 3 µm thick sections from formalin-fixed paraffin embedded (FFPE) tissues. IHC staining was performed using a Bond Max automated staining system (Leica) using the antibodies: anti-Ascl1 (Abcam #211327, 1:400), anti-Chromogranin (Abcam #52983, 1:250), anti-Synaptophysin (Abcam #32127, 1:1000). GLuc and Cas9 staining was performed manually using the antibodies: anti-GLuc (Prolume Ltd, 1:1000), anti-Cas9 (Cell Signaling #19526, 1:400). Images were acquired using the Leica Aperio Versa slide-scanner and Leica Aperio eSlide Manager software v. 1.0.3.37. IHC images were analyzed quantitatively using the Aperio ImageScope software v. 12.3.2.8013. Tumors were marked and outlined by individuals blinded to the experimental setup and their area quantified in ImageScope. Tumor burden was calculated as percentage of tumor area to total lung area.

CRISPR editing assays

T7 Endonuclease I assay. For analysis of the gene editing efficiency following infection with CRISPR AVs, sgRNA target sites were PCR amplified using genomic DNA of infected cells. PCR amplicons were purified using the PCR Purification Kit (QIAGEN) and analyzed by T7 Endonuclease I Assay as described [24]. Primers for *Trp53*: forward 5'-CGT CCA ATG GTG CTT GGA CA-3 '; reverse 5 '-GGG AAG AAA CAG GCT AAC CTA ACC-3', *Rb1*: forward 5'- CTG CTG GGA TTA AAG GCA AG-3 '; reverse 5 '-CCT GCA CTC ACA CTC AGG AA-3', *Rbl2*: forward 5'- GTA CTA CAC AAG GGT GTG GGC-3 '; reverse 5 '-CGA GGG GAG CCT GTT CTT ACA AAA-3'.

CRISPR amplicon sequencing. For sequencing analysis of gene editing events, sgRNA target sites were amplified from genomic DNA of cell culture, lung or tumor samples using the primers *Trp53*: forward 5'-CGA TGG TGA TGG TAA GCC CTC-3 '; reverse 5 '-TCT AGG CTG GAG TCA ACT GTC TC-3', *Rb1*: forward 5'-AAG TAC ATT GCA GCA TCT TG-3 '; reverse 5 '-AGG TCA CTT ACG CAT GAA TA-3', *Rbl2*: forward 5'- TCC AGA CCG GCA CCC TTT GTT C-3 '; reverse 5 '-TAC TGA CCT GCG CGT TTG CCT G-3'. For multiplex sequencing of multiple samples, amplicons were barcoded by adding the following overhangs to the gene-specific primers listed above: B1: forward 5'-TCA CTG GCA-3'; reverse 5'-TAG CTG CTG GCA-3', B2: forward 5'-AGT GGT CGA-3'; reverse 5'-GTA CAT GGT CGA-3', B3: forward 5'-CTA TAC TGT G-3'; reverse 5'-AGA GCA CTG TG-3', B4: forward 5'-CGG ACA AAA G-3'; reverse 5'-TGT TCC AAA AG-3', B5: forward 5'-GTC TAG CCA CC-3'; reverse 5'-ACT AGC CAC C-3'. PCR products were purified as described before and their concentration was determined using a NanoDrop™ 2000 spectrophotometer (Thermo Fisher). Barcoded PCRs for *Trp53*, *Rb1* and *Rbl2* were pooled and sequencing libraries were prepared using the NEBNext Ultra DNA Library Prep Kit (NEB) and sequenced on a MiSeq platform (Illumina) with the MiSeq Reagent Kit v3 (600-cycle) or MiSeq Reagent Kit v2 (500-cycles). Editing events were analyzed with CRISPResso2 [37].

CRISPR Off-Target Analysis. Possible off-target sites of the *Trp53*, *Rb1* and *Rbl2* sgRNAs were identified using the CRISPRoff Tool version 1.2 beta [38]. The list of predicted off-targets was filtered for intragenic location and presence of an "NGG" PAM and sorted by CRISPRoff score (Additional file 3). The Top10 hits for each of the *Trp53*, *Rb1* and *Rbl2* sgRNAs were PCR amplified from genomic tumor DNA (Additional file 4) and analyzed for mutations by Sanger sequencing.

Software and statistical analysis

All statistical analyses were performed with GraphPad Prism 8 software. All graphs show mean values obtained with n biological replicates, and error bars in all figures represent standard deviation (SD), unless indicated otherwise. A *P*-value 0.05 was used as the threshold level for significance. For Kaplan–Meier survival curves, the log-rank test was applied. Two groups were tested for statistically significant differences by a two-sided unpaired t-test; multiple groups were tested by 1way ANOVA in conjunction with a post hoc multiple comparison test. Experimental schemes were generated with BioRender.com.

Results

Generation of conditional GLuc reporter mice

To enable in vivo labelling of cells with GLuc for blood-based monitoring of tumors, we have first generated a GLuc transgenic knock-in mouse *Gt(ROSA)26Sor*$^{tm2(CAG-GLuc)Thst}$ (short: *Rosa26*$^{LSL-GLuc}$ or LSL-GLuc) (Fig. 1a). GLuc expression is under control of the strong, ubiquitously active synthetic CAG promoter and rendered conditional to Cre recombinase activity by insertion of a *loxP*-flanked transcriptional stop cassette (LSL). To test the inducibility of GLuc in different organs, we excised the LSL-cassette from the germline by crossing LSL-GLuc and *Prm*-Cre mice [33] and compared GLuc activity in organ lysates from LSL-GLuc and GLuc littermates (Fig. 1b, c). GLuc activity in LSL-GLuc mice was not significantly different from background luminescence in non-GLuc-transgenic control mice, indicating that expression is not leaky (Fig. 1c). Removal of the LSL cassette led to strong induction of GLuc activity in all analyzed organs (Fig. 1b), exceeding the background level by, on average, more than 4 orders of magnitude (73,118-fold; $P < 0.0001$; Fig. 1c). For longitudinal monitoring of cells using GLuc blood levels, it is essential that GLuc is secreted at a constant rate resulting in stable blood activity levels over time. When monitoring the blood of animals over 4 months, luciferase blood activity in GLuc mice was more than 4 orders of magnitude higher than in non-Cre expressing LSL-GLuc mice (mean 13,595-fold; $P < 0.0001$), with little to no variation over time (Fig. 1d, e). Again, transgene expression was not leaky as blood levels in LSL-GLuc mice were not significantly different from controls (Fig. 1e). We conclude that the LSL-GLuc reporter mouse is suitable to monitor cellular processes by non-leaky expression and stable secretion of GLuc.

In vivo labelling of tumors with GLuc

In previous studies, tumor cells were labelled ex vivo with GLuc by, for example, lentiviral transduction to monitor

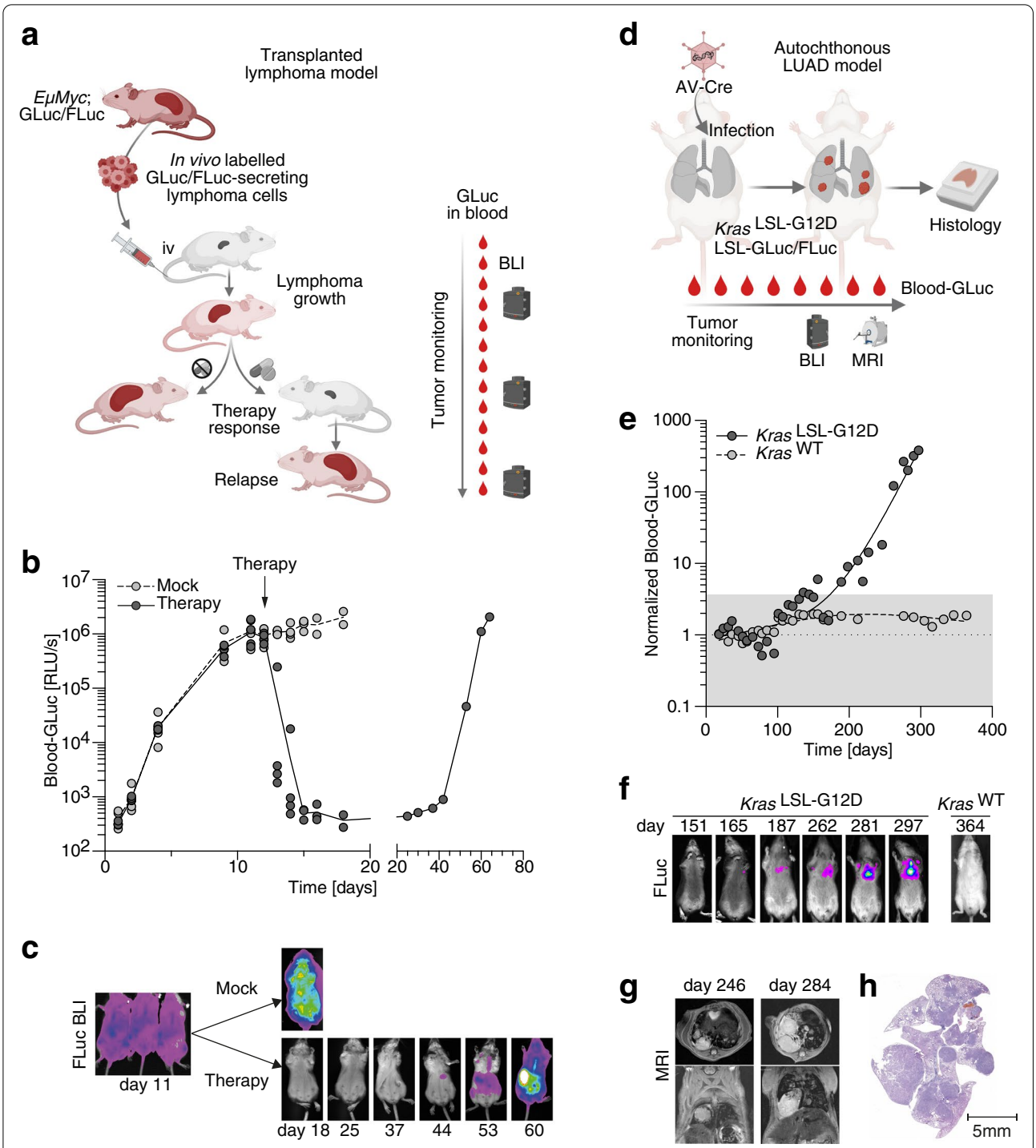

Fig. 2 Monitoring classic tumor models with GLuc. a-c Monitoring of in vivo labelled transplanted lymphomas with GLuc. **a** Experimental scheme. Red color symbolizes GLuc activity. BLI, bioluminescence imaging. **b** Time course of GLuc activity in blood samples of mice transplanted with lymphoma cells from *EμMyc;Rosa26*$^{GLuc/FLuc}$ mice. Data points represent individual mice. **c** BLI of representative mice at different time points after mock or cyclophosphamide treatment. **d-h** Monitoring of non-transplanted (autochthonous) lung adenocarcinoma with GLuc. **d** Experimental scheme. **e** Temporal development of blood GLuc activity in mice of indicated genotype. **f** Longitudinal BLI of mice with indicated genotype. **g** Sequential MRI of the *Kras*$^{LSL-G12D}$ mouse. **h** H&E stain of the *Kras*$^{LSL-G12D}$ mouse lung at time of sacrifice All error bars indicate SD, all data points represent biological replicates/individual mice. BLI, bioluminescence imaging; MRI, magnetic resonance imaging; LUAD, lung adenocarcinoma

their growth after transplantation into mice [20–22, 24, 27]. However, many primary tumor cells either fail to grow in culture or loose characteristic properties. For instance, Myc-induced Burkitt-like B cell lymphomas tend to develop chemotherapy resistance when cultured in vitro [39]. To test if luciferase-transgenic mice can be used for in vivo labelling and therapy monitoring of Myc-induced lymphomas, we generated *EμMyc* mice with GLuc and, for comparison, classical non-secreted firefly luciferase (FLuc) transgenes (Fig. 2a). Freshly explanted, in vivo GLuc/FLuc-labelled lymphoma cells were transplanted into recipients and disease development was monitored based on GLuc blood levels (Fig. 2b). GLuc activity progressively increased in the blood of all animals by more than 3 orders of magnitude by day 11, when lymphoma disease was independently confirmed by bioluminescence imaging (BLI) for FLuc activity (Fig. 2c). On day 12, half of the animals received a single dose of cyclophosphamide chemotherapy, causing a > 1000-fold decrease in GLuc blood levels over the next two days and absence of FLuc BLI signals on day 18. All untreated animals showed progressively increased GLuc blood levels and FLuc BLI signals before reaching the humane study endpoint with extensive lymphoma burden. One of the treated mice died from relapse after two months. This was preceded by a parallel increase in GLuc blood and FLuc BLI signals. These observations underline that in vivo labelling with both luciferases similarly enabled longitudinal monitoring of therapy responses. However, while the distress caused by anesthesia is limiting the BLI examination frequency, small-volume, 10–20 µl blood samples needed for GLuc activity measurements could be obtained much more frequently, yielding a high temporal resolution for capturing fast dynamic processes such as therapy responses.

We next explored using LSL-GLuc reporter mice for monitoring of non-transplanted tumors developing in an autochthonous model of $Kras^{G12D}$ oncogene-driven lung adenocarcinoma. For this, we generated a mouse carrying a germline knock-in of the Cre-inducible $Kras^{LSL-G12D}$ oncogene [30] in conjunction with the conditional LSL-GLuc and LSL-FLuc alleles (Fig. 2d). Upon intratracheal infection with Cre-expressing adenovirus (AV-Cre), the $Kras^{LSL-G12D}$ mouse developed multiple lung adenomas and adenocarcinomas accompanied by a parallel increase in GLuc blood activity and thoracic FLuc bioluminescence 5–10 months after infection (Fig. 2e-h). Of note, a mouse carrying luciferase alleles but no oncogene did not show detectable increases in GLuc or FLuc activity following AV-Cre infection confirming a tumor-derived origin of the signals (Fig. 2e-f). Together these pilot experiments demonstrated the suitability of LSL-GLuc reporter mice for in vivo labelling of tumor cells and monitoring tumor growth.

Flexible toolkit for rapid assembly of CRISPR-adenoviruses

The natural tropism for the respiratory epithelium makes adenoviral vectors (AVs) particularly efficient for lung-specific delivery of Cre and activation of Cre-inducible germline-encoded transgenes such as $Kras^{LSL-G12D}$ [30, 40–42]. Moreover, the large transgene packaging capacity makes AVs also exceptionally well suited to deliver larger genetic cargo such as CRISPR nucleases for lung-specific induction of somatic cancer mutations [15, 43, 44]. However, the most commonly used adenovirus (serotype 5) consists of a large linear, 36-kb, double-stranded DNA molecule, which makes cloning adenoviral vectors more laborious than, for example, lentiviral or adeno-associated vectors. To more rapidly produce CRISPR-adenoviruses (CRISPR-AVs) delivering Cre-recombinase together with CRISPR nucleases, consisting of *Streptococcus pyogenes* Cas9 (SpCas9) and gene-specific sgRNAs, we have developed a cloning toolkit which uses Golden Gate cloning with type IIs restriction endonucleases [45] for the flexible assembly of multiple expression cassettes and Gateway recombineering [46] for the final integration of the complete multi-cistronic assembly into the adenoviral vector genome [47].

In the first step, sgRNAs targeting the genes of interest are designed and cloned into the puromycin-selectable SpCas9-encoding pX459 plasmid [48] (Fig. 3a). For modelling small cell lung cancer (SCLC), we targeted *Trp53* and *Rb1*, the mouse homologues of the human genes *TP53* and *RB1*, which are mutated in > 90% of all SCLC patients [1]. For each target gene, multiple sgRNAs with low off-target scores (Additional file 3) were cloned into pX459, transfected into NIH3T3 mouse fibroblasts and evaluated for induction of insertion and

(See figure on next page.)

Fig. 3 Toolkit for cloning CRISPR adenoviruses. **a** Multiple candidate sgRNAs targeting cancer genes of interest are cloned into plasmids co-expressing Cas9 and a puromycin resistance gene for functional validation in cell culture. **b** Selected validated sgRNA expression cassettes including U6 promoter and sgRNA scaffold are PCR amplified using primer pairs adding a BbsI recognition site and a 4-bp motif specifying the position in the final vector construct. **c** Optional cloning of PCR amplicons for sequence verification by Sanger sequencing. **d** Release of complementary overhangs by BbsI. **e** Golden Gate assembly of multiple BbsI-digested sgRNA-cassettes with BsaI-digested shuttle vectors containing expression cassettes for Cre + Cas9 or Cre only. **f** Gateway recombination cloning of modified sgRNA-containing shuttle vectors into the adenoviral vector backbone (pAd/PL-Dest destination vector). **g** Release of linear adenoviral DNA by PacI digest. **h** Transfection of Ad293 cells for production and amplification of infectious AV particles

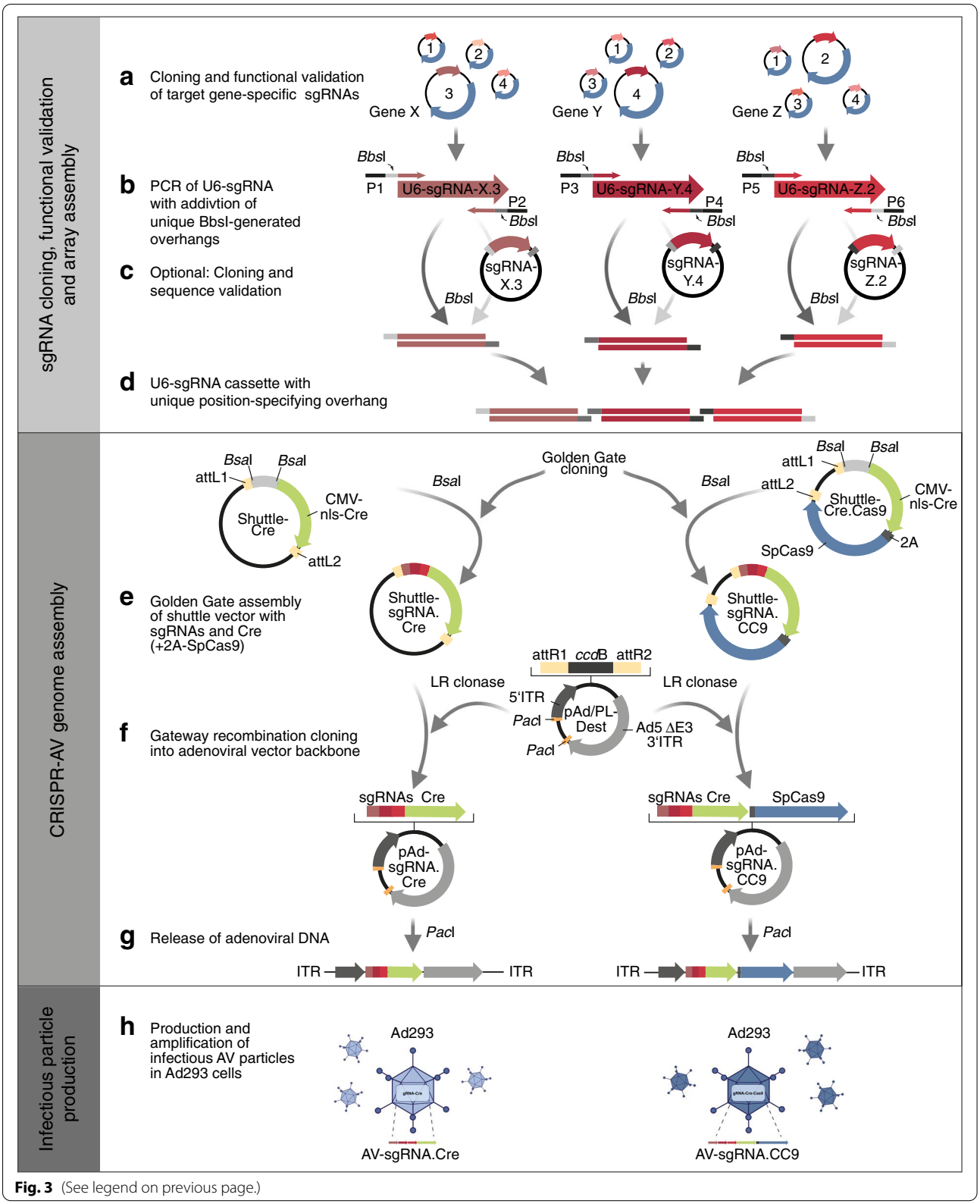

Fig. 3 (See legend on previous page.)

deletion (indel) mutations at the genomic sgRNA target sites. Functionally validated U6 promoter-driven sgRNA expression cassettes were PCR-amplified from pX459 plasmids using primers containing binding sites for the type IIs restriction enzyme BbsI, which releases a unique 4-bp overhang for later assembly with other expression cassettes for sgRNAs, SpCas9 and Cre (Fig. 3b). As an optional step, the PCR amplicons were cloned into a compatible vector for sequence validation (Fig. 3c). Eventually, multiple sgRNA amplicons were digested with BbsI (Fig. 3d) and assembled into a BsaI-restriction site of a shuttle vector containing a CMV promoter-driven Cre-2A-SpCas9 expression cassette flanked by attL recombination sites for Gateway recombination cloning (Fig. 3e). The entire assembly comprising all sgRNAs, Cre and Cas9 was recombined into attR sites of a destination vector containing a first generation (E1/E3-deleted) adenoviral vector genome (Fig. 3f). For production of infectious viral particles, the recombinant adenovirus genome was released from the plasmid by PacI restriction digest (Fig. 3g) and transfected into Ad293 cells for multiple rounds of viral amplification and purification [40] (Fig. 3h). We have hereby developed a versatile cloning system for the rapid generation of adenoviral CRISPR vectors expressing different sgRNA combinations in conjunction with Cre and SpCas9.

Monitoring CRISPR-induced lung tumorigenesis using GLuc blood-levels

We next investigated whether a *Trp53* (P) and *Rb1* (R) targeting CRISPR-AV (AV-PR.CC9) induces lung tumors that can be monitored using GLuc blood levels (Fig. 4a). Confirming the anticipated function, NIH3T3 fibroblasts infected with AV-PR.CC9 induced frameshift-causing *Trp53* and *Rb1* indel mutations as shown by T7 endonuclease assay (Fig. 4b) and resulted in markedly reduced protein expression of p53 and Rb (Fig. 4c). Next, LSL-GLuc mice were infected with AV-PR.CC9 by intratracheal injection. After 1 week, we detected widespread Cas9 and GLuc expression in lung sections by immunohistochemistry (Fig. 4d) and insertion/deletion mutations in *Trp53* and *Rb1* at the sgRNA target site by next generation sequencing (NGS) with a mutation frequency of 6.8% and 6.4%, respectively (Fig. 4e, f). More detailed evaluation of the indel spectrum revealed mostly 1 to 5-bp deletions that were larger and more heterogenous in *Trp53* than *Rb1* (Fig. 4e, f). In parallel, we infected LSL-GLuc mice with AV-C.CC9, which expresses a non-targeting control sgRNA. Tumor development was monitored for up to 15 months (Fig. 4g, h). While none of the AV-C.CC9 infected control mice developed tumors, AV-PR.CC9 mice monitored by magnetic resonance imaging (MRI) started showing tumor nodules 8 months post infection (Fig. 4g). Tumorigenesis proceeded with variable kinetics and reached the experimental endpoint after 9 to 15 months (Fig. 4h). The median survival of AV-PR.CC9-infected LSL-GLuc mice was not significantly different from infected wild-type mice (363 vs 393 days, $P=0.7354$; Fig. 4h) and comparable to conditional *Trp53/Rb1* germline-mutant mouse models for SCLC [49, 50], indicating that neither GLuc expression nor the mechanism of mutagenesis alters the time course of SCLC development.

Histological examination of tumors showed the typical morphology of small cell lung cancer with multiple mitotic figures, dense sheets of tumor cells and fine granular chromatin (Fig. 5a). In line, the majority of tumors stained strongly positive for the neuroendocrine marker synaptophysin and the lineage-specifying transcription factor Ascl1 (Fig. 5a). At the time of sacrifice most animals displayed substantial metastasis, mostly to the liver and in some cases also to the kidney and ovary, showing expression of neuroendocrine markers similar to the primary lung tumors (Fig. 5b, c). Successful GLuc-labelling of tumor cells was confirmed by positive GLuc staining of lung tumor nodules and metastases (Fig. 5a-c). GLuc blood activity started to exceed background levels in individual mice as early as 5 months post infection and increased progressively by a mean 265-fold (range: 10 to 776-fold) until reaching the humane study endpoint (Fig. 5d). Immunohistochemistry confirmed that GLuc expression, similar to neuroendocrine tumor markers, was confined to tumor nodules and largely absent from the adjacent non-tumor tissues (Fig. 5a), strongly suggesting that GLuc activity in blood samples is predominantly derived from tumor cells rather than normal lung.

(See figure on next page.)

Fig. 4 SCLC induction by adenoviral delivery of CRISPR nucleases. **a** Experimental scheme for SCLC induction and monitoring with adenoviral vectors (AV) expressing Cre and *Trp53/Rb1*-targeting Cas9 nucleases. **b** Validation of sgRNA function by T7 endonuclease I assay using genomic DNA from uninfected and AV-PR.CC9 infected NIH3T3 cells. NTC, no template control. **c** Western Blot of mouse embryonic fibroblasts (MEF) infected with AV-PR.CC9 showing Cas9 expression and downregulation of p53 and Rb1 protein levels. β-actin is shown as loading control. **d** Immunohistochemistry for GLuc and Cas9 expression in the lung of mice 1 week after intratracheal AV-PR.CC9 infection. **e,f** Mutation spectrum of **e** *Trp53* exon 6 and **f** *Rb1* exon 17 sgRNA target loci (flanked by dashed lines). Shown are sequencing reads of the most abundant indel mutations at the sgRNA target site. **g** Sequential MRI of a representative mouse showing tumor progression. Shown are frontal and transversal sections with tumors marked in blue. **h** Kaplan–Meier survival plot of WT and LSL-GLuc mice infected with indicated CRISPR-AVs (AV-C.CC9 + GLuc: $n=12$; AV-PR.CC9 + GLuc: $n=8$; AV-PR.CC9 no GLuc: $n=3$). Shown are median survival and P-values from Log-rank (Mantel-Cox) test

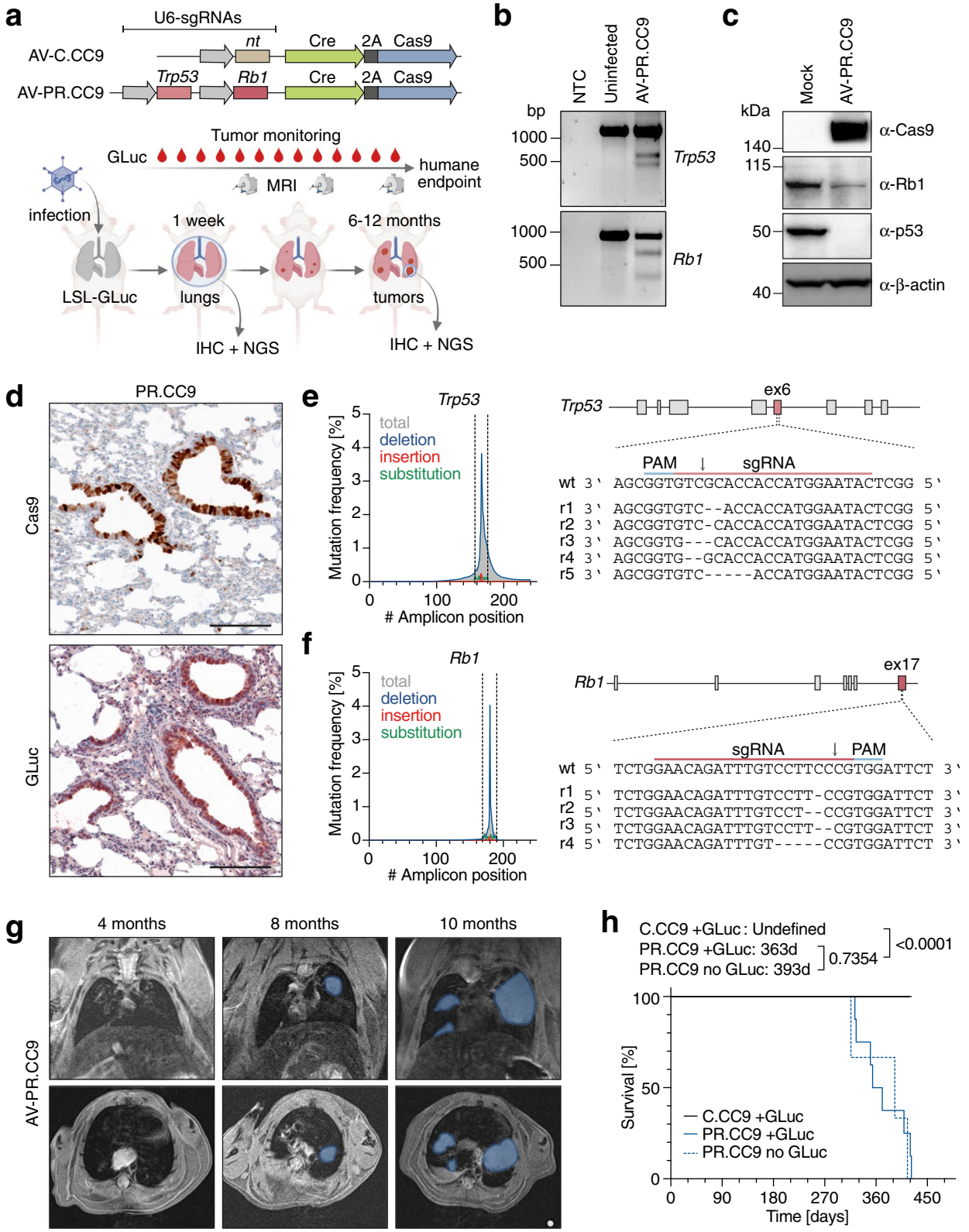

Fig. 4 (See legend on previous page.)

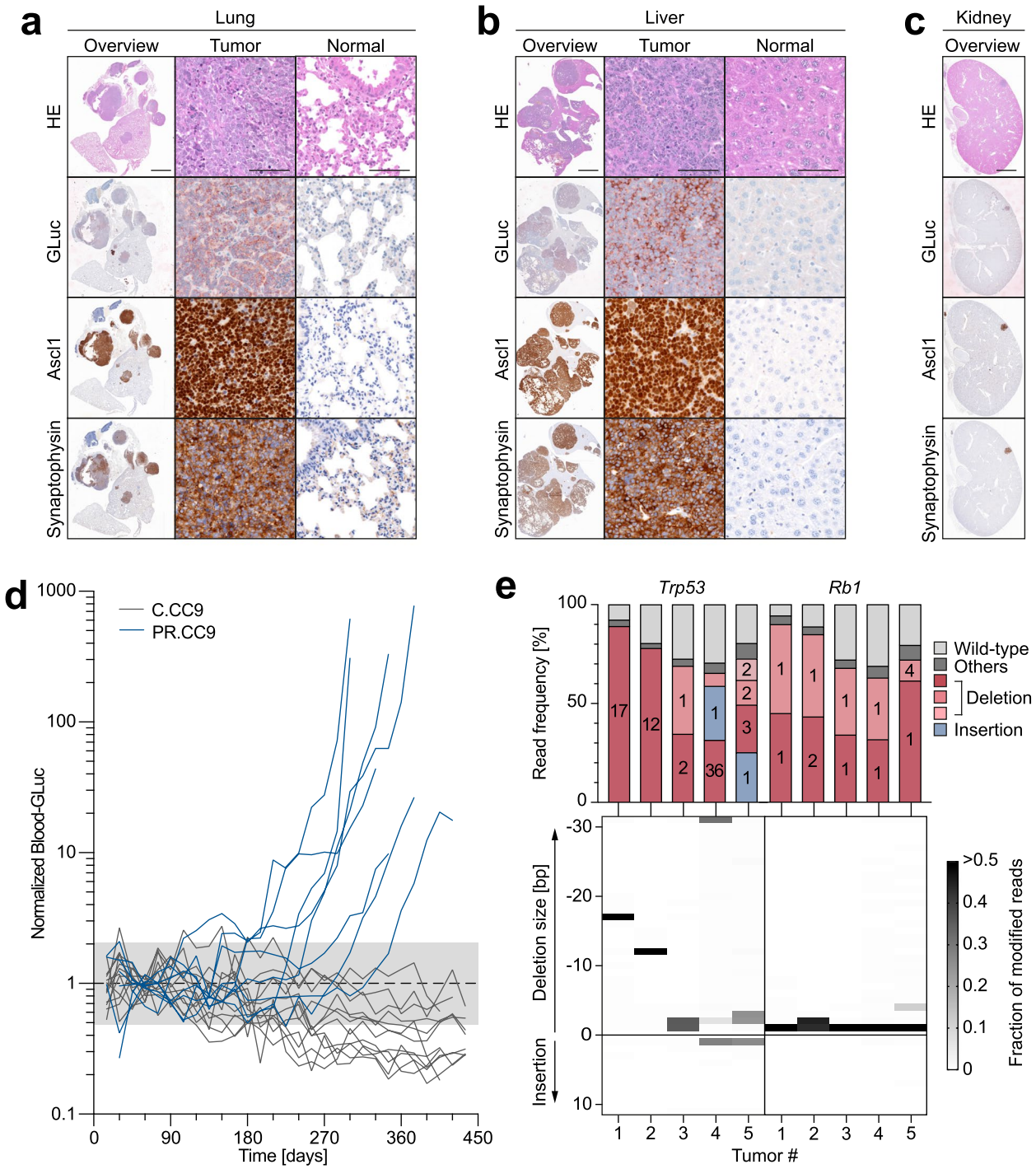

Fig. 5 Molecular characterization and GLuc-based monitoring of CRISPR-induced SCLC. **a-c** Histological analysis of AV-PR.CC9 induced **a** primary lung tumors and metastases to the **b** liver and **c** kidney. Shown are representative H&E and immunohistochemical stains for GLuc and NE lineage markers (Ascl1, Synaptophysin). **d** Temporal development of blood GLuc activity in individual mice following infection with indicated AVs (AV-C.CC9 $n=12$; AV-PR.CC9 $n=8$). Shaded area represents the GLuc background activity. **e** *Trp53* and *Rb1* mutation spectra of single AV-PR.CC9 tumors from 5 different mice. Top graph, shown is the frequency of wild-type and mutant reads. For mutant reads, all mutations with a frequency of > 5% are color-coded as deletions or insertions and labelled with the number of deleted or inserted base pairs. Less frequent mutations are summarized as 'others'. Bottom graph, shown is the size distribution of indel mutations for each tumor. The frequency is each indel mutations is encoded in grayscale

To confirm that tumors originate from cells with CRISPR-AV induced gene mutations, we sequenced the *Trp53* and *Rb1* genes of single tumors from 5 individual mice by NGS (Fig. 5e). In comparison to the low frequency of modified reads two weeks after adenoviral infection (Fig. 4e, f), tumors contained an average of 80% modified reads (*Trp53*: 0.79 ± 0.09; *Rb1*: 0.81 ± 0.11) (Fig. 5e). The mutant read frequency correlated significantly between the two genes ($R^2 = 0.88$, $P = 0.0188$), suggesting that the tumors originate from double-mutant cells. The percentage of approximately 20% unmodified reads is in line with the expected percentage of non-tumor cells populating the tumor stroma. Most tumors showed one or two (equally frequent) dominant mutant sequences, underlining that tumors are clonal in origin. Tumors 4 and 5 showed additional less frequent mutant sequences, possibly derived from adjacent tumor nodules. Similar as previously observed in AV-PR.CC9-infected lungs 1 week post infection and consistent with erroneous DSB repair via NHEJ, all *Rb1* and *Trp53* tumor mutations were indel mutations. Compared to mostly frameshift-inducing small deletions of 1, 2 or 4 nucleotides in *Rb1*, *Trp53* indels were more variable in size and nature. In addition to frameshift-inducing deletions, we also observed several in-frame mutations of 3, 12 or 36 base pairs. As the targeted *Trp53* exon 6 encodes a part of the DNA binding domain of the p53 transcription factor, which is notoriously sensitive to even subtle mutations, these in-frame mutations are likely loss-of-function mutations deficient in tumor suppression. Together, the observed mutation spectrum confirms that the tumors monitored by GLuc blood levels are indeed resulting from the anticipated *Trp53* and *Rb1* mutations rather than potential off-target mutations.

Comparative monitoring of genetically distinct tumor subtypes using GLuc blood-levels

We next explored whether GLuc-blood levels are suitable to monitor differences in tumorigenesis caused by distinct co-mutations. As a model we chose to monitor the impact of *Rbl2/p130* (L) mutations, which are recurrent co-mutations in SCLC patient tumors and accelerate SCLC tumorigenesis in mouse models [1, 15, 50]. Given the limited packaging capacity of 1st generation AVs, insertion of a third sgRNA cassette into the SpCas9-Cre co-expressing AV vector backbone resulted in strongly reduced virus titers. To overcome the resulting delivery challenges, we crossed LSL-GLuc with LSL-Cas9 mice and used compound conditional transgenic LSL-Cas9/LSL-GLuc mice with Cre-inducible expression of GLuc and Cas9 [14]. This allowed us to omit Cas9 from the CRISPR-AV and instead introduce one or more additional sgRNA cassettes. Using this strategy, we generated CRISPR-AVs expressing Cre (without SpCas9) together with sgRNA combinations targeting *Trp53* and *Rb1* (AV-PR.Cre), *Trp53*, *Rb1* and *Rbl2* (AV-PRL.Cre) or a non-targeting control sgRNA (AV-C.Cre) (Fig. 6a). The AVs were validated in vitro by infection of Cas9-expressing NIH3T3 cells, confirming efficient induction of indel mutations at all three target loci (Fig. 6b). Infection of LSL-Cas9 fibroblasts showed successful Cre-mediated activation of Cas9 expression and depletion of the targeted gene products at the protein level (Fig. 6c).

Lung sections from AV-infected LSL-Cas9/LSL-GLuc mice showed efficient induction of Cas9 and GLuc expression (Fig. 6d) and accumulation of small *Trp53*, *Rb1* and *Rbl2* indel mutations (Fig. 6e). When monitoring infected mice for development of lung cancer symptoms, the PR.Cre group showed similar kinetics of tumorigenesis as our previous PR.CC9 group (median survival 350 days; Figs. 6f and 4h). In contrast, PRL.Cre infected mice showed a significantly reduced median survival of only 210 days (Fig. 6f). GLuc labelling did not seem to affect the outcome, as non-GLuc transgenic LSL-Cas9 mice infected with these AVs showed similar survival (Additional file 1). GLuc blood-levels increased in both PR.Cre and PRL.Cre groups by far more than 2 orders of magnitude until the time of sacrifice with no significant difference between the two groups (median fold change PR.Cre: 293-fold; PRL.Cre: 335-fold; $P = 0.7971$; Fig. 6g,

(See figure on next page.)

Fig. 6 GLuc monitoring of SCLC induced by adenoviral sgRNA delivery to Cas9 mice. **a** Experimental scheme for SCLC induction and monitoring with adenoviral vectors (AV) expressing Cre and *Trp53/Rb1/Rbl2*-targeting sgRNAs. **b** Validation of sgRNA function by T7 endonuclease I Assay using genomic DNA from uninfected and AV-PRL.Cre infected NIH3T3-Cas9 cells. NTC, no template control. **c** Western Blot of LSL-Cas9 fibroblasts infected with AV-PR.Cre and AV-PRL.Cre showing downregulation of p53, Rb1 and Rbl2/p130 protein levels. β-actin is shown as loading control. **d** Immunohistochemistry for GLuc and Cas9 expression in the lung of mice 2 weeks post infection. Scale bar, 50 µm. **e** Mutation spectrum of *Trp53*, *Rb1* and *Rbl2* sgRNA target loci (flanked by dashed lines). **f** Kaplan–Meier survival plot of LSL-GLuc mice infected with indicated CRISPR-AVs (AV-C.Cre: $n = 14$; AV-PR.Cre: $n = 12$; AV-PRL.Cre: $n = 8$). Shown are median survival and P-values from Log-rank (Mantel-Cox) test. **g** Temporal development of blood GLuc activity in mice from **f** following infection with indicated AVs. Shaded area represents the GLuc background activity. **h** Total fold change in blood-GLuc activity over the course of tumor development. *P*-values from Tukey's multiple comparisons test. **i** Time point when blood-GLuc activity reached its maximum. *P*-value from an unpaired, two-sided t-test. **j** Time difference between the time of sacrifice (survival) and the time point when blood-GLuc activity was first elevated, i.e. exceeded the background range. **k** Correlation between time of sacrifice (survival) and the time point when blood-GLuc activity was first elevated. Shown is the linear regression with 95% confidence interval All error bars indicate SD, all data points represent biological replicates/individual mice

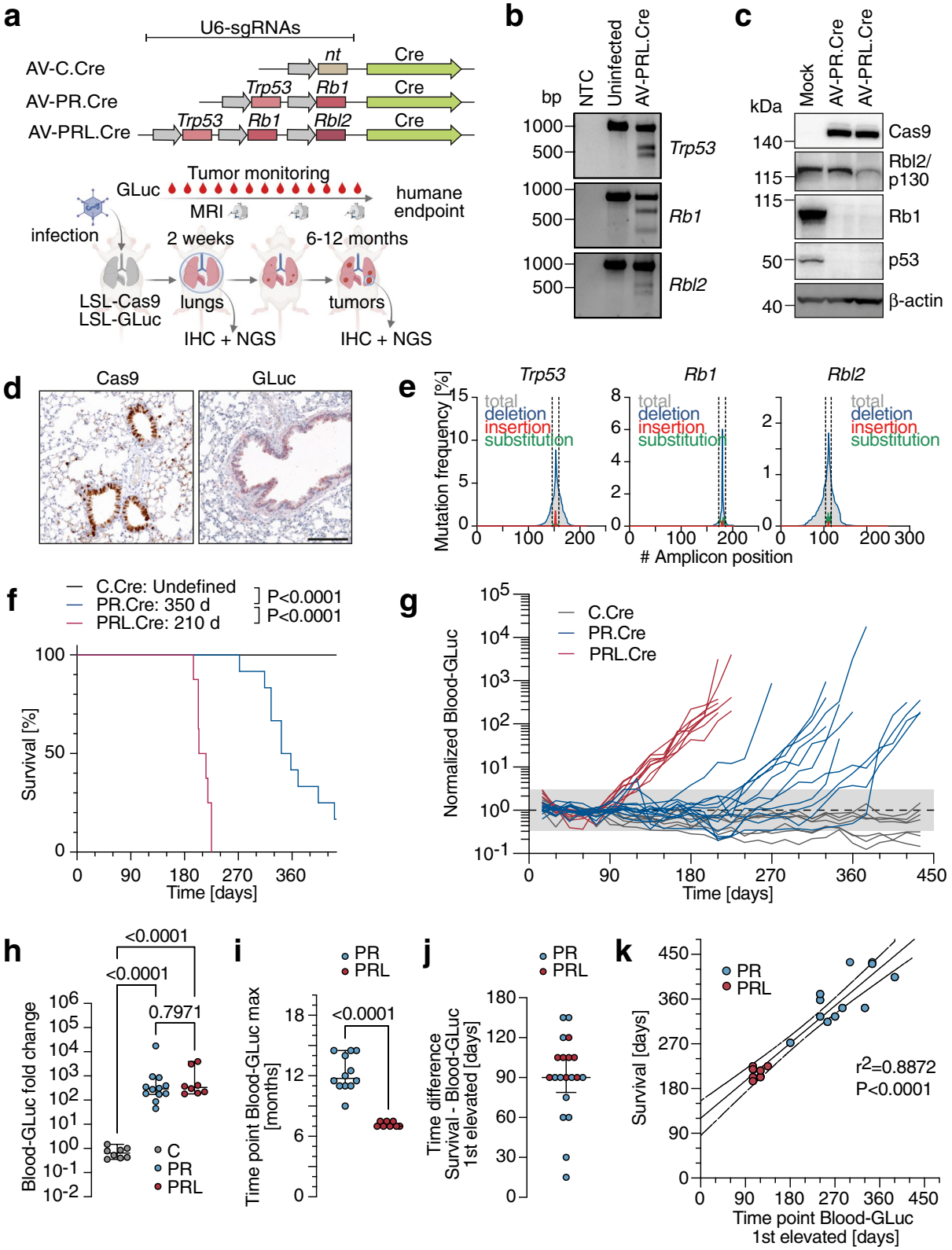

Fig. 6 (See legend on previous page.)

h). In the C.Cre control group, GLuc blood-levels did not change significantly (median 0.6580-fold; $P=0.0846$). Notably, although the fold change in GLuc blood-levels was not significantly different between PR.Cre and PRL.Cre mice, PRL.Cre mice reached the maximum GLuc blood-levels already after 7.2 ± 0.3 months, compared to 12.3 ± 1.8 months in PR.Cre mice ($P<0.0001$, Fig. 6i), mirroring the differences in survival. Interestingly, GLuc blood activity exceeded the background level, operationally defined as the average activity in the first three months, by more than 3 standard deviations approximately 3 months (PR.Cre: 82 ± 38 days, PRL.Cre: 101 ± 11 days) before reaching its maximum level at the time of sacrifice (Fig. 6j). Importantly, this early detection time point correlated with the clinically defined experimental endpoint "survival" ($r^2=0.8872$, $P<0.0001$; Fig. 6k), validating GLuc blood levels as a suitable early detection marker for autochthonous lung tumors.

MRI of representative mice suggested that the *Rbl2* co-mutation increases both the number of developing tumors and their growth rate (Fig. 7a). This impression was confirmed by histological examination of lungs at the time of sacrifice (Fig. 7b, c). Although mice from the PRL.Cre group survived 5 months shorter, quantitative image analysis revealed a 1.4-fold higher tumor burden ($P=0.0191$), which was mostly attributable to an increased number of tumors (3.0-fold, $P=0.0017$) that were only slightly smaller in size compared to tumors from PR.Cre mice (0.61-fold, $P=0.0285$; Fig. 7c).

Tumors from both groups expressed GLuc and the whole set of neuroendocrine markers, characterizing both groups as small cell lung cancer (Fig. 7b). Since Cas9 is constitutively expressed after Cre recombination, IHC confirmed this by positive Cas9 staining of tumor sections (Fig. 7b). Sequencing analysis of tumor nodules of 5 mice from each group showed *Trp53* and *Rb1* mutant allele frequencies of > 80% in all samples (Fig. 7d). Importantly, all PRL tumors also showed > 80% of mutant *Rbl2* reads identifying triple mutant cells as the cell of origin. Moreover, sequencing of predicted sgRNA off-target sites detected only in one of the tumors a single intronic base substitution (Additional file 3), excluding off-target editing as a cause of enhanced tumorigenesis in the PRL group. As seen in our previous PR.CC9 group (Fig. 5e), *Rb1* mutations were mostly small 1 bp deletions (Fig. 7d). In contrast, *Trp53* and *Rbl2* indel mutations were more diverse in size, allowing deeper insight into the clonal architecture of each analyzed tumor. While the majority of PR tumors showed 2 mutant *Trp53* alleles, PRL tumors more often contained a higher number of different *Trp53* and *Rbl2* mutations. When sequencing cell lines established from explanted SCLC tumors, the frequency of wild-type reads strongly decreased (Additional file 2). However, PRL cell lines still showed a higher number of different indel mutations than PR cell lines (Additional file 2). This strongly suggests that PR tumors are mostly monoclonal in origin, whereas PRL tumors more often consist of more than one clone. The number of tumors calculated by histological image analysis (Fig. 7c) is therefore likely an underestimation of the true number of tumor clones growing in the lungs of the PRL.Cre mouse group.

We conclude that blood-based GLuc monitoring provides an inexpensive and simple to implement technique for accurately assessing the impact of genetic factors such as co-mutations on tumor development and growth.

Discussion

Over the last decade, mouse models for cancer have improved significantly, mimicking increasingly well the spontaneous processes of tumor development, initiated by the genetic transformation of somatic cells at their natural site of origin [8]. In particular, the application of somatic mutagenesis with CRISPR nucleases has been a gamechanger that makes modelling of human cancer mutations in the mouse easier than ever [9, 10]. As more and more personalized treatment approaches with molecular drugs are developed, mouse models that accurately recapitulate the genetics of the human disease become essential preclinical tools. Nevertheless, the majority of preclinical research, especially drug testing, is still performed using subcutaneously transplanted xenograft tumors, as it was common practice already decades ago. A major reason is that tracking subcutaneous tumor growth is inexpensive and quick, whereas monitoring the development and orthotopic tumor growth in

(See figure on next page.)

Fig. 7 Rbl2 co-mutations accelerate SCLC tumorigenesis. **a** Sequential MRI of a representative AV-PR.Cre and AV-PRL.Cre infected mouse illustrating different kinetics of tumorigenesis. Shown are frontal and transversal sections with tumors marked in color. **b** Histological analysis of AV-PR.Cre and AV-PRL.Cre induced lung tumors. Shown are representative H&E and immunohistochemical stains for Cas9, GLuc and NE lineage markers (Ascl1, Synaptophysin, Chromogranin). **c** Quantitative analysis of SCLC tumor burden, tumor number and tumor size in AV-PR.Cre ($n=12$) and AV-PRL.Cre ($n=17$) infected mice. Shown is mean ± SD and P-values from unpaired, two-sided t-tests. **d** *Trp53*, *Rb1* and *Rbl2* mutation spectra of single tumors from 5 different mice of each group. Top graph, shown is the frequency of wild-type and mutant reads. For mutant reads, all mutations with a frequency of > 5% are color-coded as deletions or insertions and labelled with the number of deleted, inserted or substituted base pairs. Less frequent mutations are summarized as 'others'. Bottom graph, shown is the size distribution of indel mutations for each tumor. The frequency of each indel mutations is encoded in grayscale

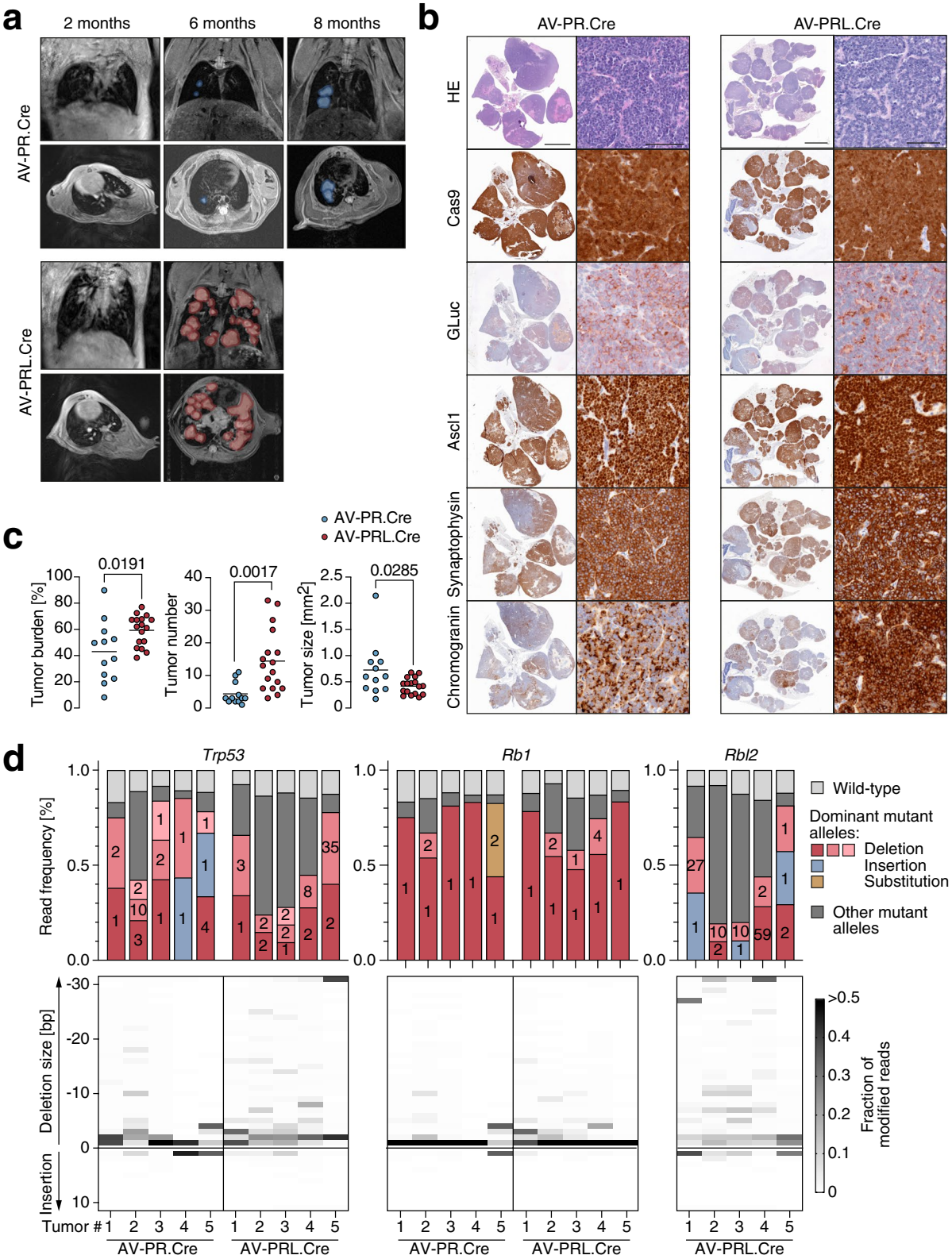

Fig. 7 (See legend on previous page.)

inner organs requires sophisticated small animal imaging technology and a highly trained staff [51]. Even though imaging is largely considered a non-invasive refinement method according to the 3R principles, it relies on anesthesia to restrain the animals and their gross motion and often also requires injection of contrast agents, tracers or luminescence substrates to visualize the tumor properly. This increases the image acquisition time by the anesthetic induction and recovery time and strongly reduces the possible throughput in cohort studies [52, 53]. Moreover, repeated anesthesia required for longitudinal studies, the exposure to ionizing radiation and the use of contrast agents also have consequences on the physiology of the animal and impose still poorly understood physical and mental distress on the animals [53, 54]. To make better use of the more human-like cancer disease models for preclinical studies, monitoring techniques are needed that provide a higher throughput at a lower cost—ideally while simultaneously minimizing distress to the animals.

An alternative to imaging is monitoring of tumor growth using biomarkers secreted by tumor cells into the blood. The monitoring of tumor-related marker proteins has been routine practice in cancer screening and clinical monitoring of cancer patients for relapse since decades [55] and has attracted even more attention in the recent years as liquid biopsy-based, ctDNA analyses have emerged as an effective strategy for non-invasive genetic cancer assessment in many stages of patients' monitoring [56]. However, not all tumors secrete specific marker proteins and the amount of blood needed for ctDNA analysis is restricting its use in small animal models. Different from the clinical tumor markers and ctDNA, secreted luciferases have the advantage of an excellent signal-to-noise ratio, a high dynamic range over several orders of magnitude, and—being actively secreted in an energy-consuming process—a direct relationship of signal to cell viability [20, 57]. As such, secreted *Gaussia* and *Cypridina* luciferases enable a blood-based tumor monitoring with high sensitivity and specificity using small-volume (10-20 µl) blood samples [20, 21, 27]. However, this requires the tumor cells to be labelled with the luciferases which is commonly achieved by transfection or retroviral transduction prior to their implantation into mice. While this works excellent for various transplanted mouse tumor models [22, 25, 26], the need for ex vivo labelling has prevented its use in autochthonous tumor models. The conditional GLuc-transgenic reporter mouse, developed in our study, overcomes this limitation and allows in situ labelling of cells by temporospatially controlled expression of Cre recombinase. Coupling Cre-mediated GLuc induction to tumor induction is achieved either by simultaneous Cre-mediated recombination of germline-encoded mutations, as demonstrated in the *Kras*^{G12D}-driven lung adenocarcinoma model (Fig. 2d-h), or by co-delivery of Cre with components of cancer-inducing CRISPR nucleases, as demonstrated in the SCLC models (Figs. 4, 5, 6 and 7). Importantly, in vivo GLuc labelling does not alter the disease time course as wild-type and LSL-GLuc mice with CRISPR-induced SCLC have indistinguishable survival and tumor phenotype (Fig. 4h). Notably, tumor cells which cannot be propagated or loose characteristic properties in vitro, can be labelled in vivo with the GLuc transgene and then directly allografted into cohorts of experimental animals for preclinical drug studies (Fig. 2a-c).

Of note, not all AV-infected cells that recombine the GLuc transgene develop into a tumor and will generate a background of non-transformed GLuc expressing cells. In our experiments, AV infection increased the background GLuc luminescence of wild-type or non-infected mice (Fig. 1d) by approximately fivefold and this level was maintained for at least 3 months. We exploited the increase in background luminescence as an indicator of successful AV infection and compensated for it in the analysis by normalizing all GLuc measurements to the post-infection background activity level. In the later course of tumorigenesis, blood-GLuc activity increased further by more than 4 orders of magnitude until the humane endpoint was reached, highlighting a high dynamic range that is not compromised by the initial infection-related increase in luminescence background. In contrast, GLuc background activity decreased over time in non-tumor control mice (Figs. 5d, 6g), suggesting that GLuc-expressing epithelial cells are continuously replaced by non-recombined, GLuc-negative progenitors or stem cells.

Despite providing a highly quantitative measure of the viable tumor load in each animal, secreted luciferases are not ideal for localizing the tumors by imaging. In principle, tumors can be imaged using GLuc [20], but as tumors grow larger and blood-GLuc levels increase, systemically applied luciferase substrate is often completely metabolized in the blood before reaching the tumor so that the tumor signal is effectively disguised [27]. Nevertheless, GLuc-based monitoring of tumor load can be combined with bioluminescence imaging (BLI) using mice double transgenic for a secreted and a non-secreted luciferase, provided that both luciferase signals can be discriminated. As GLuc metabolizes coelenterazine, we used luciferin-consuming firefly luciferase (FLuc) as a non-secreted partner-luciferase for imaging (Fig. 2). While BLI and blood-GLuc measurements provided congruent results, BLI was temporally restricted to one examination per week because of animal welfare regulations. In contrast, small-volume blood samples of up to 1% of the animal's total blood volume, i.e. up to 20 µl in mice, are

allowed to be drawn daily for a period of two weeks [58], giving a much higher temporal resolution of tumor load measurement and facilitating studies into the dynamics of fast processes such as tumor therapy (Fig. 2b). Alternatively, tumors can also be imaged by other technologies such as MRI. While we could only analyze some exemplary animals with multiple techniques in parallel, these animals showed similar results (Fig. 2e-g). A perfect correlation, however, would not even be expected considering that morphological imaging by MRI or CT insufficiently discriminates viable and necrotic tumor volumes and that BLI signals are strongly influenced by light absorption dependent on the emitted wavelength, tissue depth and type and fur color [59]. On the other side, blood-GLuc activity might be affected by differences in tumor vascularization, an issue that has so far not been explored, but should be considered when testing, for example, anti-angiogenic drugs.

Another important consideration for preclinical drug studies is that tumors need to be detectable early enough before the humane endpoint is reached to provide a time window sufficiently large to evaluate therapy responses. As in particular immunotherapies often show first therapeutic effects only several weeks after the first dose, this issue becomes increasingly important as research into immunotherapies is exploding. Notably, blood-GLuc levels were first elevated in our SCLC models on average 3 months before the animals reached the humane endpoint (Fig. 6j) and this early detection timepoint correlated significantly with the survival time of the animal (Fig. 6k). Especially in autochthonous tumor models, where the time course of tumor development varies strongly between different animals, blood-GLuc levels appear optimal to repeatedly screen larger animal cohorts for disease onset with minimal cost and effort. Once tumor growth is evident in blood samples, blood-GLuc monitoring could be complemented specifically by more sophisticated imaging techniques if, for example, exact tumor localization is required. Similarly, blood-GLuc monitoring can be implemented to screen therapy cohorts of treated mice long-term for evidence of relapse, as demonstrated in Fig. 2b, again followed by complementary imaging techniques to localize the site of relapse (Fig. 2c).

Tumor induction by CRISPR-induced somatic cancer gene mutations is a rising technology, that not only suffers from easily accessible monitoring strategies but also from nuclease delivery issues [9, 10]. Adenoviral vectors (AVs) with their natural tropism for the respiratory epithelium are optimally suited for highly efficient gene transfer to the lung. Moreover, mouse cells are naturally non-permissive to human adenovirus replication providing an additional level of safety in mouse experiments. In addition, owing to the large size of their genome, already first-generation AVs have a sufficiently large packaging capacity to deliver SpCas9 nucleases together with Cre for lung tumor induction (Figs. 4 and 5). However, the large size of the genome also makes AVs more difficult to engineer than smaller lentiviral or adeno-associated vectors. We have therefore provided a flexible cloning toolkit to rapidly assemble AVs for expression of Cre, SpCas9 and variable combinations of sgRNAs. Of note, while AV genomes could be assembled that express three sgRNA cassettes together with Cre and SpCas9, these were not efficiently packaged into viral particles. For expression of three (or more) sgRNAs we therefore recommend using LSL-Cas9 mice in conjunction with an AV that expresses sgRNAs and Cre only. Although Cas9 will be expressed constitutively in this case (Fig. 7b), adenoviral transgene (sgRNA) expression is only transient, thus intrinsically preventing long-term nuclease activity. In fact, we did not observe differences in the kinetics and efficiency of tumor induction comparing SCLC induction with either AV-PR.CC9 (Figs. 4 and 5) or AV-PR.Cre (Figs. 6 and 7). Alternatively, Cre could be co-delivered with the nuclease and three or more sgRNAs by a single AV by switching to smaller orthogonal CRISPR nucleases (such as SaCas9, Cpf1 or CasMINI), to smaller crRNA arrays cleaved in vivo by Cpf1 or endogenous RNases or to helper-dependent 'gutless' AVs with almost unlimited packaging capacity [12, 13, 60–62].

In all SCLC tumors that were analyzed by deep sequencing, the total mutant read frequency exceeded 70%, consistent with a small subpopulation of genetically wild-type stromal and immune cells (Figs. 5e and 7d). The vast majority of mutations were deletions, followed by a smaller number of insertions and substitutions. In all cases, these occurred at the sgRNA target site and were predicted to disrupt protein function either by inducing a frameshift or by mutating or deleting functionally critical residues. Each PR tumor contained one to two dominant mutant alleles in the two target genes, indicating a clonal origin of the tumor nodule. In the case of PRL tumors, most tumors contained more than two dominant alleles in each of the three target genes, suggesting that the analyzed tumor nodules originated from more than a single cell. This is likely attributable to the previously reported high efficiency of SCLC induction by additional inactivation of *Rbl2* [15, 50], a gene known to be essential for maintaining cell cycle quiescence [63]. Together the deep sequencing analysis confirmed that the SCLC development measured by increasing blood-GLuc levels originated from tumors containing the desired gene mutations and accurately captures differences in tumorigenesis resulting from different sets of CRISPR-induced driver mutations.

Conclusion

Our study describes a new GLuc reporter mouse for monitoring autochthonous tumors using luciferase measurements in blood samples. In addition, we provide a flexible toolkit for generating adenoviral vectors that, when used in conjunction with the conditional GLuc reporter mouse, simultaneously induce somatic mutations in cancer driver genes and label the resulting tumors with GLuc for blood-based monitoring. The combination of reporter mouse and adenoviral vector system will facilitate the use of autochthonous mouse tumor models in preclinical research by making tumor screening and monitoring of genetically-engineered orthotopic tumors considerably less time-consuming, less expensive and less burdening for the animals.

Abbreviations

AV: Adenoviral vector; AAV: Adeno-associated virus; GLuc: Gaussia princeps luciferase; FLuc: Firefly luciferase; GEMM: Genetically engineered mouse model; LSL: LoxP-Stop-loxP; SCLC: Small cell lung cancer; NSCLC: Non-small cell lung cancer; CRISPR: Clustered Regularly Interspaced Short Palindromic Repeats; Cas9: CRISPR-associated 9 protein; sgRNA: Single guide RNA; TME: Tumor microenvironment; BLI: Bioluminescence imaging; MRI: Magnetic resonance imaging; CT: Computed tomography; NGS: Next generation sequencing; IHC: Immunohistochemistry.

Supplementary Information

The online version contains supplementary material available at https://doi.org/10.1186/s12943-022-01661-2.

Additional file 1: Survival of non-GLuc transgenic SCLC mice. LSL-Cas9 mice (without GLuc transgene) were intratracheally infected with either AV-C.Cre, AV-PR.Cre or AV-PRL.Cre as depicted in Fig. 6a. Shown is the Kaplan-Meier survival plot with group size, median survival and P-values from Log-rank (Mantel-Cox) test

Additional file 2: Mutation spectra of SCLC cell lines. Cell lines were established from AV-PR.Cre (n=3) and AV-PRL.Cre (n=5) SCLC tumors and analyzed by deep sequencing of the sgRNA target regions in *Trp53*, *Rb1* and *Rbl2*. Depicted is the frequency of wild-type and mutant reads. For mutant reads, the Top5 mutations are color-coded as deletions or insertions and labelled with the number of deleted, inserted or substituted base pairs. Less frequent mutations are summarized as 'others'.

Additional file 3: sgRNA off-target analysis. *Trp53*, *Rb1* and *Rbl2* sgRNAs were analyzed for potential off-targets using the CRISPRoff Tool version 1.2. Shown are the Top10 hits with an intragenic location and "NGG" PAM. The Top10 hits for each of the *Trp53*, *Rb1* and *Rbl2* sgRNAs were PCR amplified using genomic tumor DNA from 3 AV-PR.Cre and 3 AV-PRL.Cre infected mice. PCR amplicons were analyzed for mutations by Sanger sequencing. Results are shown color-coded. Identified on-target and off-target mutations are shown in detail. Off-target mutations were all heterozygous missense mutations.

Additional file 4: Primers used for sgRNA off-target analysis.

Acknowledgements

Authors thank Sigrid Bischofsberger, Antje Grzeschiczek, Björn Geißert, Angela Mühling, Lara Kauer and employees of the animal facility of Marburg University for technical and experimental support. We acknowledge support by the Medical Core Facilities Genomics, Small Animal Imaging and Mouse Pathology.

Authors' contributions

Conceptualization: TS; Molecular biology experiments: NM, FS, MW, JF, MN, KK; Generation of GLuc reporter mouse: AS, TBr; Mouse tumor experiments: NM, FS, AMK, SE, OT; Mouse histopathology: FH, AP; Bioinformatics: MM; Next generation sequencing: AN; Funding acquisition: TBr, TBo, RS, OT, TS; Writing – Original Draft: NM, OT, TS; Writing – Review and Editing: all. The author(s) read and approved the final manuscript.

Authors' information

Not applicable.

Funding

Open Access funding enabled and organized by Projekt DEAL. This work was supported by grants from BMBF (031L0063), Deutsche Forschungsgemeinschaft (TRR81/3 109546710 Project A10 and A12, TI 1028/2–1, STI 182/13–1, GRK2573, BO 1639/9–1), German Center for Lung Research (DZL), State of Hesse (LOEWE iCANx), von Behring-Röntgen Stiftung (65–0004 and 66-LV06), Deutsche Krebshilfe (111250, 70112623 and 111444), Deutsche José Carreras Leukämie Stiftung e.V. (09 R/2018). The funding bodies were not involved in the design of the study and collection, analysis, and interpretation of data and in writing the manuscript.

Availability of data and materials

All of the materials, reagents and data generated during the current study are available from the corresponding authors upon request.

Declarations

Ethics approval and consent to participate

Not applicable.

Consent for publication

Not applicable.

Competing interests

The authors declare that they have no competing interests.

Author details

[1]Institute of Molecular Oncology, Universities of Giessen and Marburg Lung Center (UGMLC), Member of the German Center for Lung Research (DZL), Philipps-University, Marburg, Germany. [2]Clinic of Diagnostic and Interventional Radiology, Philipps-University, Core Facility 7T-small animal MRI, Marburg, Germany. [3]Mouse Pathology and Electron Microscopy Core Facility, Department of Neuropathology, Philipps-University, Marburg, Germany. [4]Genomics Core Facility, Philipps-University, Marburg, Germany. [5]Department of Cardiac Development and Remodeling, Member of the German Center for Lung Research (DZL), Max-Planck-Institute for Heart and Lung Research, Bad Nauheim, Germany. [6]Department of Biochemistry, Justus Liebig University, Giessen, Germany. [7]Max-Planck Institute for Heart and Lung Research, Member of the German Center for Lung Research (DZL), Member of the Cardio-Pulmonary Institute (CPI), Bad Nauheim, Germany. [8]Institute for Lung Health (ILH), Justus Liebig University, Giessen, Germany.

Received: 29 March 2022 Accepted: 22 September 2022
Published online: 03 October 2022

References

1. George J, Lim JS, Jang SJ, Cun Y, Ozretic L, Kong G, et al. Comprehensive genomic profiles of small cell lung cancer. Nature. 2015;524:47–53.
2. Gridelli C, Rossi A, Carbone DP, Guarize J, Karachaliou N, Mok T, Petrella F, Spaggiari L, Rosell R. Non-small-cell lung cancer. Nat Rev Dis Primers. 2015;1:15009.
3. Kwon MC, Berns A. Mouse models for lung cancer. Mol Oncol. 2013;7:165–77.
4. Mascaux C, Angelova M, Vasaturo A, Beane J, Hijazi K, Anthoine G, et al. Immune evasion before tumour invasion in early lung squamous carcinogenesis. Nature. 2019;571:570–5.

5. Guerin MV, Finisguerra V, Van den Eynde BJ, Bercovici N, Trautmann A. Preclinical murine tumor models: a structural and functional perspective. Elife. 2020;9:e50740.
6. Olson B, Li Y, Lin Y, Liu ET, Patnaik A. Mouse Models for Cancer Immunotherapy Research. Cancer Discov. 2018;8:1358–65.
7. Mendes N, Dias Carvalho P, Martins F, Mendonca S, Malheiro AR, Ribeiro A, Carvalho J, Velho S. Animal Models to Study Cancer and Its Microenvironment. Adv Exp Med Biol. 2020;1219:389–401.
8. Sanchez-Rivera FJ, Jacks T. Applications of the CRISPR-Cas9 system in cancer biology. Nat Rev Cancer. 2015;15:387–95.
9. Weber J, Rad R. Engineering CRISPR mouse models of cancer. Curr Opin Genet Dev. 2019;54:88–96.
10. van der Weyden L, Jonkers J, Adams DJ. The use of CRISPR/Cas9-based gene editing strategies to explore cancer gene function in mice. Curr Opin Genet Dev. 2021;66:57–62.
11. Truong DJ, Kuhner K, Kuhn R, Werfel S, Engelhardt S, Wurst W, Ortiz O. Development of an intein-mediated split-Cas9 system for gene therapy. Nucleic Acids Res. 2015;43:6450–8.
12. Xu X, Chemparathy A, Zeng L, Kempton HR, Shang S, Nakamura M, Qi LS. Engineered miniature CRISPR-Cas system for mammalian genome regulation and editing. Mol Cell. 2021;81(4333–4345):e4334.
13. Ehrke-Schulz E, Schiwon M, Leitner T, David S, Bergmann T, Liu J, Ehrhardt A. CRISPR/Cas9 delivery with one single adenoviral vector devoid of all viral genes. Sci Rep. 2017;7:17113.
14. Platt RJ, Chen S, Zhou Y, Yim MJ, Swiech L, Kempton HR, et al. CRISPR-Cas9 knockin mice for genome editing and cancer modeling. Cell. 2014;159:440–55.
15. Ng SR, Rideout WM 3rd, Akama-Garren EH, Bhutkar A, Mercer KL, Schenkel JM, Bronson RT, Jacks T. CRISPR-mediated modeling and functional validation of candidate tumor suppressor genes in small cell lung cancer. Proc Natl Acad Sci U S A. 2020;117:513–21.
16. Oser MG, Sabet AH, Gao W, Chakraborty AA, Schinzel AC, Jennings RB, et al. The KDM5A/RBP2 histone demethylase represses NOTCH signaling to sustain neuroendocrine differentiation and promote small cell lung cancer tumorigenesis. Genes Dev. 2019;33:1718–38.
17. Hong D, Knelson EH, Li Y, Durmaz YT, Gao W, Walton E, et al. Plasticity in the Absence of NOTCH Uncovers a RUNX2-Dependent Pathway in Small Cell Lung Cancer. Cancer Res. 2022;82:248–63.
18. Wang Y, Tseng JC, Sun Y, Beck AH, Kung AL. Noninvasive imaging of tumor burden and molecular pathways in mouse models of cancer. Cold Spring Harb Protoc. 2015;2015:135–44.
19. Markova SV, Larionova MD, Vysotski ES. Shining Light on the Secreted Luciferases of Marine Copepods: Current Knowledge and Applications. Photochem Photobiol. 2019;95:705–21.
20. Wurdinger T, Badr C, Pike L, de Kleine R, Weissleder R, Breakefield XO, Tannous BA. A secreted luciferase for ex vivo monitoring of in vivo processes. Nat Methods. 2008;5:171–3.
21. Tannous BA. Gaussia luciferase reporter assay for monitoring biological processes in culture and in vivo. Nat Protoc. 2009;4:582–91.
22. Vogiatzi F, Brandt DT, Schneikert J, Fuchs J, Grikscheit K, Wanzel M, et al. Mutant p53 promotes tumor progression and metastasis by the endoplasmic reticulum UDPase ENTPD5. Proc Natl Acad Sci U S A. 2016;113:E8433–42.
23. Klimovich B, Mutlu S, Schneikert J, Elmshauser S, Klimovich M, Nist A, Mernberger M, Timofeev O, Stiewe T. Loss of p53 function at late stages of tumorigenesis confers ARF-dependent vulnerability to p53 reactivation therapy. Proc Natl Acad Sci U S A. 2019;116:22288–93.
24. Wanzel M, Vischedyk JB, Gittler MP, Gremke N, Seiz JR, Hefter M, et al. CRISPR-Cas9-based target validation for p53-reactivating model compounds. Nat Chem Biol. 2016;12:22–8.
25. Gremke N, Polo P, Dort A, Schneikert J, Elmshauser S, Brehm C, et al. mTOR-mediated cancer drug resistance suppresses autophagy and generates a druggable metabolic vulnerability. Nat Commun. 2020;11:4684.
26. Brichkina A, Bertero T, Loh HM, Nguyen NT, Emelyanov A, Rigade S, et al. p38MAPK builds a hyaluronan cancer niche to drive lung tumorigenesis. Genes Dev. 2016;30:2623–36.
27. Charles JP, Fuchs J, Hefter M, Vischedyk JB, Kleint M, Vogiatzi F, et al. Monitoring the dynamics of clonal tumour evolution in vivo using secreted luciferases. Nat Commun. 2014;5:3981.
28. Srinivas S, Watanabe T, Lin CS, William CM, Tanabe Y, Jessell TM, Costantini F. Cre reporter strains produced by targeted insertion of EYFP and ECFP into the ROSA26 locus. BMC Dev Biol. 2001;1:4.
29. Dooley AL, Winslow MM, Chiang DY, Banerji S, Stransky N, Dayton TL, et al. Nuclear factor I/B is an oncogene in small cell lung cancer. Genes Dev. 2011;25:1470–5.
30. Jackson EL, Willis N, Mercer K, Bronson RT, Crowley D, Montoya R, Jacks T, Tuveson DA. Analysis of lung tumor initiation and progression using conditional expression of oncogenic K-ras. Genes Dev. 2001;15:3243–8.
31. Adams JM, Harris AW, Pinkert CA, Corcoran LM, Alexander WS, Cory S, Palmiter RD, Brinster RL. The c-myc oncogene driven by immunoglobulin enhancers induces lymphoid malignancy in transgenic mice. Nature. 1985;318:533–8.
32. Song J, Willinger T, Rongvaux A, Eynon EE, Stevens S, Manz MG, Flavell RA, Galan JE. A mouse model for the human pathogen Salmonella typhi. Cell Host Microbe. 2010;8:369–76.
33. O'Gorman S, Dagenais NA, Qian M, Marchuk Y. Protamine-Cre recombinase transgenes efficiently recombine target sequences in the male germ line of mice, but not in embryonic stem cells. Proc Natl Acad Sci U S A. 1997;94:14602–7.
34. Timofeev O, Koch L, Niederau C, Tscherne A, Schneikert J, Klimovich M, et al. Phosphorylation Control of p53 DNA-Binding Cooperativity Balances Tumorigenesis and Aging. Cancer Res. 2020;80:5231–44.
35. Timofeev O, Klimovich B, Schneikert J, Wanzel M, Pavlakis E, Noll J, et al. Residual apoptotic activity of a tumorigenic p53 mutant improves cancer therapy responses. EMBO J. 2019;38:e102096.
36. Timofeev O, Schlereth K, Wanzel M, Braun A, Nieswandt B, Pagenstecher A, Rosenwald A, Elsasser HP, Stiewe T. p53 DNA binding cooperativity is essential for apoptosis and tumor suppression in vivo. Cell Rep. 2013;3:1512–25.
37. Thorrez L, Vandenburgh H. Challenges in the quest for "clean meat." Nat Biotechnol. 2019;37:215–6.
38. Alkan F, Wenzel A, Anthon C, Havgaard JH, Gorodkin J. CRISPR-Cas9 off-targeting assessment with nucleic acid duplex energy parameters. Genome Biol. 2018;19:177.
39. Schmitt CA, Rosenthal CT, Lowe SW. Genetic analysis of chemoresistance in primary murine lymphomas. Nat Med. 2000;6:1029–35.
40. Luo J, Deng ZL, Luo X, Tang N, Song WX, Chen J, et al. A protocol for rapid generation of recombinant adenoviruses using the AdEasy system. Nat Protoc. 2007;2:1236–47.
41. He TC, Zhou S, da Costa LT, Yu J, Kinzler KW, Vogelstein B. A simplified system for generating recombinant adenoviruses. Proc Natl Acad Sci U S A. 1998;95:2509–14.
42. DuPage M, Dooley AL, Jacks T. Conditional mouse lung cancer models using adenoviral or lentiviral delivery of Cre recombinase. Nat Protoc. 2009;4:1064–72.
43. Maddalo D, Manchado E, Concepcion CP, Bonetti C, Vidigal JA, Han YC, et al. In vivo engineering of oncogenic chromosomal rearrangements with the CRISPR/Cas9 system. Nature. 2014;516:423–7.
44. Hartmann O, Reissland M, Maier CR, Fischer T, Prieto-Garcia C, Baluapuri A, et al. Implementation of CRISPR/Cas9 Genome Editing to Generate Murine Lung Cancer Models That Depict the Mutational Landscape of Human Disease. Front Cell Dev Biol. 2021;9:641618.
45. Engler C, Kandzia R, Marillonnet S. A one pot, one step, precision cloning method with high throughput capability. PLoS ONE. 2008;3:e3647.
46. Hartley JL, Temple GF, Brasch MA. DNA cloning using in vitro site-specific recombination. Genome Res. 2000;10:1788–95.
47. Russell WC. Update on adenovirus and its vectors. J Gen Virol. 2000;81:2573–604.
48. Ran FA, Hsu PD, Wright J, Agarwala V, Scott DA, Zhang F. Genome engineering using the CRISPR-Cas9 system. Nat Protoc. 2013;8:2281–308.
49. Meuwissen R, Linn SC, Linnoila RI, Zevenhoven J, Mooi WJ, Berns A. Induction of small cell lung cancer by somatic inactivation of both Trp53 and Rb1 in a conditional mouse model. Cancer Cell. 2003;4:181–9.
50. Schaffer BE, Park KS, Yiu G, Conklin JF, Lin C, Burkhart DL, Karnezis AN, Sweet-Cordero EA, Sage J. Loss of p130 accelerates tumor development in a mouse model for human small-cell lung carcinoma. Cancer Res. 2010;70:3877–83.
51. Serkova NJ, Glunde K, Haney CR, Farhoud M, De Lille A, Redente EF, et al. Preclinical Applications of Multi-Platform Imaging in Animal Models of Cancer. Cancer Res. 2021;81:1189–200.
52. Hildebrandt IJ, Su H, Weber WA. Anesthesia and other considerations for in vivo imaging of small animals. ILAR J. 2008;49:17–26.
53. Balaban RS, Hampshire VA. Challenges in small animal noninvasive imaging. ILAR J. 2001;42:248–62.

54. Tremoleda JL, Kerton A, Gsell W. Anaesthesia and physiological monitoring during in vivo imaging of laboratory rodents: considerations on experimental outcomes and animal welfare. EJNMMI Res. 2012;2:44.
55. Duffy MJ. Tumor markers in clinical practice: a review focusing on common solid cancers. Med Princ Pract. 2013;22:4–11.
56. Siravegna G, Mussolin B, Venesio T, Marsoni S, Seoane J, Dive C, et al. How liquid biopsies can change clinical practice in oncology. Ann Oncol. 2019;30:1580–90.
57. Liu S, Su Y, Lin MZ, Ronald JA. Brightening up Biology: Advances in Luciferase Systems for in Vivo Imaging. ACS Chem Biol. 2021;16:2707–18.
58. Morton DB, Abbot D, Barclay R, Close BS, Ewbank R, Gask D, et al. Removal of blood from laboratory mammals and birds. First report of the BVA/FRAME/RSPCA/UFAW Joint Working Group on Refinement. Lab Anim. 1993;27:1–22.
59. Darne C, Lu Y, Sevick-Muraca EM. Small animal fluorescence and bioluminescence tomography: a review of approaches, algorithms and technology update. Phys Med Biol. 2014;59:R1-64.
60. McCarty NS, Graham AE, Studena L, Ledesma-Amaro R. Multiplexed CRISPR technologies for gene editing and transcriptional regulation. Nat Commun. 2020;11:1281.
61. Ran FA, Cong L, Yan WX, Scott DA, Gootenberg JS, Kriz AJ, et al. In vivo genome editing using Staphylococcus aureus Cas9. Nature. 2015;520:186–91.
62. Zetsche B, Gootenberg JS, Abudayyeh OO, Slaymaker IM, Makarova KS, Essletzbichler P, et al. Cpf1 is a single RNA-guided endonuclease of a class 2 CRISPR-Cas system. Cell. 2015;163:759–71.
63. Litovchick L, Sadasivam S, Florens L, Zhu X, Swanson SK, Velmurugan S, et al. Evolutionarily conserved multisubunit RBL2/p130 and E2F4 protein complex represses human cell cycle-dependent genes in quiescence. Mol Cell. 2007;26:539–51.

Publisher's Note

Supplemental Figure 1

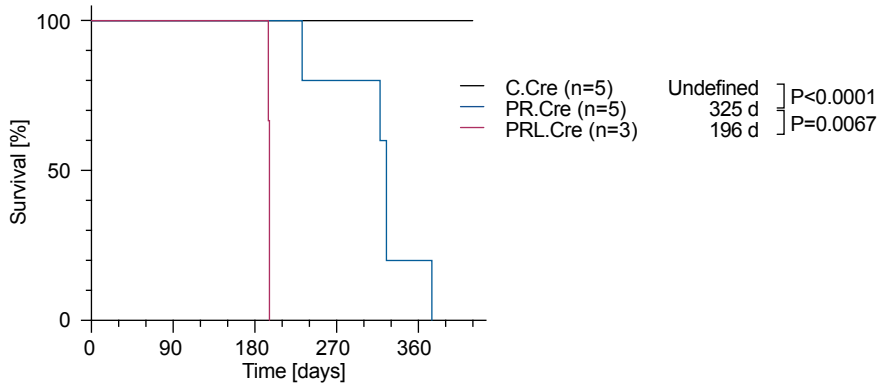

Supplemental Figure 2